Des microtubules à la mitose - Fonctions du cytosquelette au cours de la division des cellules eucaryotes

Jean-Philippe Kleman

Diplôme d'Habilitation à Diriger les Recherches

Spécialité : Biologie
Université Joseph Fourier – Grenoble I

Des microtubules à la mitose - Fonctions du cytosquelette au cours de la division des cellules eucaryotes.

Présenté par

Jean-Philippe KLEMAN

Laboratoire des Protéines du Cytosquelette
Institut de Biologie Structurale "Jean-Pierre Ebel"

Soutenue le 4 février 2004

Composition du jury :

Dr Bruno Goud	Rapporteur
Dr Carl Mann	Rapporteur
Dr Didier Job	Rapporteur
Pr Eva Pebay-Peyroula	
Pr Jean-Claude Boucaut	
Dr Robert L. Margolis	

"La théorie, c'est quand on sait tout et que rien ne fonctionne. La pratique, c'est quand tout fonctionne et que personne ne sait pourquoi. Ici, nous avons réuni théorie et pratique : rien ne fonctionne... et personne ne sait pourquoi!"

Albert Einstein

Pour Théo et Simon.

Table des matières

Curriculum Vitae

KLEMAN Jean-Philippe, Chercheur au Commisariat à l'Energie Atomique depuis 1996
Né le 4 juillet 1967 à Paris, 16ème arrondissement

Adresse professionelle Laboratoire des Protéines du Cytosquelette
Institut de Biologie Structurale «Jean-Pierre Ebel»
41, rue Jules Horowitz
38027 Grenoble cedex 1

Téléphone professionel 04 38 78 92 19
Adresse électronique jpk@ibs.fr

Diplomes et titres universitaires

Baccalauréat	Série C	1985
Normalien	Ecole Normale Supérieure de Lyon	1987-1991
Magistère	Ecole Normale Supérieure de Lyon & Université Claude Bernard Lyon I Licence de Biochimie Licence de Biologie Cellulaire et Moléculaire Maitrise de Biologie Cellulaire et Moléculaire Diplôme d'Etude Approfondie de Différenciation, Génétique et Immunologie Rang 8	1987-1990 1987-1988 1987-1988 1988-1989 1989-1990
DEA		
Thèse de Doctorat	"Etude des Formes des Collagènes de Types V et XI" Direction Pr. M. van der Rest Soutenue devant l'Université Claude Bernard Lyon I le 20 décembre 1993 Mention Très Honorable avec Félicitations	1990-1993

Direction de travaux

J'ai dirigé ou participer à la direction des travaux de plusieurs chercheurs post-doctoraux et d'étudiants au cours des années passées. Je suis à l'origine de la venue au laboratoire du Dr Caroline Reynaud (2001-2003) avec qui j'ai travaillé sur l'étude de TD-60. J'ai eu par ailleurs la possibilité de travailler pendant leur stage post-doctoral avec les Drs Cristiana Mollinari (1999-2001) et Cristina Pacios-Bras (depuis 2003).
J'encadre également depuis juillet 2003 Maxime Parisotto, étudiant de Master 2 (Biologie Structurale et Nanobiologie) sur un projet portant sur l'étude biochimique et fonctionnelle de la protéine des kinétochores TD-60. J'ai obtenu pour ce projet le pré-flêchage d'un financement CFR du CEA pour la rentrée universitaire 2004.
J'ai encadré depuis 2000 le stage de DEA (Biologie Structurale et Fonctionnelle) puis la thèse de Denis Bouvier (financement CFR du CEA 2001-2004) sur le thème de l'étude biochimique et structurale de l'interaction STOP-calmoduline. Ce travail est réalisé en partenariat avec le laboratoire de Résonance Magnétique Nucléaire de l'Institut.

Dans le cadre des stages de Maîtrise universitaire (durée 2 mois), j'ai encadré les travaux d'Henri Cabrière («Surexpression et caractérisation de la protéine F-STOP : établissement de la liaison F-STOP-Microtubule»; 1999), et d'Aurélie Enjalbert («Etablissement de la liaison STOP-Calmoduline»; 2000).
J'ai encadré le stage de fin d'étude (stage de 3 mois, IUT de l'Université Clermont I) de Catherine Bonnichon («Préparation, purification et caractérisation de systèmes protéiques régulateurs du cytosquelette : La protéine F-STOP et la calmoduline, La protéine TD-60 au cours de la cytokinèse»; 2000) et d'Anne-Cécile Birgi («Localisation et rôle de la protéine PRC1 au cours de la cytokinèse»; 2001).
J'ai également encadré le stage de BTS de Sandrine Jobase (durée 1 mois «Caractérisation de systèmes protéiques régulateurs du cytosquelette : La protéine STOP et la calmoduline»; 2002).

Activités d'enseignement

A la suite de ma scolarité à l'Ecole Normale Supérieure de Lyon, j'ai bénéficié pour ma thèse de doctorat d'une bourse d'Allocataire Moniteur Normalien, incluant une charge d'enseignement (96 heures équivalent TP par an). J'ai encadré les travaux pratiques de biochimie de première année de Magistère de Biologie Moléculaire et Cellulaire (ENS-Lyon). J'ai aussi dispensé pour ces mêmes étudiants des séances de travaux dirigés qui portaient sur les techniques d'analyse biochimique des protéines et sur l'étude d'articles scientifiques.

Depuis 1992, je suis membre du jury du concours d'entrée à l'Ecole Normale Supérieure de Lyon. Dans ce cadre, j'ai été chargé des épreuves orales de biologie cellulaire (1992-2002) et de T.I.P.E. (Travaux d'Intérêt Personnel Encadrés, 2003) ainsi que du secrétariat du concours (1992-1995), et ponctuellement correcteur des épreuves écrites. En 1997, j'ai été chargé de la rédaction du sujet écrit de biologie pour l'épreuve commune des Ecoles Normales Supérieures de Lyon et de Cachan.

Liste des publications

1. Kleman, J. P., Hartmann, D. J., Ramirez, F., et van der Rest, M. 1992 The human rhabdomyosarcoma cell line A204 lays down a highly insoluble matrix composed mainly of alpha 1 type-XI and alpha 2 type-V collagen chains, Eur J Biochem 210, 329-335.

2. Giry-Lozinguez, C., Kleman, J. P., et van der Rest, M. 1994 Modules et interactions moléculaires au sein des matrices extracellulaires, Médecine/Science 12, 1234-1243.

3. Moradi-Ameli, M., Rousseau, J. C., Kleman, J. P., Champliaud, M. F., Boutillon, M. M., Bernillon, J., Wallach, J., et Van der Rest, M. 1994 Diversity in the processing events at the N-terminus of type-V collagen, Eur J Biochem 221, 987-995.

4. Fichard, A., Kleman, J. P., et Ruggiero, F. 1995 Another look at collagen V and XI molecules, Matrix Biol 14, 515-531.

5. Kleman, J. P., Giry-Lozinguez, C., et van der Rest, M. 1995 Diversity and modularity of extracellular matrix macromolecules at the gene and protein levels, J Hepatol 22, 3-9.

6. Kleman, J. P., Aeschlimann, D., Paulsson, M., et van der Rest, M. 1995 Transglutaminase-catalyzed cross-linking of fibrils of collagen V/XI in A204 rhabdomyosarcoma cells, Biochemistry 34, 13768-13775.

7. Chantalat, L., Skoufias, D. A., Kleman, J. P., Jung, B., Dideberg, O., et Margolis, R. L. 2000 Crystal structure of human survivin reveals a bow tie-shaped dimer with two unusual alpha-helical extensions, Mol Cell 6, 183-189.

8. Mollinari, C., Kleman, J. P., Jiang, W., Schoehn, G., Hunter, T., et Margolis, R. L. 2002 PRC1 is a microtubule binding and bundling protein essential to maintain the mitotic spindle midzone, J Cell Biol 157, 1175-1186.

9. Mollinari, C., Reynaud, C., Martineau-Thuillier, S., Monier, S., Kieffer, S., Garin, J., Andreassen, P. R., Boulet, A., Goud, B., Kleman, J. P., et Margolis, R. L. 2003 The Mammalian Passenger Protein TD-60 Is an RCC1 Family Member with an Essential Role in Prometaphase to Metaphase Progression, Dev Cell 5(2), 295-307.

10 Bouvier, D., Vanhaverbeke, C., Simorre, J. P., Arlaud, G. J., Bally, I., Forge, V., Margolis, R. L., Gans, P., et Kleman, J. P. 2003 Unusual Ca(2+)-Calmodulin Binding Interactions of the Microtubule-Associated Protein F-STOP, Biochemistry 42, 11484-11493.

11. Robinson, P. J., Wang, X., Xue, J., Assaf, B. T., Kemp, B. E., Larsen, M. R., Milburn, P. J., Kleman, J. P., et Margolis, R. L. 2003 Phosphorylation of N-STOP on Ser-537 by cGMP-dependent protein kinase in nerve terminals is regulated by Ca^{2+}-calmodulin, J Neurochem, manuscrit en préparation.

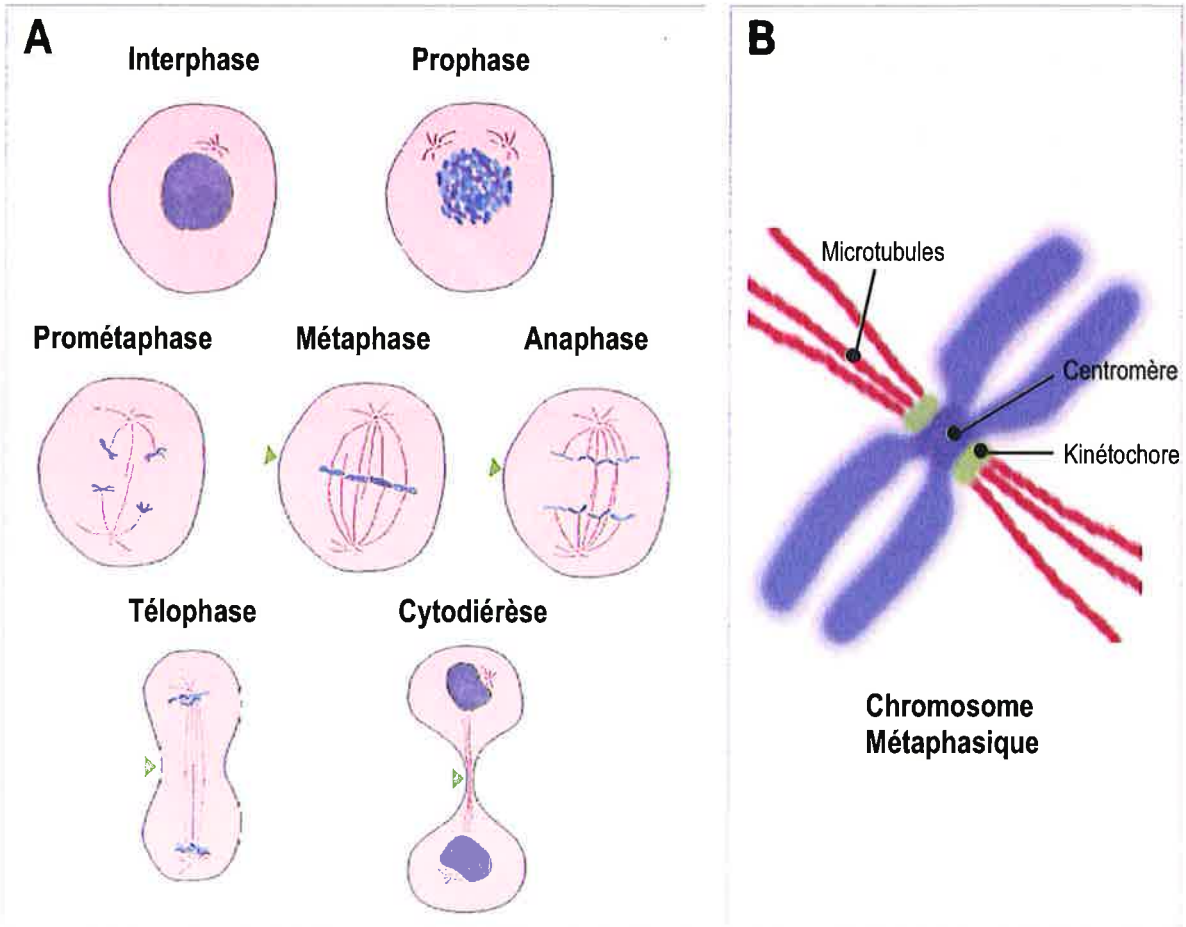

Figure 1: A) Les grandes étapes de la mitose.
Sont représentés dans ce schéma l'ADN en bleu et les microtubules en rouge. En fin d'interphase, un seul centrosome (centre organisateur des microtubules) est visible à proximité du noyau. Dès le début de la prophase, l'ADN se condense, l'enveloppe nucléaire disparait, et le centrosome se duplique pour migrer de part et d'autre des chromosomes. En prométaphase, les microtubules forment le fuseau mitotique. Ils s'associent aux kinétochores des chromosomes (voir B), et permettent l'alignement des chromosomes qui est obtenu en métaphase. Lorsque les chromosomes sont parfaitement alignés, la cellule rentre en anaphase. Les bras des chromosomes se séparent et migrent grâce aux microtubules vers les pôles. Les microtubules dont l'extrémité reste libre forment un réseau chevauchant au centre de la cellule. Ces microtubules dits interkinétochoriens permettent l'assemblage des protéines du disque télophasique, où la cellule débute sa constriction (télophase) jusqu'à la séparation des cellules filles au cours de la cytodiérèse. Les microtubules interkinétochoriens forment alors le corps intermédiaire. Les pointes des flèches représentent l'emplacement du sillon de division, visible dès la télophase, et marqué dans la cellule par la présence des protéines passagères. Ces protéines participent à la formation du disque télophasique.
B) Représentation d'un chromosome typique en métaphase.
Le chromosome métaphasique possède 2 brins d'ADN dupliqué lors de la phase de réplication du stock génétique (Phase S). Les deux bras sont en contact par le centromère sur lequel se forme le kinétochore. Cette structure permet la liaison aux microtubules du fuseau mitotique. Elle présente habituellement une organisation lamellaire apposée au centromère. La couronne fibreuse externe est la zone d'attachement des microtubules.

Introduction

Mon parcours scientifique se partage en deux périodes principales. D'une part la période DEA-Thèse de doctorat (IBCP, Lyon), et d'autre part la période post-doctorale, immédiatement suivie de mon recrutement à l'IBS (Grenoble). Ce document est volontairement limité aux travaux correspondant à cette dernière période. Seul un bref résumé de mes activités antérieures est inclu en annexe.

Au cours des années passées dans le Laboratoire des Protéines du Cytosquelette de Robert Margolis, et en fonction de mes centres d'intérêts, j'ai cherché à mettre en place des projets transversaux impliquants les groupes de structuralistes de l'Institut. Mon travail axé sur les relations entre les éléments du cytosquelette et les contrôles du cycle cellulaire, m'a conduit à développer deux programmes. Ces projets portent sur des protéines associées au cytosquelette, et plus particulièrement aux microtubules du fuseau mitotique, cette structure impliquée dans l'alignement puis la ségrégation des chromosomes au cours de la mitose (figure 1A). Le cytosquelette est essentiel aux régulations du cycle cellulaire. Au laboratoire, nous avons choisi de développer ces projets à partir du modèle constitué par les cellules eucaryotes de mammifères.

Je me suis tout particulièrement intéressé aux complexes formés par le couple centromère-kinétochore. Les kinétochores sont assemblés lors de la mitose sur les centromères et permettent en particulier l'ancrage des microtubules du fuseau aux chromosomes (figure 1B). Les kinétochores sont également le siège des contrôles lors de la transition métaphase-anaphase, et sont impliqués dans la mise en place du disque télophasique, l'organite qui permet la séparation physique des cellules filles (cytodiérèse). Parmi les protéines constituantes, les protéines dîtes "passagères des chromosomes" forment une classe particulière, définie par leur localisation spécifique au cours de la mitose. Présentes sur les kinétochores en métaphase, ces protéines migrent le long des microtubules inter-kinétochoriens en anaphase (figure 1A) pour participer à la formation, au centre de la cellule, du disque télophasique (figure 2). Le premier membre de cette famille mis en évidence a été INCENP (INner CENtromere Protein, références *1, 2*). Depuis lors, 3 autres protéines passagères ont été identifiées, la survivine, la kinase Aurora B, et TD-60 (*3-7*). Ces protéines portent des fonctions essentielles pour la transition métaphase-anaphase d'une part, et la cytodiérèse d'autre part, en participant à la formation du disque télophasique dans la zone où débutera la division physique des 2 futures cellules filles.

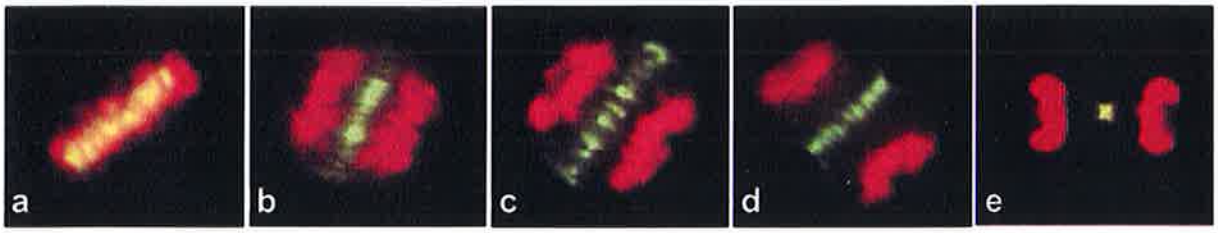

Figure 2 : Localisation de TD-60 (vert) et des chromosomes (rouge) au cours de la mitose.
TD-60 montre la localisation typique d'une protéine passagère. Elle est concentrée sur les centromères des chromosomes en métaphase (a). Après la transition métaphase-anaphase, la protéine migre depuis les kinétochores vers la zone centrale du fuseau (anaphase, insert b). En fin d'anaphase (c) la protéine se concentre pour former le disque télophasique, où s'initie la formation du sillon de division (d). En fin de division (e), TD-60 est localisée sur le corps intermédiaire, entre les deux cellules filles (Clichés LPC, IBS-CEA).

Depuis 1999, j'ai pris en charge avec les Dr C. Reynaud et C. Mollinari l'identification et la caractérisation de la protéine passagère TD-60 (antigène de 60kDa du Disque Télophasique). Son implication dans le clivage des cellules filles avait été suggéré au laboratoire (*7*), mais sa séquence et ses fonctions biologiques exactes restaient encore largement obscures. Cette protéine participe à la formation d'une structure associée aux microtubules et mise en place au cours de l'anaphase, le disque télophasique (*7*), qui est directement impliquée dans la signalisation de la zone dans laquelle débute la formation du sillon de division. Nous avons démontré que cette protéine passagère était un nouveau membre de la famille RCC1 qui possède un rôle dans la transition métaphase-anaphase. Ce travail récemment publié (*8*) fait l'objet d'une section de ce document. J'ai également contribué à la caractérisation de la survivine. Cette protéine passagère avait été découverte en 1997 pour son rôle anti-apoptotique (*9*), et était connue pour s'associer aux microtubules du fuseau mitotique (*10*). Elle possède à son extrémité amino terminale un domaine BIR (Baculovirus Inhibitor of apoptosis Repeat), et une longue hélice alpha (45 résidus) dans sa partie C-terminale. La structure cristallographique résolue (*11*) a permis de montrer que la survivine était un dimère formé par l'interaction tête-bêche des domaines BIR avec l'extrémité proximale de l'hélice alpha. Pour des raisons de concision, je ne développerai pas plus avant ces travaux, mais le lecteur intéressé pourra se référer au tiré à part

présenté à la fin de ce document.

Les protéines passagères participent toutes à la formation du disque télophasique, probablement en formant un complexe fonctionnel (*4, 12*). Au cours de notre travail sur TD-60, nous nous sommes intéressé à une autre protéine localisée dans la zone centrale du fuseau en anaphase et impliquée dans la division des cytoplasmes en fin de mitose, PRC1 (Protein Required for Cytokinesis 1 , référence *13*). Nous avons mis en évidence par une étude de dissection moléculaire et de biologie cellulaire, que cette protéine est responsable de l'association latérale des microtubules en fin de mitose et participe ainsi à l'élaboration du sillon de division (*14*). Ces donnés ainsi que les développements actuels de ce projet sont exposés dans ce document.

Une autre partie de mon travail a porté sur la protéine STOP (Stable Tubule Only Polypeptide; voir chapitre II page 13). J'ai travaillé en liaison avec le laboratoire CS (Didier Job, DRDC) sur les aspects structuraux de la protéine associée aux microtubules stables des fibroblastes, F-STOP (*15*). Dans les conditions physiologiques, F-STOP n'est associée aux microtubules que lors de la mitose (*16*). Il s'agit de la forme la plus courte des membres de la famille des STOP, dont le premier à avoir été décrit est la forme neuronale N-STOP (*17, 18*). Les protéines STOP sont toutes issues d'un gène unique, et stabilisent les microtubules en particulier au froid où à la dilution. Cette propriété est inhibée en présence de calmoduline calcique, par un mécanisme qui implique une interaction directe entre la protéine STOP et la calmoduline (Pour une revue, voir référence *19*). Au cours de la mitose, le recrutement spécifique de F-STOP sur les microtubules du fuseau où est également présente la calmoduline (*20*) suggère que l'interaction de ces deux partenaires pourrait être liée à une fonction physiologique de F-STOP. Dans le cadre de ce projet, j'ai encadré depuis 3 ans un étudiant en thèse de doctorat, Denis Bouvier, en collaboration avec le Laboratoire de Résonance Magnétique Nucléaire de l'institut, afin d'étudier les caractéristiques structurales du complexe formé par la F-STOP et la calmoduline calcique. Le travail réalisé par Denis Bouvier a permis de montrer un mode de liaison inhabituel entre un motif de cette F-STOP et la calmoduline (*21*).

Chapitre I : Les kinétochores, le disque télophasique et les protéines passagères

Le kinétochore est la structure supra-moléculaire qui s'assemble sur les centromères des chromosomes lors de la mitose. Ce macro-complexe est le siège de nombreux contrôles qui sont indispensables à la régulation de l'avancement normal en mitose. Sa fonction première est de permettre la liaison des chromosomes avec le fuseau mitotique de microtubules. Cette structure est donc impliquée de la ségrégation correcte des chromosomes au cours de la division cellulaire (*22*). Le kinétochore est pourtant largement méconnu, et si certains de ses constituants sont maintenant identifiés, leurs fonctions au sein de cette structure complexe restent encore obscures.

Un des enjeux majeurs dans la compréhension de la mitose est aujourd'hui l'analyse des relations structurales et fonctionnelles dans ces macro-structures impliquant à la fois l'ADN du centromère, des protéines de structure et les protéines de contrôle (protéines du point de contrôle mitotique). Parmi les composants des kinétochores, les protéines passagères se relocalisent pendant la mitose, depuis la partie centromérique des kinétochores vers la zone centrale du fuseau en prenant appui sur les microtubules (*23*). Dans le cadre de l'étude des protéines passagères et de leurs fonctions en mitose, j'ai participé à plusieurs résultats importants du laboratoire. Il s'agit en particulier de la résolution de la structure de la survivine (*11*), travail sous la responsabillité de D. Skoufias (en collaboration avec le O. Dideberg, IBS, Laboratoire de Cristallogénèse Moléculaire), mais aussi la purification, le séquençage, le clonage et la caractérisation de TD-60 (*8*), un travail pour lequel j'ai en partie encadré plusieures post-doctorantes, Cristiana Mollinari (1999-2001), Caroline Reynaud (2001-2003) et Cristina Pacios-Bras (depuis février 2003), et enfin pour l'étude de PRC1 (C. Mollinari), une protéine du disque télophasique impliquée dans le déroulement de la cytodiérèse (*14*).

PRC1, une protéine impliquée dans la structuration du disque télophasique

Analyse fonctionnelle des domaines de la protéine PRC1

PRC1 est une protéine directement impliquée dans la phase finale de la mitose (*13*) au cours de laquelle les microtubules kinétochoriens participent au clivage des cellules filles en formant le disque télophasique. Cet organite dépourvu de membrane est mis en place par l'intermédiaire des microtubules et des protéines passagères pour remplir cette fonction primordiale. Nous avons montré que PRC1 participe à l'assemblage d'un disque télophasique fonctionnel (référence *14 et travaux en cours*). En effet, PRC1 possède la capacité de stabiliser des assemblages de microtubules antiparallèles, ce qui est le cas des microtubules du disque télophasique.

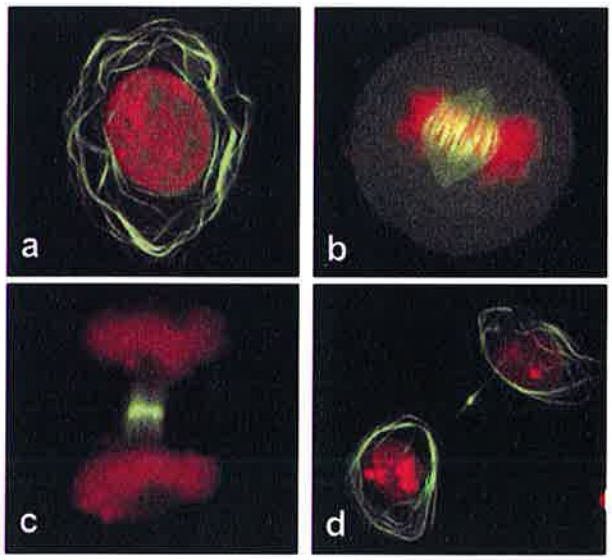

Figure 3: Visualisation de PRC1 surexprimée dans les cellules HeLa au cours du cycle cellulaire.
La fusion GFP-PRC1 apparaît en vert, l'ADN est coloré en rouge. PRC1 est colocalisée avec le réseau des microtubules au cours du cycle. La surexpression modifie profondément les microtubules en interphase (a, formation de pelotes), mais la cellule reste capable de réaliser la mitose normalement (b: métaphase; c: cytodiérèse). Lors du cycle suivant (d), les microtubules forment de nouveau des assemblages compacts dans le cytoplasme.

L'activité d'assemblage des microtubules par PRC1 est régulée *in vivo* par une phosphorylation dépendante du cycle cellulaire (*13*). Au cours de notre travail, nous avons montré par transfection de PRC1 ou de son mutant non phosphorylable, qu'à l'état non phosphorylée, PRC1 participe à l'assemblage latéral des microtubules de la zone centrale du fuseau pendant la cytodiérèse. Après transfection d'un ADN codant pour PRC1 dans les cellules HeLa, la présence non-physiologique de la protéine dans le cytoplasme génère un assemblage anormal des microtubules interphasiques (figure 3). En l'absence de l'activité kinase responsable de la phosphorylation de PRC1 en mitose, les microtubules cytoplasmiques apparaissent sous forme de pelotes compactes. En début de mitose, l'action des kinases dépendantes du cycle phosphoryle PRC1 qui n'est alors plus capable de réaliser cet assemblage. En fin de mitose, la perte de l'activité kinase induit la

formation de ces assemblages de microtubules qui participent alors au déroulement de la cytodiérèse (*14*). Pourtant, *in vitro*, PRC1 même après phosphorylation, reste capable de générer des faisceaux compacts par assemblage des microtubules formés par la tubuline purifiée (données non figurées). Il semble donc que la régulation de l'activité d'assemblage de PRC1 en fonction de son état de phosphorylation soit le résultat de l'interaction fonctionelle avec une ou plusieurs protéines spécifiques de la mitose. En collaboration avec Tony Hunter (Salk Institute, San Diego, USA), nous avons en effet montré que l'expression d'un mutant non-phosphorylable modifiait profondément l'aspect et la dynamique du fuseau en mitose, en formant des assemblages latéraux des microtubules du fuseau avant la transition métaphase-anaphase (*14*).

Afin de mieux comprendre l'origine de ces observations, nous avons entamé une étude des domaines

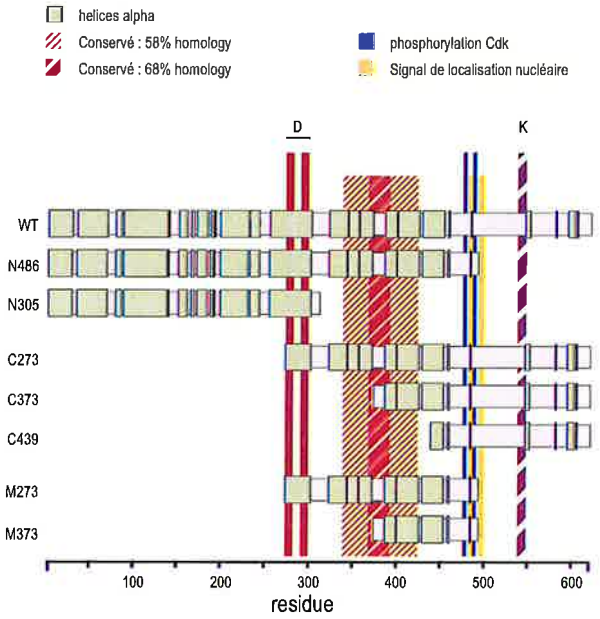

	Interphase		Mitose		
	Assemblage des MTs	Noyau*	Localisation aux MTs	Zone de clivage	Corps intermédiaire
WT	OUI	OUI	OUI	OUI	OUI
N486	OUI	NON	OUI	OUI	OUI
N305	NON	NON	NON	OUI	OUI
C273	OUI	OUI	OUI	OUI	OUI
C373	NON	OUI	NON	NON	NON
C439	NON	OUI	NON	NON	NON
M273	OUI	NON	OUI	NON	NON
M373	NON	OUI	NON	NON	NON

* Concentration spécifique

Figure 4: Constructions de PRC1 et propriétés des domaines de la protéine.
Le schéma représente les différentes constructions de PRC1 réalisées, et figure les régions d'intérêts. Les noms donnés aux différentes constructions N-terminales, C-terminales ou médianes, reprennent la position de la coupure par rapport au résidu correspondant de la séquence sauvage (WT). La séquence de PRC1 présente un signal de localisation nucléaire bipartite (jaune) accolé aux deux thréonines cibles de la phosphorylation dépendante du cycle cellulaire. Les régions D et K correspondent aux boites de destruction potentielles impliquées dans la dégradation spécifique de la protéine. Les zones hachurées correspondent aux régions les plus conservées des séquences homologues suivantes : AAC02688 et AAH05140 Homo sapiens; AAH05475 Mus musculus; AAF47965 et AAF47966 Drosophila melanogaster; CAC17794/17795/17796 Nicotiana tabacum; CAB82688 et BAB08676 Arabidopsis thaliana, après alignement multiple (ClustalW). Le tableau résume les propriétés principales observées après transfection dans les cellules de construction de ces différents mutants. Sont répertoriées les capacités des constructions de la protéine exogène à assembler les microtubules (MTs) du cytoplasme en interphase et de se localiser dans le noyau. En mitose, sont indiquées les capacités des constructions à se colocaliser avec les microtubules du fuseau, à se concentrer dans la zone de clivage ou dans la partie centrale du corps intermédiaire avant la séparation physique des cellules filles.

de PRC1. Nous avons ainsi cloné des mutants de délétion de la protéine que nous avons étudié à la fois *in cellulo* et *in vitro*, ce qui nous a permis de mettre en évidence des domaines distincts de la protéine, responsables de la liaison aux microtubules et de l'activité d'assemblage d'une part, et de la relocalisation sur le corps intermédiaire en fin de mitose d'autre part (figure 4). Nos données ne permettent pourtant pas de définir clairement la relation qui pourrait exister entre les sites de phosphorylation et la genèse des faisceaux de microtubules. En effet, tout les mutants qui sont correctement localisés sur les microtubules mitotiques sont aussi responsables de la formation de pelotes cytoplasmiques (*14*).

Structure du disque télophasique et cytodiérèse

Dans le cadre de cette étude de la protéine PRC1, réalisée par Dr. C. Mollinari, et maintenant en poste à Rome (Campus Bio-Medico Libera Università), nous avions proposé que PRC1 participe à la formation du disque télophasique en permettant l'assemblage latéral des microtubules interkinétochoriens (*14*). Nos

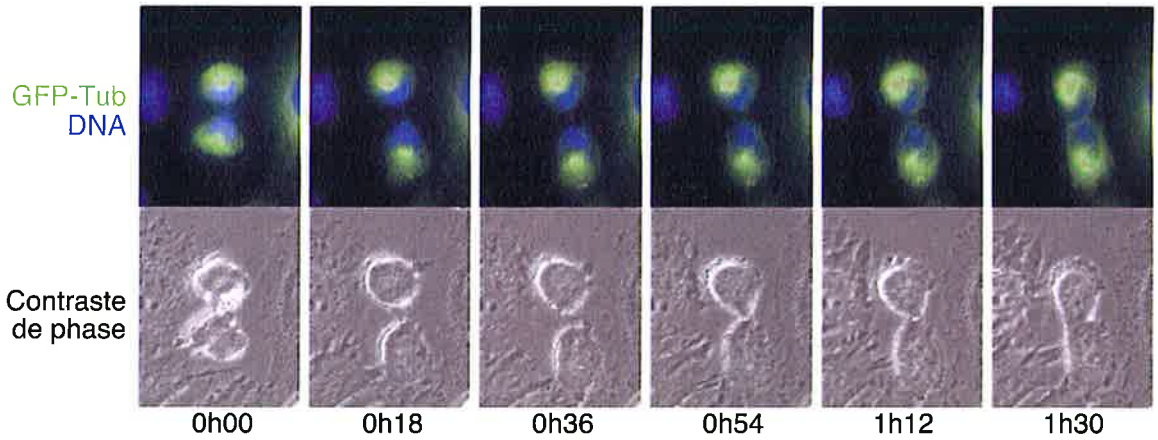

Figure 5: Séquence au cours du temps de l'évolution des cellules HeLa après suppression de PRC1 par interférence à l'ARN :
La galerie montre 6 clichés extraits d'un film couvrant 1h30 d'une cellules Hela traitée par RNAi contre PRC1, et montrant l'échec de la cytodiérèse. En haut, marquage de l'ADN par le Hoecsht 33342 (colorant vital, bleu), et GFP-tubuline (vert). En bas, images en contraste de phase correspondantes. La cellule est filmée depuis le début de la télophase (temps 0h00), et montre la formation d'un sillon de division marqué, en absence de microtubules entre les deux stocks chromosomiques. En fin d'aquisition, les deux cellules filles refusionnent pour former une cellule binucléées. Clichés obtenus sur la plateforme de vidéo-microscopie du laboratoire CS (DRDC, Grenoble, Y. Saoudi).

expériences récentes montrent que lorsque PRC1 est supprimé par interférence à l'ARN, les cellules ne parviennent plus à réaliser la cytodiérèse et deviennent binucléées. Dans ces conditions, la partie centrale du fuseau mitotique bien que désorganisée, reste cependant capable de recruter les protéines passagères impliquées dans les fonctions du disque télophasique, à l'exception notable de MKLP1 (Mitotic Kinesin Like Protein 1) qui disparaît de la zone centrale. MKLP1 fait partie d'un complexe, la centralspindline, qui serait

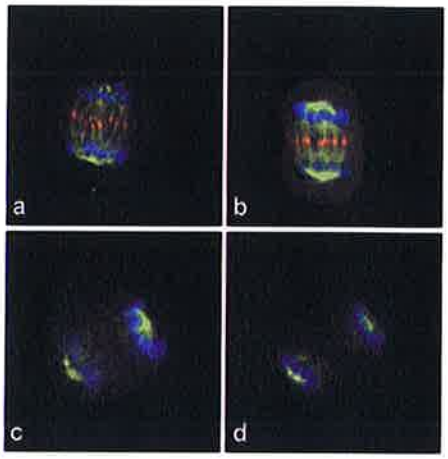

Figure 6: Images confocales des cellules HeLa contrôles ou après suppression de PRC1 par interférence à l'ARN :
Figures de mitose (a et c, anaphases; b et d, télophases) des cellules contrôles (a et b) ou essais (c et d) présentant un marquage triple après fixation. En vert la GFP-tubuline (GFP-tubuline stabilisée dans la lignée Hela), en bleu les chromosomes, et en rouge MgcRacGAP. Les cellules essais sans PRC1 présentent une profonde désorganisation de la partie centrale du fuseau, et perdent totalement la centralspindline, visualisée ici par le marquage de MgcRacGAP. Clichés C. Mollinari.

impliqué dans l'assemblage des microtubules lors du clivage des cellules filles (*24*). La disparition de MKLP1 pourrait ainsi expliquer l'échec en cytodiérèse des cellules dépourvues de PRC1.

Nous avons récemment utilisé les techniques de vidéo-microscopie (Laboratoire CS, DRDC) afin de suivre en temps réel l'évolution des cellules dépourvues de PRC1 (collaboration avec Dr S. Jablonski, Fox Chase Cancer Center, Philadelphie, USA). Nous avons constaté grâce aux séquences enregistrées, que les cellules restaient capables de former un sillon de division très marqué. Dans ces conditions pourtant, le pont cytoplasmique n'est jamais coupé, et les cellules filles refusionnent en fin de mitose pour former une cellule binucléée (figure 5). Ces données ne sont toutefois pas en accord avec les fonctions actuellement admises de la centralspindline. En effet, ce complexe formé de MKLP1 et de MgcRacGAP, un facteur d'activation de la petite GTPase Rac, homologue humain du facteur de la drosophile RotundRacGAP (*25*), est décrit comme permettant la mise en place de l'anneau contractile d'actino-myosine responsable de la constriction membranaire (*26*). En effet, une étude très récente montre que l'activité de MgcRacGAP est modifiée après phosphorylation par la protéine passagère Aurora B, et que MgcRacGAP modifie alors sa spécificité pour Rac1 en aquérant une spécificité d'activation de RhoA, une GTPase impliquée dans les fonctions de l'actine en mitose. Ces données suggèrent que la centralspindline serait un acteur majeur de la cytodiérèse en permettant les fonctions de l'anneau d'actine pendant le clivage (*27*). Nos données actuelles montrent que la suppression de PRC1 par interférence à l'ADN conduit également à la disparition de MgcRacGAP de la zone centrale du fuseau des cellules traitées (figure 6). Nos résultats suggèrent donc que l'absence de centralspindline n'empêche en rien la constriction liée au fonctionnement de l'anneau d'actine, mais bloque

seulement la coupure du pont cytoplasmique entre les cellules filles. Nos résultats mettent également en avant le rôle primordial des protéines du disque télophasique, et plus spécifiquement les protéines passagères, dans la formation de l'anneau d'actine cortical. Nous poursuivons actuellement ce travail afin de confirmer ces résultats originaux. Pour cela, nous allons vérifier la présence des autres acteurs de la constriction, en particulier l'anilline, une protéine qui intéragit avec l'actine et les septines lors de la formation de l'anneau d'actine responsable de la constriction membrannaire (*28*).

La protéine passagère TD-60

Au cours des 3 dernières années, nous avons identifié la séquence nucléotidique ainsi que la structure primaire de TD-60, une nouvelle protéine passagère. L'étude de ces protéines est un thème important du laboratoire. Nous travaillons depuis plusieurs années sur TD-60 et ses fonctions au sein du disque télophasique (*5, 29, 30*). Cette structure encore mal définie est formée dans la zone précise où a lieu le clivage des cellules filles, par l'association fonctionelle de protéines comme PRC1, MKLP1 mais aussi les protéines passagères. Le disque télophasique est ainsi considéré comme responsable de la localisation correcte, dans l'espace et dans le temps, de la constriction entre les deux futures cellules filles. Les protéines passagères, la survivine, Aurora B, INCENP et TD-60 se délocalisent pendant l'anaphase, des kinétochores vers le disque télophasique (figure 2 et référence *23*). INCENP, Aurora B et la survivine forment entre elles

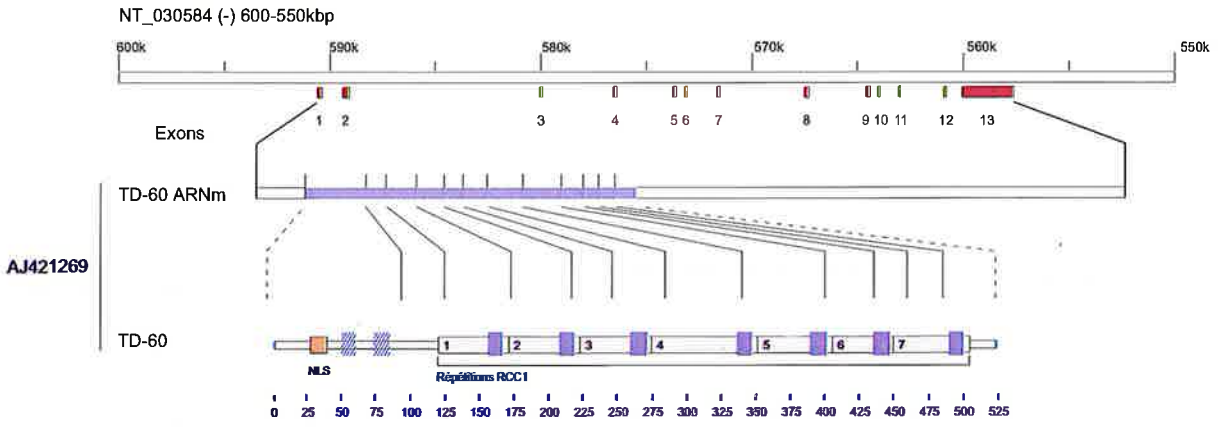

Figure 7: Représentation schématique de l'organisation du gène, de l'ARN messager et de la protéine TD-60.
Le gène codant pour la protéine TD-60 est présent dans l'entrée génomique NT_030584 correspondant au chromosome 1 humain. 13 exons (rectangles rouges) constituent la partie transcrite en ARNm, formant un transcrit de 4kb. La trame de lecture ouverte (rectangle bleu) est traduite en une protéine de 522 résidus. Cette séquence présente, dans sa région C-terminale, 7 régions analogues aux domaines RCC1 (rectangles verts 1-7). La partie N-terminale ne présente pas d'homologie connue en dehors d'un signal de localisation nucléaire potentiel (NLS) et de 2 signatures de type RCC1 dans un contexte différent des domaines RCC1 classiques (PROSITE RCC1-2). Les séquences ARN et protéiques sont déposés à GenBank (AJ421269).

un complexe dont la fonction est essentielle dans la progression en mitose. L'un de ses composants, Aurora B est une kinase dont l'activité semble avoir un rôle déterminant. Il a été montré récemment que son activité kinase pourrait être régulée par la formation du complexe formé par les protéines passagères (*31*). En outre, l'activité kinase d'Aurora B phosphoryle spécifiquement MgcRacGAP, le partenaire de MKLP1 dans la centralspindline, et cette phosphorylation régule la fonction de MgcRacGAP durant la cytodiérèse (*27*).

Clonage et caractérisation de TD-60

En collaboration avec Jérôme Garin (DRDC, CP), nous avons obtenu dès fin 1999 des séquences partielles de fragments de TD-60 par spectrométrie de masse en mode tandem. Ces séquences ont permis d'identifier rapidement une trame de lecture ouverte présente dans un ensemble d'entrées EST correspondant à une protéine potentielle de 60 kDa. Cette trame de lecture est également retrouvée dans un large fragment génomique humain issu de la base HTGs (NT_030584). Le gène est présent au locus 1p36.13 du chromosome 1 humain (figure 7).

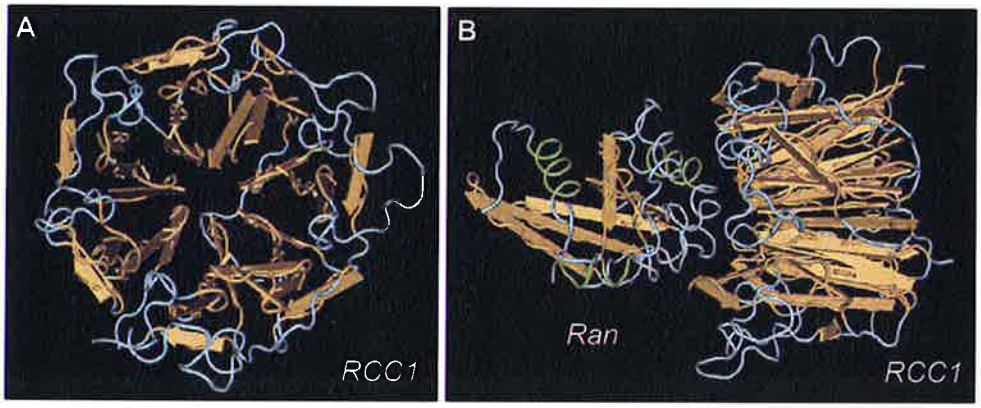

Figure 8 : Représentation des données cristallographiques de RCC1.
Structure cristallographique (1,7Å) de RCC1 (A) et du complexe Ran-RCC1 (B) d'après l'entrée PDB 1I2M. Les brins sont figurés par les flèches brunes, les hélices en vert, et les boucles en bleu. On peut noter la structure « tout β» de RCC1, formée par la répétition de 7 domaines formant un tonneau. L'interaction avec Ran se fait par des résidus situés sur l'entrée du tonneau. Représentation obtenue par le logiciel Cn3D à partir des coordonnées PDB.

L'analyse de la séquence de TD-60 que j'ai déposé à GenBank (AJ421269), montre que la protéine clonée est un nouvel analogue de RCC1, une protéine impliquée dans l'importation nucléaire (*32*). La structure de RCC1 est formé par la répétition de 7 domaines RCC1, et forme un anneau riche en feuillets β. Ces 7 domaines sont conservés dans TD-60, ce qui suggère que son repliement serait proche de la structure tertiaire de RCC1 (figure 8). RCC1 agit comme un facteur d'échange (GEF) pour une petite GTPase de la famille Ras-like, Ran. Récemment, il a été montré que Ran est impliquée dans la régulation de la formation des microtubules du fuseau mitotique (*33*). Par analogie, cela nous a conduit à proposer un rôle en mitose pour TD-60 de type facteur d'échange.

TD-60 est-elle un facteur d'échange ?

En collaboration avec Bruno Goud de l'institut Curie (Paris), nous avons réalisé une étude de l'affinité de la protéine TD-60 pour les différentes GTPases monomériques représentatives de la famille Ras-like; Ran, Rab6, Rac1, RhoA et cdc42. Nous avons montré par double-hybride que seule Rac1 présentait une affinité potentielle pour TD-60. Ce résultat était inattendu car les facteurs d'échange des protéines de la famille Rac1 sont très différents de RCC1, l'analogue de TD-60. Nous avons confirmé ces résultats par l'étude de l'interaction de ces protéines *in vitro* (*8*). Ces dernières expériences montrent que TD-60 possède une affinité préférentielle pour la forme sans nucléotide de Rac1 (figure 9), une propriété caractéristique des

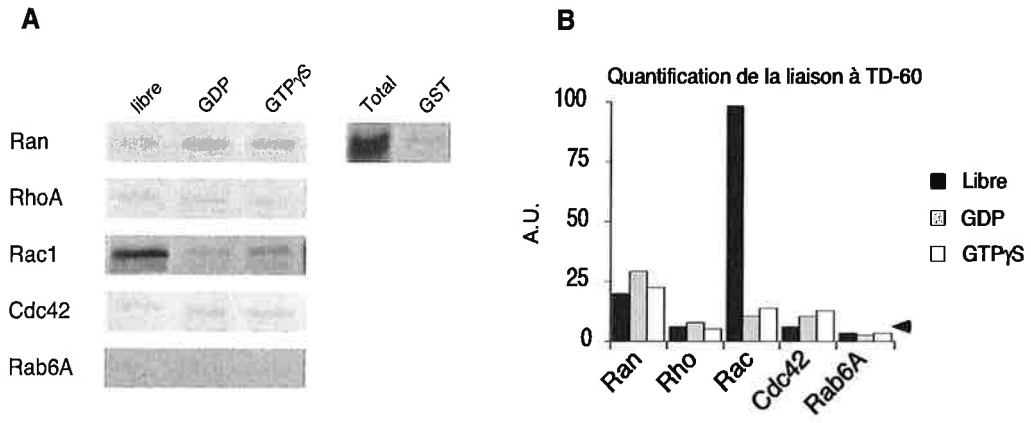

Figure 9 : Liaison de TD-60 aux différentes GTPases :
A) La protéine TD-60 produite par traduction in vitro est testée pour sa liaison aux différentes GTPases chargées en présence de GDP, GTP non hydrolysable, ou sans nucléotide, dans un test «GST pull-down». Les fractions retenues sont analysées par autoradiographie sur gel. L'encart présente le taux basal de liaison sur la GST seule. B) quantification par phosphoimager des autoradiographies présentées en A. La liaison à Rac1 sans nucléotide est spécifiquement supérieure à celles obtenues sur les autres GTPases ou en présence de Rac1 chargée par les nucléotides. Le taux basal est représenté par une pointe de flèche.

GEFs. Cela suggère que TD-60 est en effet une GEF spécifique de Rac1, et que Rac1 pourrait avoir un rôle jusqu'alors non décrit dans la progression en mitose.

Actuellement, nous débutons l'étude des domaines fonctionnels de TD-60. La partie correspondant aux répétitions RCC1 a été cloné dans un vecteur double-hybride. Les résultats préliminaires indiquent que c'est bien ce domaine qui est responsable de l'interaction spécifique de TD-60 avec Rac1. Nous souhaitons maintenant exprimer et purifier cette région de la protéine à partir d'un système de surexpression bactérien afin d'en réaliser une étude biochimique complète. En outre, l'étude structurale de cette protéine sera entreprise par diffraction des rayons X après cristallisation. cette protéine purifiée pourra être cristallisée soit seule, soit en complexe avec Rac1. Par comparaison avec la structure connue de RCC1 avec Ran (Figure 9B et référence *34*), l'analyse de la structure du complexe permettra alors de mieux comprendre l'origine de la grande spécificité de TD-60 pour Rac1.

TD-60 est indispensable à la formation d'un kinétochore fonctionnel

La suppression de TD-60 par interférence à l'ARN a été réalisé au laboratoire par le Dr C. Reynaud. Ses expériences montrent que l'absence de TD-60 provoque un blocage des cellules en amont de la métaphase (prométaphase), avec une désorganisation profonde des kinétochores, entraînant la perte de l'attachement des microtubules du fuseau (figure 10). La métaphase correspond à l'étape de la division cellulaire où les chromosomes, à l'aide du fuseau mitotique, s'alignent à l'équateur de la cellule. Pour cela, les microtubules s'associent aux kinétochores, et permettent le mouvement des chromosomes. Le kinétochore est alors le siège de nombreuses régulations liées au fonctionnement des protéines du point de contrôle. L'activité de ces dernières permet la blocage du cycle des cellules tant que l'alignement des chromosomes n'est pas achevé, afin que les stocks chromosomiques des futures cellules filles soient rigoureusement identiques (*35*). Nous avons ainsi pu montrer que, contrairement aux autres protéines passagères dont l'absence engendre une levée du point de contrôle mitotique, la suppression de TD-60 bloque indéfiniment les cellules en prométaphase, en inhibant l'association des microtubules aux kinétochores. Les dérégulations du fonctionnement des kinétochores sont en particulier responsables de très nombreux cas de cancers (*36*). La participation de TD-60 dans ces fonctions kinétochoriennes et son rôle de facteur d'échange potentiel de Rac1 ouvre de nombreuses pistes pour la poursuite de ces travaux.

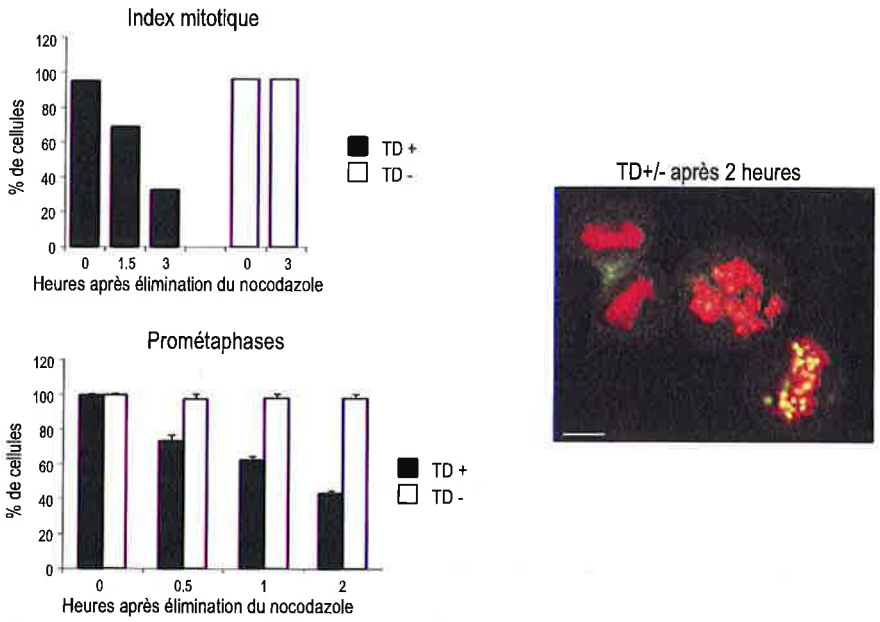

Figure 10 : Les cellules HeLa dépourvues de TD-60 après RNAi sont bloquées en prométaphase :
Les cellules HeLa traitées par interférence à l'ARN spécifique de TD-60 ont été bloquées au nocodazole (synchronisation des cellules en prophase). Après élimination du nocodazole, le nombre de cellule en mitose dans les expériences témoins (présence de TD-60 : TD+) et essais (TD-) est rapporté au nombre total de cellules dans l'échantillon (haut). L'index mitotique ainsi mesuré montre que les cellules dépourvues de TD-60 sont bloquées en mitose. En bas, parmi les cellules en mitose, on peut distinguer les cellules en prométaphase. Si ce nombre décroit régulièrement dans les cellules témoins, le nombre de prométaphases reste constant dans les cellules dépourvues de TD-60. A droite, image typique d'un champ observé 2 heures après le élimination du nocodazole. On observe une cellule négative pour TD-60 (TD-) en prométaphase, et deux cellules positives pour TD-60 (TD+) en télophase (à gauche) ou en métaphase (à droite). Le marquage TD-60 apparait en vert; le marquage de l'ADN est en rouge. Echelle : 10µm.

Perspectives expérimentales

L'étude biochimique et structurale de TD-60 est un des projets que je souhaite approfondir. Je dirige actuellement un étudiant de Master II sur ce sujet. Ce projet met également en jeu une collaboration avec le groupe de Stefan Dimitrov à l'Institut Albert Bonniot de Grenoble (Clonage de l'orthologue de xénope). Ces travaux constituent une étape primordiale dans l'étude de cette nouvelle protéine, avec en particulier la création des outils pour l'étude de son activité "facteur d'échange" (collaboration avec B. Goud, Institut Curie, Paris), ainsi que l'étude structurale par cristallisation sous forme native ou en complexe avec la petite GTPase Rac1 par exemple (J. Fontecilla, LCCP, IBS). Ce travail nous amène à étudier séparément les deux domaines de la protéine, d'une part la partie N-terminale (120 résidus) comprenant notamment un signal de localisation nucléaire potentiel, et la partie C-terminale constituée par les 7 répétitions caractéristiques du domaine RCC1. Nous nous intéresserons aux ligands protéiques de ce domaine, y compris les petites GTPases, dans le cadre de la caractérisation biochimique de l'activité GEF. Les résidus responsables de la spécificité de RCC1 pour Ran sont connus. Ces résidus sont différents dans TD-60, et nous nous attacherons à caractériser l'importance de ces variations dans la spécificité de TD-60 pour Rac1.

En outre, nous souhaitons caractériser les protéines associées aux différents domaines de TD-60, ainsi que leurs interactions dans la structuration du macro-complexe protéique qu'est le kinétochore fonctionnel. L'effort sera fait en particulier sur l'identification des relations avec les autres protéines passagères, Aurora B par exemple, une kinase dont l'activité pourrait modifier TD-60, et ainsi réguler ses fonctions. Un site potentiel de phosphorylation par Aurora B est en effet présent dans hTD-60 (*Homo sapiens*) et conservé dans xTD-60 (*Xenopus laevis*), mais absent de RCC1. Dans ce dernier exemple, la production de la protéine nous permettra de débuter l'étude des sites de phosphorylation au niveau biochimique, ainsi que leurs implications dans les fonctions de TD-60 *in cellulo*. Un autre partenaire potentiel de TD-60 dans le kinétochore pourrait être CENP-A. Cette protéine analogue à l'histone H3 est un constituant spécifique des centromères, où il remplace H3 dans les nucléosomes de cette région du chromosome. RCC1 est quant à elle associée à la chromatine par l'intermédiaire des histones H2A et H2B, suggérant qu'une interaction de TD-60 avec CENP-A, si elle était démontrée, pourrait rendre compte de la localisation spécifique de TD-60 aux centromères.

Chapitre II : Dynamique des microtubules : Etude de la protéine F-STOP

La question biologique fondamentale que nous souhaitons aborder concerne la compréhension des mécanismes de régulation de la dynamique des assemblages microtubulaires. STOP est un modèle d'étude bien adapté pour mieux comprendre, au niveau moléculaire, les interactions multiples des microtubules avec leurs effecteurs directs et indirects (Pour une revue récente voir *19*). En effet, la protéine STOP semble être directement impliquée dans la dynamique des microtubules du fuseau mitotique, et contrôlée par un des effecteurs de la transduction du signal : la calmoduline. STOP pourrait donc être au centre d'une régulation dépendant non seulement du cycle cellulaire, mais aussi des voies de signalisation.

La protéine F-STOP est la forme d'épissage alternatif non-neuronale de N-STOP, une protéine associée aux microtubules stables des axones (*18, 37, 38*). La structure du gène murin décrite récemment montre que le promoteur permettant la transcription de F-STOP réside dans le premier exon des isoformes longues tel N-STOP (*39*). STOP est capable de stabiliser *in vitro* les microtubules au froid ou à la dilution, ainsi qu'en

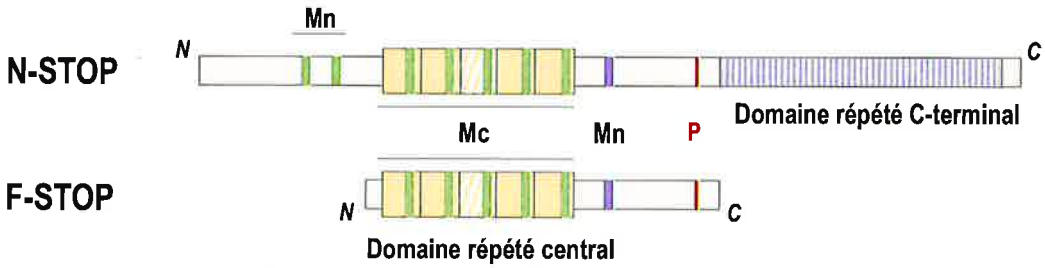

Figure 11: représentation des isoformes N et F-STOP.
Sont figurés le domaine central formé de répétitions comprenant le motif Mc (vert), ainsi que les domaines amino et carboxy-terminaux des deux protéines. On notera la présence d'un domaine C-terminal caractéristique de la forme N (neuronale), ainsi que la présence de motifs Mn (bleu) de liaison à la calmoduline et aux microtubules dans les régions flanquant le domaine central. Le site noté P (rouge) correspond au site de phosphorylation par la PKG. Ce site est présent sur toutes les isoformes de STOP.

présence de calcium ou des actifs dépolymérisants les microtubules comme le nocodazole (*40, 41*). Dans le cas de la forme F-STOP, cette capacité à stabiliser les microtubules pourrait être liée à sa fonction, puisque F-STOP s'associe physiologiquement avec certains des microtubules du fuseau mitotique (les microtubules du pôle aux kinétochores) mais pas avec les microtubules cytoplasmiques pendant l'interphase (*16*). Au cours de la mitose, la calmoduline, un inhibiteur de la stabilisation par STOP des microtubules, est présente sur le fuseau mitotique (*20*), ce qui suggère que ces deux acteurs pourraient faire partie d'une même voie de contrôle ou de signalisation au cours de la division cellulaire.

Liaison STOP-Calmoduline

La calmoduline (CAM) est un ligand des STOPs. Cette liaison étant encore très mal connue il y a peu, j'ai initié une étude structurale afin de caractériser la formation de ce complexe (partenariat avec le LRMN). À ces fins, nous avons utilisé le clone VU-1 de calmoduline synthétique qui nous a été donné par D.M. Watterson (*42*). Les sites de liaison de la calmoduline sur STOP ont été récemment définis dans une étude exhaustive utilisant une cartographie d'interaction sur une série de peptides chevauchants issu de la séquence primaire (*43*). Cette étude montre en particulier que deux motifs distincts de STOP (Motifs Mc et Mn, voir figure 11) possèdent à la fois la capacité de lier la calmoduline et de participer à la stabilisation des microtubules. Les motifs Mc seraient impliqués dans la résistance des microtubules au froid, alors que les motifs Mn participeraient à la résistance des microtubules au actifs dépolymérisant, en particulier le nocodazole (*43*). Notre modèle d'étude est basé sur un peptide de synthèse modèle d'une des 5 répétitions de la région centrale répétée de STOP (motif "Mc", figure 11). Afin de caractériser cette liaison au niveau structural, une étude par diverses techniques d'analyse, en particulier RMN, a été menée par Denis Bouvier, étudiant en thèse (3ème année, financement CFR du CEA), sous la co-direction de Pierre Gans (LRMN), et de moi-même. Ce projet commun à nos deux laboratoires, implique également une chercheuse post-doctorale, Dr Cécile Vanhaverbeke (contrat CEA).

Nous avons en particulier montré que la liaison de ce peptide de STOP était inhabituelle pour les ligands calcium-dépendants de la calmoduline. En effet, les résultats que nous avons obtenus montrent que la liaison est restreinte à la partie C-terminale de la calmoduline, qui reste alors dans une conformation étendue. Expérimentalement, la liaison du peptide à la calmoduline a été suivie par des mesures de fluorescence intrinsèque du tryptophane. Ce résidu présent uniquement dans le peptide était une sonde de choix pour suivre les modifications d'environnement engendrées par la liaison du peptide à la calmoduline calcique. Cette technique nous a permis de montrer que la liaison était à la fois spécifique de la présence de calcium, et sensible à la force ionique, ce qui n'est pas le cas des ligands classiques de la calmoduline. L'utilisation d'une sonde extrinsèque (Dansyl), a permis de montrer que le domaine C-terminal de la calmoduline pouvait se substituer à la calmoduline entière dans la liaison du peptide Mc. Ces données ont ainsi permis

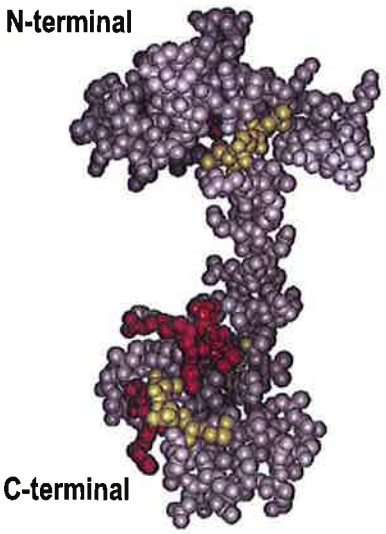

Figure 12: Modèle des régions modifiées de la calmoduline en présence du peptide "Mc" de STOP.
Les variations des déplacements chimiques observés par RMN ont été reportés selon leurs intensités croissantes (du jaune vers le rouge) sur la structure de la calmoduline.

de confirmer les résultats obtenus par résonance magnétique nucléaire, et qui montrent que la majorité des résidus de la calmoduline affectés par la liaison au peptide sont situés dans la partie C-terminale de la protéine (figure 12). Des données récentes de la littérature montrent l'existence d'autres cas inhabituels de liaison entre la calmoduline calcique et ses ligands (*44-46*), et nos résultats renforcent donc l'importance de ces modes alternatifs de liaison à la calmoduline dans les régulations cellulaires. Les résultats obtenus ont donné lieu récemment à une publication (*21*).

Nous avons maintenant débuté une étude structurale plus approfondie de la liaison calmoduline-STOP. L'un des aspect est l'attribution complète de la structure de la calmoduline dans le complexe formé, ainsi que la comparaison de cette structure avec celle décrite pour le peptide homologue de MARCKS (*44, 45*). Ce dernier peptide est un modèle pour l'étude de la liaison de la protéine MARCKS à la calmoduline calcique, interaction impliquant là aussi essentiellement le domaine C-terminal de la calmoduline. A ces fins, Cécile Vanhaverbeke a réalisé les spectres RMN du complexe de la calmoduline avec le motif Mc de STOP, afin d'en déduire la mobilité relative des parties N et C-terminales l'une par rapport à l'autre. En parallèle, l'étude de la forme globale du complexe calmoduline-peptide par diffusion des rayons X aux petits angles (SAXS) a été initié (collaboration avec Stéphanie Finet; ESRF). Les données préliminaires obtenues indiquent que la calmoduline liée au module Mc conserve une conformation étendue très proche de celle de la calmoduline calcique.

Phosphorylation de STOP

Dans le cadre d'une collaboration avec le laboratoire de Phil Robinson (CMRI, Sydney Australie) , nous avons démontré que les protéines STOP possédaient toutes un site de phosphorylation spécifique par la kinase dépendante du cGMP (PKG). La PKG est une kinase ubiquitaire. Dans les neurones, l'activité de la PKG est en particulier liée aux phénomènes de plasticité synaptique ou de « long term potentiation » (LTP) et de « long term depotentiation » (LTD) (*47*). Ces phénomènes sont largement impliqués dans un dysfonctionnement nerveux conduisant à la schizophrénie humaine. Il est intéressant de noter qu'Annie

$_{282}$D R R R I R [S] L Y S E P $_{293}$

Figure 13: Phosphorylation spécifique de F-STOP par la PKG.
Autoradiographie des protéines recombinantes F-STOP et de ses mutants de la sérine cible 288 par une alanine (S288A) ou par un acide glutamique (S288E) après phosphorylation *in vitro* en présence d'ATP radiomarqué et de PKA ou de PKG. Deux expériences indépendantes sont représentées. La sérine phosphorylée est indiquée par un cadre dans la séquence protéique correspondante de F-STOP.

Andrieux (DRDC, CS) a montré récemment que la suppression de STOP chez les souris, conduisait à un comportement assimilable à la schizophrénie, associé à des perturbations importantes de la LTP et de la LTD (*48*). Notre étude a permis de démontrer que les isoformes de STOP sont des substrats spécifiques de la PKG. Nous avons identifié par séquençage et par spectrométrie de masse (MALDI-TOF), le résidu sérine de STOP phosphorylé en présence de PKG (figure 13). Nous avons également montré que la phosphorylation PKG-dépendante de STOP est inhibée par la calmoduline (figure 14), ce qui suggère que la liaison STOP-calmoduline pourrait être responsable de l'inhibition observée. Ces données sont actuellement en préparation pour publication (*49*).

Figure 14: Phosphorylation de F-STOP par la PKG en présence de calcium-calmoduline.
La protéine F-STOP recombinante (0,5µg par essai) est phosphorylée en présence de PKG et d'ATP radiomarqué après préincubation de concentration croissantes de calmoduline (0 à 60 µg/mL) en présence ou en absence de 200µM calcium. Les protéines ainsi traitées sont séparés par electrophorèse et soumises à une autoradiographie. La flèche indique la position de la protéine F-STOP.

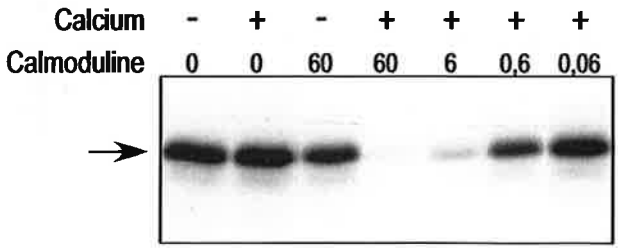

Perspectives expérimentales

L'ensemble des résultats que nous avons obtenus, et les données de la littérature suggèrent donc un lien important entre la régulation potentielle de STOP par la PKG et la liaison à la calmoduline. Une partie importante du travail à venir est maintenant de comprendre comment la liaison à la calmoduline peut modifier la capacité de STOP à être phosphorylé par la PKG sur un résidu très éloigné des motifs Mc ou Mn. Nous avons ainsi débuté l'étude de la liaison entre la calmoduline calcique et un peptide issu du motif Mn de F-STOP (voir figure 11). Les résultats préliminaires indiquent que le motif Mn lierai la calmoduline de manière similaire à celle que nous avons décrites pour le motif Mc. Si la protéine F-STOP paraît largement déstructurée en solution (données non publiées), la partie C-terminale comprenant le motif Mn, pourrait présenter une structure tertiaire en présence de calmoduline. Ces possibilités sont actuellement en cours d'étude par Denis Bouvier et Cécile Vanhaverbeke sous ma responsabilité (manuscrit en préparation).

Nous souhaitons également comprendre quel est l'effet physiologique de cette phosphorylation sur l'activité de STOP. Je suis ainsi allé mettre en place à Sydney (CMRI; novembre 2001) les outils permettant de tester l'influence de la phosphorylation sur la capacité de STOP à se lier ou à stabiliser les microtubules. Les résultats obtenus *in vitro* sur des protéines purifiées, indiquent que les caractéristiques du comportement de STOP vis-à-vis des microtubules ne sont pas altérées par la phosphorylation de manière directe. Toutefois, la phosphorylation d'extraits synaptiques par la PKG montre une délocalisation de la protéine phosphorylée de la fraction liée aux membranes (et aux microtubules) vers la fraction soluble (figure 15). Nous pensons qu'*in*

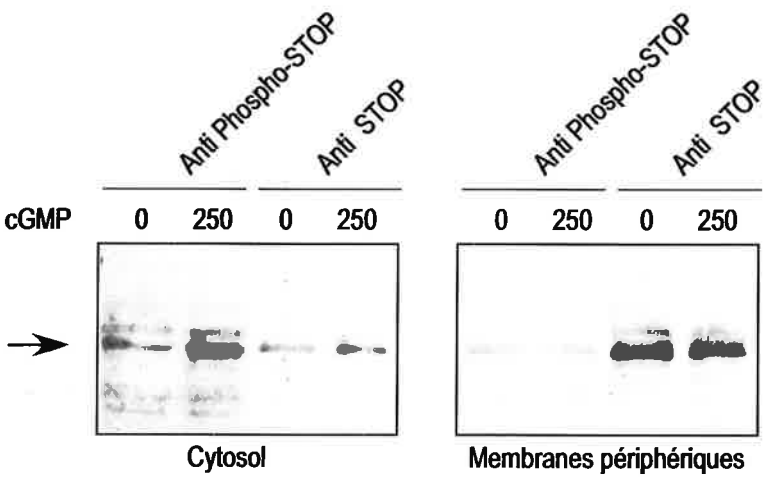

Figure 15: La phosphorylation de STOP par la PKG dans les extraits de synaptosomes.
Les extraits membranaires (membranes périphériques) ou solubles (cytosol) de synaptosomes stimulés ou non par 250µM de 8-pCPT-cGMP, sont séparés par électrophorèse puis transférés avant d'être immunocolorés par les anticorps spécifique de la STOP ou de la séquence phosphorylée de STOP. Les immunotransferts montrent que si la grande majorité de la protéine STOP reste associée à la fraction membranaire, la forme phosphorylée est spécifiquement relarguée dans la fraction soluble après activation de l'activité kinase de la PKG.

vivo, l'inhibition de la phosphorylation par la CAM permet la localisation de STOP sur les microtubules du fuseau mitotique. Afin de confirmer ces hypothèses, j'ai construit des mutants de F-STOP où la sérine cible est mutée soit en acide glutamique (mimant la phosphorylation) soit en alanine (mutant non-phosphorylable). Ces constructions pourront être exprimées après transfection de cellules de mammifère en présence ou en absence de constructions fluorescentes (GFP) de la calmoduline et de son mutant C-terminal, afin d'étudier les mécanismes physiologiques des fonctions de STOP au cours de la mitose par microscopie confocale ou résolue dans le temps.

A plus long terme, ce programme sera rapproché des études auxquelles je participe par ailleurs au laboratoire (Cf. chapitre I), en particulier l'étude des protéines du kinétochore, la structure qui permet la liaison mécanique et fonctionnelle des microtubules aux chromosomes au cours de la mitose. Dans un premier temps, nous chercherons à identifier par "pull-down" les partenaires de STOP sous ses formes mutées pour la phosphorylation en présence ou en absence de calmoduline. L'identification des partenaires fonctionnels et structuraux de STOP au cours de la mitose permettra de mettre en place comme nous l'avons déjà fait pour le complexe STOP-calmoduline, un programme de biologie structurale portant sur les éventuels partenaires identifiés. Le fait que la calmoduline interagisse avec la protéine STOP par sa seule partie C-terminale conduit à faire l'hypothèse qu'un troisième partenaire pourrait en effet s'associer avec le complexe STOP-calmoduline.

Tirés à part

Page 33:
Chantalat, L., Skoufias, D. A., Kleman, J. P., Jung, B., Dideberg, O., et Margolis, R. L. **2000** Crystal structure of human survivin reveals a bow tie-shaped dimer with two unusual alpha-helical extensions, Mol Cell 6, 183-189.

Page 41:
Mollinari, C., Kleman, J. P., Jiang, W., Schoehn, G., Hunter, T., et Margolis, R. L. **2002** PRC1 is a microtubule binding and bundling protein essential to maintain the mitotic spindle midzone, J Cell Biol 157, 1175-1186.

Page 53:
Mollinari, C., Reynaud, C., Martineau-Thuillier, S., Monier, S., Kieffer, S., Garin, J., Andreassen, P. R., Boulet, A., Goud, B., Kleman, J. P., et Margolis, R. L. **2003** The Mammalian Passenger Protein TD-60 Is an RCC1 Family Member with an Essential Role in Prometaphase to Metaphase Progression, Dev Cell 5(2), 295-307.

Page 67:
Bouvier, D., Vanhaverbeke, C., Simorre, J. P., Arlaud, G. J., Bally, I., Forge, V., Margolis, R. L., Gans, P., et Kleman, J. P. **2003** Unusual Ca(2+)-Calmodulin Binding Interactions of the Microtubule-Associated Protein F-STOP, *Biochemistry 42*, 11484-11493

JCB Article

PRC1 is a microtubule binding and bundling protein essential to maintain the mitotic spindle midzone

Cristiana Mollinari,[1] Jean-Philippe Kleman,[1] Wei Jiang,[2] Guy Schoehn,[3] Tony Hunter,[4] and Robert L. Margolis[1]

[1]Institut de Biologie Structurale J-P Ebel (CEA-CNRS), 38027 Grenoble cedex 1, France
[2]Department of Biochemistry, New York University Medical Center, New York, NY 10016
[3]EMBL Grenoble Outstation, 38042 Grenoble cedex, France
[4]The Salk Institute, La Jolla, CA 92037

Midzone microtubules of mammalian cells play an essential role in the induction of cell cleavage, serving as a platform for a number of proteins that play a part in cytokinesis. We demonstrate that PRC1, a mitotic spindle-associated Cdk substrate that is essential to cell cleavage, is a microtubule binding and bundling protein both in vivo and in vitro. Overexpression of PRC1 extensively bundles interphase microtubules, but does not affect early mitotic spindle organization. PRC1 contains two Cdk phosphorylation motifs, and phosphorylation is possibly important to mitotic suppression of bundling, as a Cdk phosphorylation-null mutant causes extensive bundling of the prometaphase spindle. Complete suppression of PRC1 by siRNA causes failure of microtubule interdigitation between half spindles and the absence of a spindle midzone. Truncation mutants demonstrate that the NH_2-terminal region of PRC1, rich in α-helical sequence, is important for localization to the cleavage furrow and to the center of the midbody, whereas the central region, with the highest sequence homology between species, is required for microtubule binding and bundling activity. We conclude that PRC1 is a microtubule-associated protein required to maintain the spindle midzone, and that distinct functions are associated with modular elements of the primary sequence.

Introduction

Mitosis is a highly regulated process characterized by dramatic and coordinated morphological changes to ensure the fidelity of chromosome segregation. Cytokinesis occurs at the final stage of mitosis and is accomplished by the contraction of an acto-myosin ring that leads to daughter cell separation at the midbody (Cao and Wang, 1990). A number of proteins accumulate at the midzone of the mammalian mitotic spindle during late mitosis and have been shown to play a role in cell cleavage by antibody suppression, overexpression, or mutagenesis. Among these proteins are passenger proteins such as INCENP (Mackay et al., 1998) and survivin (Skoufias et al., 2000; Uren et al., 2000); protein kinases such as polo (Lee et al., 1995) and aurora B (Terada et al., 1998); small G-proteins such as Rho (Takada et al., 1996; Drechsel et al., 1997; O'Connell et al., 1999); and microtubule motor proteins such as CENP-E (Yen et al., 1992; Martineau-Thuillier et al., 1998), Rab6-KIFL (Hill et al., 2000), and MKLP1 (Sellitto and Kuriyama, 1988; Nislow et al., 1992). Some interactions among these proteins have been established, but specifically defined functional roles in the cleavage process are still largely unknown. Another protein that accumulates in the spindle midzone and that has a demonstrated role in sustaining cell cleavage, PRC1, has been recently described (Jiang et al., 1998). As is true of most of the other midzone proteins, the precise role of PRC1 in the cleavage process is unknown.

In late anaphase, a central mitotic spindle forms between the two separating sets of chromatids. It consists of a dense network of overlapping antiparallel microtubules (MTs)*. (Mastronarde et al., 1993). The central spindle, the site of accumulation of numerous proteins required for cell cleavage (Glotzer, 1997; Robinson and Spudich, 2000), has been demonstrated to be critical to the completion of cytokinesis (Cao and Wang, 1996; Wheatley and Wang, 1996). This is the only time in the cell cycle that a typical mammalian culture cell generates stable and bundled MTs. The molecular basis for maintenance of the midzone MT bundle is unresolved.

Address correspondence to Robert L. Margolis, Institut de Biologie Structurale J-P Ebel (CEA-CNRS), 41 rue Jules Horowitz, 38027 Grenoble cedex 1, France. Tel.: 33-43-878-9616. Fax: 33-43-878-5494. E-mail: margolis@ibs.fr

Key words: mitosis; Cdk; cytokinesis; microtubule-associated protein; cytoskeleton

*Abbreviations used in this paper: EGFP, enhanced green fluorescent protein; MT, microtubule; NLS, nuclear localization signal; siRNA, short interfering RNA; UTR, untranslated region.

The Journal of Cell Biology, Volume 157, Number 7, June 24, 2002 1175–1186
http://www.jcb.org/cgi/doi/10.1083/jcb.200111052

Here we show that PRC1 is required to maintain a stable midzone MT bundle. It is an MT binding and bundling protein in vitro, and it forms extensive MT interphase bundles when overexpressed in mammalian cells. In keeping with these results, introduction of short interfering RNAs (siRNAs) targeting PRC1 profoundly disrupts the formation of the midzone bundle and blocks cytokinesis. The effect of siRNA occurs uniquely during cell cleavage, showing PRC1 is required to maintain interdigitation between the two half spindles during anaphase.

PRC1 has an evident domain structure. The NH_2-terminal region of the protein is largely α-helical with multiple predicted coiled-coil motifs, whereas the COOH-terminal one quarter is predicted to be largely composed of β sheets and turns. Truncation mutants show that PRC1 appears to be modular. The NH_2-terminal half of the protein is required for its association with the cleavage furrow and midbody, whereas sequence within residues 273–486 is required for MT binding. Microinjection of antibody that recognizes the COOH terminus of PRC1 disrupts the function of midzone MT bundles and blocks cleavage, showing the conformation of the COOH terminus may be important to the protein's function. On the basis of our results, we conclude that the function of PRC1 is necessary for spindle integrity during late mitosis, particularly to maintain the midzone MT bundles that are essential for the completion of cell cleavage.

Results

Overexpression of PRC1 modifies the MT array in HeLa cells

PRC1 is a mitotic spindle-associated protein that is required for cytokinesis in mammalian cells (Jiang et al., 1998). Sequence analysis shows that the NH_2-terminal three quarters of the protein is largely α-helical (see Fig. 5 A) with predicted coiled-coil motifs (Fig. 1 B), whereas the COOH-terminal region is predicted to be largely composed of β-sheets and turns. At the junction between these two distinct regions there is a cluster of two Cdk phosphorylation sites, two nuclear localization motifs, and two D boxes and a Ken box (see Fig. 5 A).

In accord with previous findings (Jiang et al., 1998), native PRC1 is intranuclear in interphase (Fig. 1 A, a), and then associates with the spindle in early mitosis, being more enriched on the interdigitating MTs, and finally to the spindle midzone in late mitosis (Fig. 1 A, b and c). We have compared the distribution of PRC1 with that of TD-60, a passenger protein that localizes to the spindle midzone in late mitosis (Andreassen et al., 1991). Double immunofluorescence staining with autoimmune antiserum recognizing TD-60 and with polyclonal anti-PRC1 showed that TD-60 and PRC1 distributed to the kinetochores, and to the entire spindle, respectively, at the beginning of mitosis (Fig. 1 A, d), and then colocalized in the spindle midzone in early telophase, and to the midbody at the end of mitosis (Fig. 1 A, e and f). It is interesting to note that although both proteins are found in the midbody, PRC1 is always at the center of the intercellular bridge, in the so-called Flemming body region (Zeitlin and Sullivan, 2001), compared with the broader TD-60 distribution (Fig. 1 f). The polyclonal anti-PRC1 serum recognizes only one protein in whole-cell extracts, with the predicted mass of PRC1 (Fig. 1 C, right).

For functional analysis, we began by constructing several plasmids to express wild-type and mutant PRC1 (Fig. 1 B), including a full-length cDNA chimera with NH_2-terminal enhanced green fluorescent protein (EGFP), and a chimera with COOH-terminal EGFP. Both the $PRC1^{AA}$ mutant and $PRC1^{EE}$ mutant in which the two threonine Cdk phosphorylation sites were mutated, respectively, to alanine (T470A; T481A) or to glutamic acid (T470E; T481E), were expressed as either NH_2- or COOH-terminal EGFP chimeras. The COOH-terminal EGFP constructs have been truncated by 35 amino acids at the COOH terminus, without apparent effect on PRC1 function or localization.

The polyclonal antiserum recognizes the extreme COOH terminus of PRC1 (Jiang et al., 1998), and thus reveals overexpression of the NH_2-terminal chimera after transfection into HeLa, but does not recognize the COOH-terminal chimera (Fig. 1 C, right). The levels of overexpression of the COOH-terminal chimeras compared with the endogenous protein can be estimated by the relative intensities of the PRC1–EGFP and EGFP–PRC1 bands in cell extracts detected with anti-GFP antibody (Fig. 1 C, left).

Overexpression of the PRC1 chimeras yielded a striking phenotype. Although the endogenous protein was normally confined to the nucleus in interphase, a substantial fraction of the overexpressed protein was cytosolic and localized to brightly stained fiber arrays that ring the nucleus (Fig. 1 D, a). On entry into mitosis the filaments disappeared, and PRC1 associated with a normal mitotic spindle, with a higher concentration in the zone of overlap between antiparallel MT sets during metaphase (Fig. 1 D, b). The in vivo localization of both native and tagged-PRC1, shows an enrichment in the MTs between the two half spindles at metaphase (Fig. 1, A, d and D, b). During anaphase PRC1 remained enriched in the spindle midzone, and finally localized exclusively in the midbody during cell cleavage (Fig. 1 D, c and d). After normal cleavage, perinuclear rings reformed in the two daughter cells (Fig. 1 D, d). The rings are MT arrays rearranged by the presence of PRC1, as shown by the colocalization of PRC1 with tubulin in the rings (Fig. 2 A). After a 4-h exposure to nocodazole, an MT depolymerizing drug, both tubulin and PRC1 were dispersed (Fig. 2 A), and PRC1 was largely intranuclear. At lower doses of nocodazole, PRC1 filaments were resistant to depolymerization compared with control MTs, suggesting that PRC1 overexpression also stabilizes MTs (unpublished data).

Thus, when overexpressed, PRC1 has the capacity to rearrange the normally radial MT arrays in HeLa cells, as well as in several other cell types (unpublished data), bundling interphase MTs into perinuclear rings. This bundled ring rearrangement is commonly observed during overexpression of many MT-associated proteins in mammalian culture cells (Weisshaar et al., 1992; Barlow et al., 1994; Waterman-Storer et al., 1995; Mandelkow et al., 1996; Togel et al., 1998; Koonce et al., 1999; Smith et al., 2000).

PRC1 binds and clusters Taxol-stabilized MTs in vitro

The rearrangement of the interphase MT array and the coassociation of PRC1 with MTs suggest a specific interaction

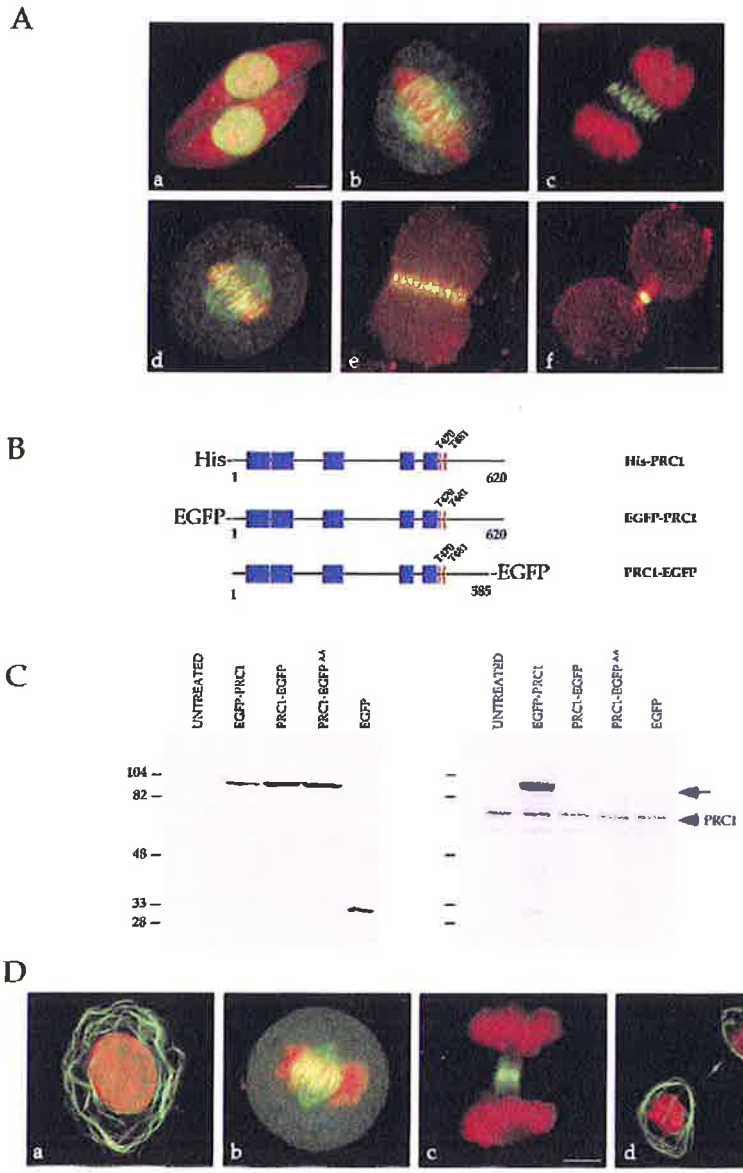

Figure 1. **The distribution of the endogenous PRC1 and its chimeras in HeLa cells.** (A) The localization of the endogenous PRC1 and TD-60. (a–c) HeLa cells were labeled with the affinity-purified antibody against PRC1 (green) and with propidium iodide for DNA (red). PRC1 is present in nuclei in interphase cells (a), and then becomes localized to the spindle upon entry into mitosis (b), and concentrates in the spindle midzone during late anaphase (c). (d–f) Double labeling of PRC1 (green) and TD-60 (red) during mitosis. (d) In metaphase, TD-60 is bound to the kinetochores at the metaphase plate, whereas PRC1 is associated with the spindle, enriched on interdigitating MTs. In late mitosis, the two antigens largely colocalize at the cleavage furrow (e) and midbody (f). PRC1 appears restricted to the Flemming body. Bars, 10 μm. (B) Schematic representation of the PRC1 chimeras. PRC1 was expressed in bacteria or HeLa cells as a tagged protein. For the first two constructs, the complete coding region of PRC1 (1–620 aa) was fused downstream to a 6×-His tag (His-PRC1) or an EGFP tag (EGFP–PRC1). The last construct allowed the expression of a COOH terminus truncation of PRC1 fused upstream to the EGFP (PRC1–EGFP). Both types of EGFP chimeras were used to overexpress the PRC1 mutant proteins. The PRC1^{AA} protein is a null phosphorylation mutant, with both Thr 470 and Thr 481 (red vertical bars) mutated into Ala. The PRC1^{EE} protein, with both the Thr 470 and Thr 481 mutated into Glu, mimics phosphorylation. The blue boxes indicate the regions of PRC1 with a high probability of multicoil formation (residues 35–85, 89–135, 210–251, 384–411, and 437–464). (C) Expression of the endogenous PRC1 and chimeras in HeLa cells. Extracts from HeLa, either untreated or transfected with one of the PRC1 chimeras (EGFP–PRC1, PRC1–EGFP, and PRC1–EGFP^{AA}), or with a control plasmid expressing only EGFP, were subjected to electrophoresis on 8% polyacrylamide gels and immunoblotted with the anti-EGFP antibody (left) or anti-PRC1 antibody (right). (Right) The anti-PRC1 antibody recognizes the endogenous PRC1 (arrowhead) in all extracts along with a band at the expected molecular mass of the EGFP–PRC1 fusion protein (arrow). PRC1–EGFP and the mutant PRC1–EGFP^{AA} fusions were not recognized because they lack the COOH- terminal residues recognized by this antibody. In contrast, the anti-EGFP antibody recognizes the unfused EGFP as well as all the three PRC1 fusion proteins. (D) The distribution of the PRC1-EGFP fusion protein in HeLa cells. During interphase, the overexpressed PRC1–EGFP protein (green) induces the formation of circular filaments around nuclei (DNA, red). In common with endogenous PRC1, overexpressed PRC1 is also in nuclei. During mitosis, the PRC1–EGFP protein is associated to a normal spindle (b), and then becomes associated to the midzone (c) and midbody at late telophase (d), similar to endogenous PRC1. The perinuclear ring filaments are evident in interphase (a) and at the end of telophase (d) but are dispersed during mitosis. Bar, 10 μm.

between PRC1 and MTs. Thus, we probed for PRC1 binding to MTs in an in vitro assay, and found that His-tagged, bacterially expressed PRC1 was entirely pelleted by Taxol-stabilized pure tubulin MTs (Fig. 2 B). In contrast, in the absence of MTs, PRC1 remained in the supernatant (Fig. 2 B). Direct microscopic observation of MTs after PRC1 binding shows complete colocalization of the two antigens, and reveals that the MTs have become extensively bundled in the presence of PRC1 (Fig. 2 C).

We have also analyzed the Taxol-stabilized MTs in the presence of His-PRC1 by electron microscopy. The bundles were extremely dense, but in favorable regions could be seen to contain clusters of aligned MTs (Fig. 2 D, left, arrow). Examination of these regions at higher magnification re-

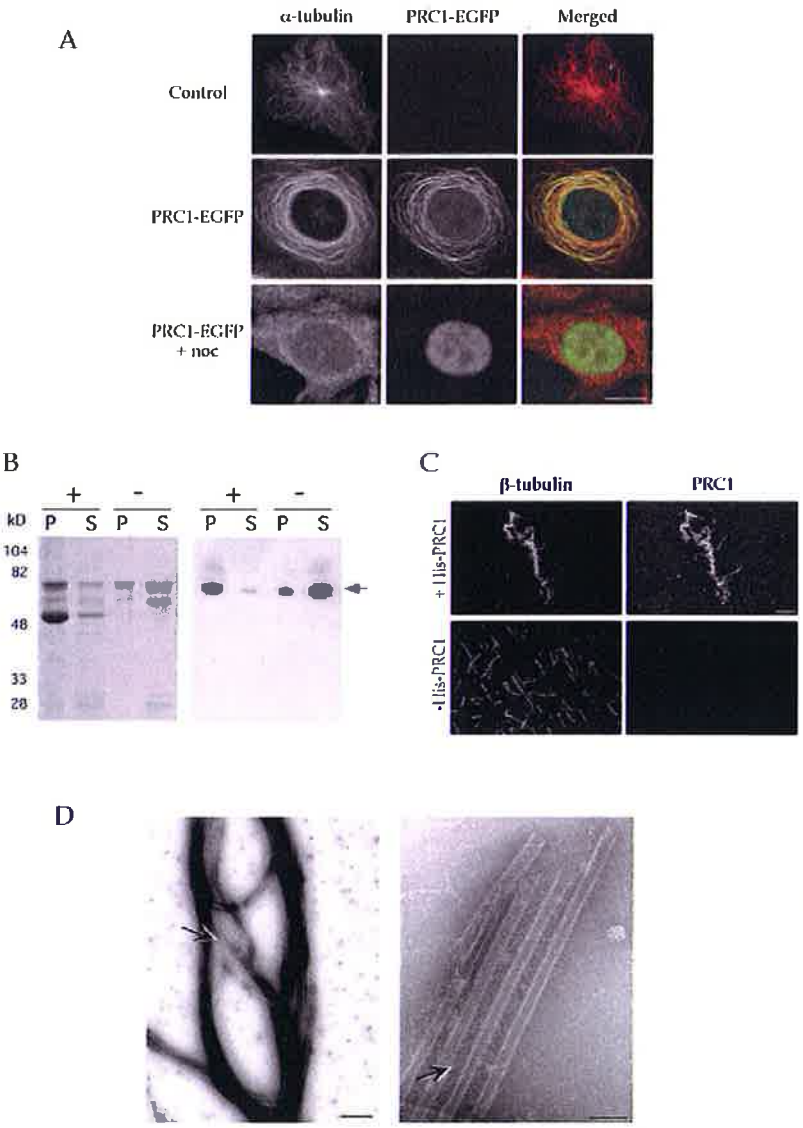

Figure 2. **PRC1 is a MT bundling protein.** (A) The overexpression of PRC1–EGFP chimera induces a circular rearrangement of the MT array. Starting from the top, the panel shows the MTs (red) focused on the centrosome in an untransfected HeLa cell. In an interphase cell overexpressing the PRC1-EGFP fusion protein (green), the circular filaments correspond to MTs (red) rearranged into a circular pattern around the nucleus. After a 4-h incubation in 1 μg/ml of nocodazole, the circular filaments are dispersed. Bar, 10 μm. (B) His-PRC1 binds in vitro MTs. His-PRC1 was incubated 10 min at 37°C in the absence (−) or presence (+) of MTs then subjected to a brief centrifugation. Pellets (P) and supernatants (S) were recovered in equal volumes of SDS-PAGE loading buffer, and samples were subjected to electrophoresis (left, Coomassie gel) and immunoblotted with the anti-PRC1 antibody (right). His-PRC1 protein is completely pelleted in the presence of MTs, whereas in the absence of MTs PRC1 remains soluble. (C) His-PRC1 induces MT bundling in vitro. Taxol-stabilized MTs were incubated in presence or absence of His-PRC1. The mixture was then deposited on top of a poly-lysine–treated coverslip which was then methanol fixed and incubated with anti–β-tubulin and anti-PRC1 antibodies. MTs appear short and unbundled in the absence of His-PRC1. After addition of His-PRC1, MTs form long highly bundled filaments. Bar, 20 μm. (D) Negatively stained electron microscopy samples. Low magnification view of bundled MTs. Arrow indicates MTs with clearly visible alignment (left). Bar, 400 nm. High magnification of aligned MTs shows PRC1 forming extensive intermicrotubule bridges (right, arrow). Bar, 40 nm.

vealed MTs in regularly spaced arrays interconnected by filamentous projections (Fig. 2 D, right). The average distance between the MTs was ~19 nm. The PRC1 filaments linking the MTs appeared to form a constant angle (~38°) with respect to the longitudinal MT axis (Fig. 2 D, right, arrow).

PRC1 is an MT-associated protein whose bundling activity is cell cycle regulated

It is remarkable that, despite a gross rearrangement of the interphase MT array, overexpressed PRC1 is associated with mitotic spindles of normal appearance (Fig. 1 D, b). The spindles of cells overexpressing PRC1 also exhibited normal function, as transfected cells routinely proceeded through normal anaphase and telophase (Fig. 1 D, c and d). In keeping with this dichotomy in interphase/mitotic behavior, we found that recently divided daughter cells, connected by a midbody following normal mitosis, contained perinuclear MT ring arrays (Fig. 1 D, d).

The capacity of PRC1 to form interphase rings but participate in normal spindle function suggests that its capacity to bundle MTs is specifically suppressed, either directly or indirectly, during early mitosis. In contrast, PRC1 strongly associates with the MT bundle that normally forms at the spindle equator during anaphase. These observations indicate that the bundling capacity of mitotic spindle-associated PRC1 might be downregulated during early mitosis, and then activated during late mitotic stages when the midzone MT bundle, necessary for cell cleavage (Cao and Wang, 1996; Wheatley and Wang, 1996), is formed. Thus, we have conducted tests to determine if there is specific downregulation of PRC1 in early mitosis, followed by a requirement for PRC1 to bundle the spindle midzone in late mitosis.

Human PRC1 has two Cdk phosphorylation sites, at T470 and T481 (Jiang et al., 1998). An attractive explanation for our observations is that Cdc2/cyclin B phosphorylation specif-

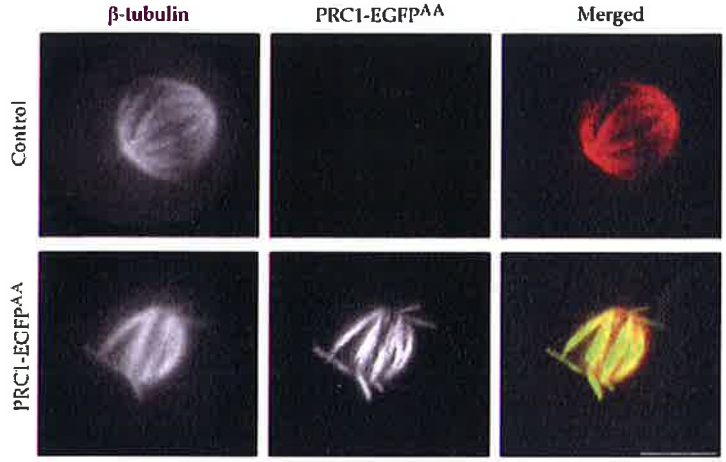

Figure 3. **Overexpression of a double PRC1 mutant lacking the two Cdk phospho-threonines creates multiple MT bundles in mitotic spindles.** A control untreated cell (top) and a cell (bottom) overexpressing PRC1–EGFP^{AA} (green), double labeled with anti–β-tubulin antibody (red), are shown. Although PRC1 distribution shows the MTs are highly bundled, the mitotic spindle preserves a bipolar shape. Bar, 10 μm.

ically downregulates PRC1 bundling capacity in early mitosis. We mutated the two Cdk-phosphorylated threonine residues to alanine, and transfected HeLa with plasmids expressing the nonphosphorylatable PRC1–EGFP^{AA} mutant. The result was striking. In early mitosis, mutant PRC1 caused extensive bundling of the MTs of the mitotic spindle (Fig. 3, bottom) compared with the morphology of a control spindle (Fig. 3, top). Despite extensive bundling, the MT arrays largely preserve a bipolar orientation. Approximately 37% of the prometaphase cells overexpressing the mutant showed such bundled spindles associated with highly condensed DNA, and no mitotic cells with such bundles were observed in anaphase, indicating the mutant blocks mitotic progression.

We also constructed a phosphorylation mimic PRC1–EGFP^{EE} mutant to determine if it had a distinct effect. Expression of this construct gave results identical to those obtained with the PRC1–EGFP^{AA} mutant (unpublished data). The EE mutant also had no effect on MT binding (see Fig. 5 C) or bundling (unpublished data) of PRC1 in vitro. We interpret these results as indicating that glutamate substitution in this case is not a good phosphorylation mimic, but instead interferes with a critical function at the phosphorylation site.

The absence of PRC1 affects midzone formation during anaphase

PRC1 is clearly required for cell cleavage, as microinjection of anti-PRC1 antibody causes cleavage failure (Jiang et al., 1998). To determine the specific role that PRC1 plays in cell cleavage, we transfected cells with siRNA to block PRC1 translation, and followed cells in which PRC1 was suppressed. Immunofluorescence analysis showed that PRC1 was substantially diminished in 30–35% of transfected cells after 24 h. Many cells could be found in which PRC1 was apparently completely absent as shown by paired PRC1-negative and -positive metaphase and early (Fig. 4 A, a) and late anaphase (Fig. 4 A, b) cells. In both cases, one cell of the pair has no detectable PRC1 (Fig. 4 A a, arrow and b, arrowhead). In accord with these observations, Western blots showed that PRC1 was strongly suppressed in the entire cell population after transfection (Fig. 4 B).

In the absence of PRC1, cells were able to progress normally in mitosis to metaphase (Fig. 4 A, a, arrow), and underwent normal chromatid segregation in anaphase (Fig. 4 A, b, arrowhead). However, cells lacking PRC1 always showed aberrant anaphase spindle morphology (Fig. 4 C). Interpolar MTs were radially dispersed, and interdigitating MTs were generally absent between the two half spindles (Fig. 4 C, a). Interestingly, even in the absence of a midzone MT bundles, cells were able to separate their sets of sister chromatids and showed partial furrowing (Fig. 4 C, b and c).

Differing degrees of severity of the phenotype were always associated with either complete or reduced levels of PRC1 expression. In some cases, midzone MTs were present, but in disarray. More often, MTs displayed no interdigitation at the spindle equator (Fig. 4 C, b), and as a result the half spindles and their chromosomes frequently rotated away from their normal alignment orthogonal to the spindle equator. However, even in the absence of midzone MTs, cells seemed to initiate furrowing then regress before completing cleavage (Fig. 4 C, d). As a result of furrow regression, cells lacking PRC1 became increasingly binucleate with time (Fig. 4 D), reaching values consistent with the PRC1 suppressed population. We conclude that the absence of PRC1 disturbs neither MT assembly nor chromosome segregation, but severely alters interzonal bundling in anaphase.

Domain structure of PRC1

The primary sequence of PRC1 has several striking features (Fig. 5 A, wt). The NH_2-terminal three quarters of the protein is predicted to be largely composed of α-helical sequence (within which are predicted coiled-coil motifs, Fig. 1), whereas the COOH-terminal region mostly contains β-sheets and turns. At the junction between these two regions there are two Cdk consensus phosphorylation sites clustered with two nuclear localization signals (NLSs). A central region of the protein, spanning residues 240–440, is highly conserved among eukaryotic species, and can be assumed to be important to the function of PRC1. PRC1 also contains putative consensus sequences for ubiquitination-dependent proteolysis, including two D boxes and a KEN box (Fig. 5 A) (Glotzer et al., 1991; Pfleger and Kirschner, 2000).

To determine the relative roles of these distinct regions of the primary structure in PRC1 function, we constructed sev-

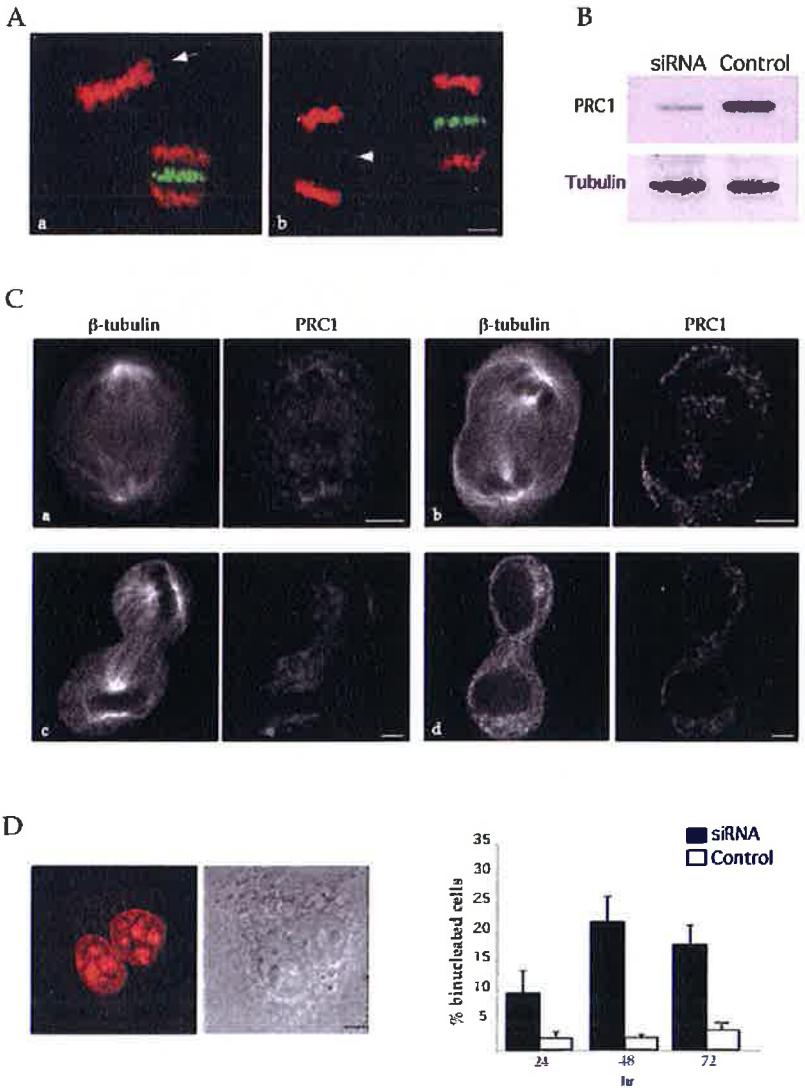

Figure 4. **Suppression of PRC1 function by siRNA disrupts midzone MTs in HeLa cells.** (A) Panels a (arrow) and b (arrowhead) show two examples of mitotic cells negative for PRC1 (green) side by side with cells expressing endogenous PRC1. (B) Western blot showing a specific decrease of PRC1 protein after siRNA transfection compared with untreated cells. The same blot was then reprobed with an anti-tubulin antibody to show equal loading of the samples. (C) HeLa cells negative for PRC1 have an altered spindle midzone. Interdigitating MTs are absent (a) or drastically reduced and disorganized (b and c) and as a consequence the two half spindles are rotated relative to the spindle axis. Cells with altered spindle midzone initiate furrowing (b and c) but do not complete cleavage (d). (D) A binucleated cell negative for PRC1. Bar, 5 μm. A histogram showing the increase in binucleated cells after siRNA transfection. A peak is reached 48 h after transfection.

eral truncation mutants (Fig. 5 A) and expressed them as GFP-tagged chimeras to assay their properties in mammalian cells. Western blots of PRC1 chimeras, expressed after transfection, showed that truncated proteins of the correct size were expressed, and that all constructs were being expressed at approximately the same level (Fig. 5 B).

Results with the different constructs are summarized in Table I. In brief, we found that MT binding during mitosis correlated with the presence of the conserved central region. Further, NH_2-terminal sequence upstream of the conserved region was required for association with the midzone of the cleavage furrow and for localization to the center of the midbody. Nuclear localization during interphase correlated with the presence of the NLS consensus sequence, as expected.

Immunofluorescence images of the different chimeras demonstrate their distinct capacities for localization (Fig. 6). The shortest COOH-terminal construct, C439, neither localizes to the mitotic spindle nor to the cleavage midzone. The construct M273, containing the central conserved region, localizes to the whole mitotic spindle but lacks sequence required to address it to the center of the midbody at the end of mitosis.

Like M273, the longer COOH-terminal construct C273 also localizes to the mitotic spindle but not to the center of the midbody in telophase. It is noteworthy that inclusion of downstream sequence causes C273 to induce stronger MT association in the mitotic spindle than M273 (Fig. 6 A). In contrast to the COOH-terminal constructs, the NH_2-terminal constructs N305 and N486 both specifically localize to the center of the midbody at the end of mitosis (Fig. 6 B, insets), whereas the longer construct, N486, localizes to the entire mitotic spindle at metaphase, the shorter N305 does not (unpublished data), reinforcing the importance of the central region in MT binding. The result with N305 demonstrates that MT binding capacity is not required for localization to the center of the midbody. These in vivo results were reinforced by in vitro MT binding assays (Fig. 5 C),

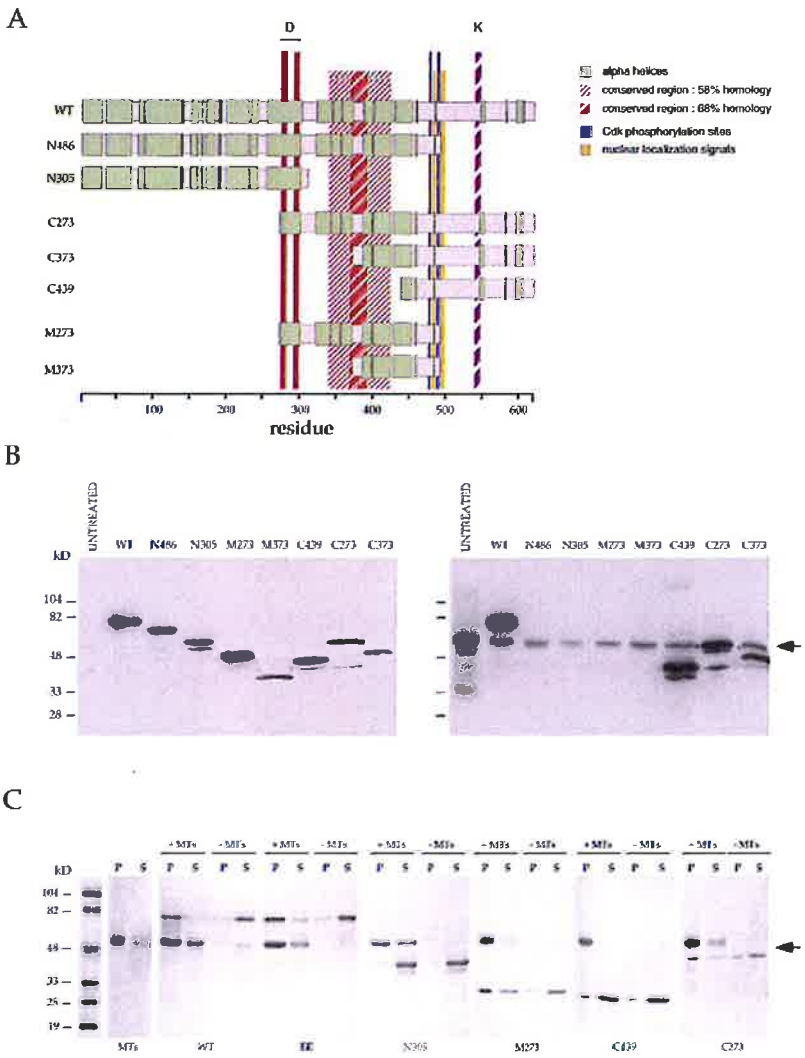

Figure 5. **Expression and properties of the PRC1 domains.** (A) Scheme representing the WT PRC1 protein and its NH_2- and COOH-terminal truncations. The different helical regions of PRC1 are indicated in the scheme along with two Cdk substrate threonines adjacent to two distinct nuclear localization signals (TPSKRRGLAPNTPGKARKL from aa 470 to 488). (D and K) Degradation boxes. Names given to the different mutants are C for COOH-terminal (number indicating the residue where the mutant commences), N for NH_2-terminal (number indicating the residue where the mutant terminates), or M for middle region (number indicating the residue where the mutant commences). The indicated percent homology is by comparison, using ClustalW, with the following sequences: AAC02688 and AAH05140 *Homo sapiens*; AAH05475 *Mus musculus*; AAF47965 and *AAF47966 Drosophila melanogaster*; CAC17794/17795/17796 *Nicotiana tabacum*; CAB82688 and BAB08676 *Arabidopsis thaliana*. Table I summarizes the distinct properties of the WT PRC1 and its truncation mutants. (B) Western blots of the different GFP-PRC1 proteins, both wild-type and mutants, expressed in HeLa cells, recognized with anti-GFP antibody (left) or anti-PRC1 antibody (right). The anti-PRC1 antibody recognizes the WT and COOH-terminal truncations along with the endogenous PRC1 (arrow). Expression levels of the different constructs are all approximately the same. (C) Coomassie-stained gels of different His-PRC1 constructs after MT binding assay in vitro. WT PRC1 and $PRC1^{EE}$ both pellet in presence of MTs. M273 and C273 also pellet (P) in presence of MTs, whereas C439 and N305 remain mostly in the supernatant (S). The arrow indicates the position of tubulin.

which showed that C273 was almost entirely bound to MTs, whereas M273 exhibited intermediate binding. In contrast, N305 and C439 did not bind to MTs in vitro.

Although the COOH-terminal domain of PRC1 does not display any particular localization or activity, it apparently influences the rest of the protein, as suggested by the difference between C273 and M273 in MT association. Further, remarkably, an antibody directed against a COOH-terminal peptide is able to disrupt cell cleavage (Jiang et al., 1998).

Table I. Properties and localization of PRC1 domains

	Interphase		Mitosis		
	MT bundling	Nuclear[a]	MT localization	Cleavage midzone	Central midbody
WT	Yes	Yes	Yes	Yes	Yes
N486	Yes	No	Yes	Yes	Yes
N305	No	No	No	Yes	Yes
C273	Yes	Yes	Yes	No	No
C373	No	Yes	No	No	No
C439	No	Yes	No	No	No
M273	Yes	No	Yes	No	No
M373	No	Yes	No	No	No

Summary of the properties and localization of wild-type PRC1 and its truncation mutants in HeLa cells. The different constructs are described in Fig. 5 A.
[a]Specific concentration.

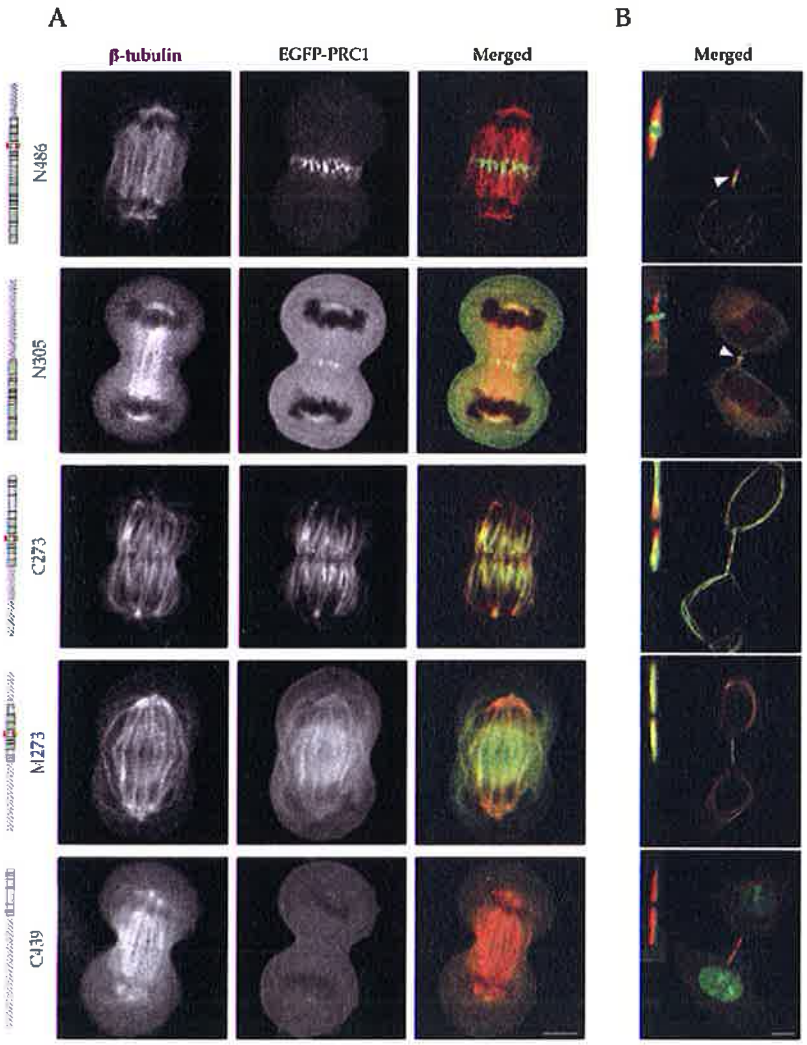

Figure 6. **PRC1 contains distinct domains with different functional capacities as determined by immunofluorescence.** To the left of the panels is shown a scheme of the different constructs studied. For each construct, anaphase (A) and telophase (B) cells are shown, stained for β-tubulin (red) and PRC1 (green). Removal of the COOH-terminus of PRC1 does not affect its ability to bind MTs (M273) nor its enrichment at the Flemming body during telophase (N486-N305) (B, arrowheads). In fact, the COOH terminus alone does not seem to be directly involved in any PRC1 activity assayed. Constructs C273 and M273 contain the region responsible for binding and bundling MTs, but they lack the signal to focus on the center of the midzone in anaphase (A), or the Flemming body during telophase (B). In (B) a closeup of the midbody (inset) is shown for each telophase cell. Bars, 5 μm.

Upon microinjection of affinity-purified anti-PRC1 antibodies, we found that spindle morphology and function were normal in early mitosis (Fig. 7, a and b), and all stages up to telophase were unchanged. However, at telophase, the usual broad MT bundle was greatly diminished by comparison to normal mitotic controls, and did not appear to extend to the cell cortex (Fig. 7 c). Thus, the effect of a COOH-terminal directed antibody is quite similar to that of PRC1 suppression by siRNA, except that the phenotype is more severe with siRNA, which affects the earlier step of midzone formation during anaphase with consequent suppression of cytokinesis. We find that ~50% of the microinjected cells fail in cleavage, as previously noted (Jiang et al., 1998).

Discussion

We have shown that human PRC1 is a MT-associated bundling protein. Both in vivo and in vitro evidence support this conclusion. The requirement for PRC1 in cell cleavage, and the bundling that is associated with PRC1 presence in the midzone of the late mitotic spindle, lead us to conclude that PRC1 functions to stabilize the midzone MT bundle, permitting completion of cell cleavage.

Many proteins concentrate at the equatorial region of the late mitotic central spindle for the purpose of participating in the cleavage event. Although many of these proteins, like PRC1, are known to be required for the cleavage process, their specific roles in cell cleavage have not as yet been defined. Some of these proteins have defined functions, acting as MT motors (Ohkura et al., 1997; Adams et al., 1998; Williams et al., 1995; Raich et al., 1998), small GTP-binding proteins and their regulators (Kishi et al., 1993; Drechsel et al., 1997; Prokopenko et al., 1999; Tatsumoto et al., 1999; Hill et al., 2000; Jantsch-Plunger et al., 2000), or protein kinases (Lee et al., 1995; Carmena et al., 1998; Madaule et al., 1998; Terada et al., 1998; Yasui et al., 1998). Their overall functions must be either to maintain the central spindle, recruit required proteins to this site, create the physical means by which the central spindle communicates to the cell cortex for the controlled deposition of myosin II and actin, or to generate the signal for the cleavage event.

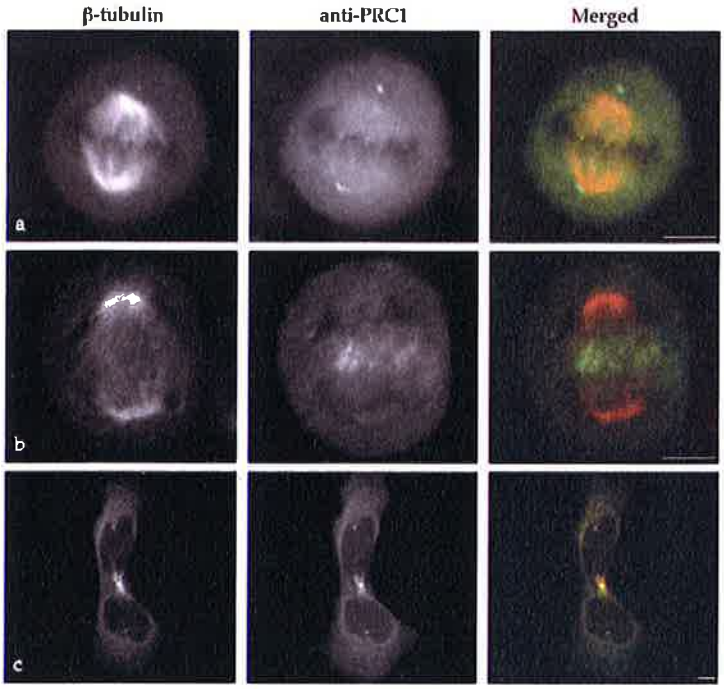

Figure 7. **The microinjection of the anti-PRC1 antibody specifically affects the formation of the midbody during telophase.** HeLa cells microinjected with the anti-PRC1 antibody, labeled with the anti–β-tubulin antibody (red) along with the anti–rabbit IgG antibody (green), are shown in the panel. Antibody microinjection does not affect the early steps of spindle formation. PRC1 is associated with the entire spindle at metaphase (a), and moves to the spindle midzone during anaphase (b), as in controls. However, during telophase (c), the midzone spindle appears as a narrow and unstructured bundle of MTs that has detached from the cell cortex. Note anti-PRC1 antiserum crossreacts with centrosomes, as previously noted (Jiang et al., 1998). Bars, 5 μm.

Considering that interdigitated midzone MTs are required for successful cytokinesis, and that passenger proteins with roles in cell cleavage collect at the center of the central spindle in late anaphase, PRC1 may be essential for these proteins to correctly localize to the cleavage furrow. Indeed, our preliminary data indicate that PRC1 has a key role in targeting the passenger proteins involved in cleavage (unpublished data). The capacity of PRC1 to specifically localize to the Flemming body in telophase, independent of its association with MTs, suggests there may be a second and important function for PRC1 during cleavage.

PRC1 phosphorylation sites and their potential function

A notable aspect of PRC1 behavior is that, despite bundling MTs when overexpressed in interphase cells, it permits normal spindle function. This result suggests that PRC1 MT bundling function is strongly downregulated in early mitosis, and then reactivated in late mitosis for the purpose of stabilizing the midzone MTs. Inactivation in early mitosis is in accord with siRNA experiments that show suppression of PRC1 does not interfere with any aspect of mitosis until cell cleavage. Among the proteins that bundle interphase MTs when overexpressed, PRC1 is, to our knowledge, unique with respect to its suppression during early mitosis.

PRC1 has two Cdk phosphorylation sites, and a null phosphorylation mutant yields an early mitotic phenotype consistent with the interpretation that phosphorylation suppresses PRC1 bundling activity, as the mutant generates MT bundles throughout the mitotic spindle. PRC1 has been shown to be a good substrate for several Cdks in vivo and in vitro (Jiang et al., 1998). It is reasonable to speculate that the mitosis-specific regulation is mediated by Cdc2 activity. Although several observations indicate a physiological role for phosphorylation of PRC1, we were unable to clearly demonstrate this because overexpression of a phosphorylation mimic EE mutant of PRC1 generates the same bundled mitotic spindle phenotype seen with the phosphorylation-null mutant, suggesting that the EE mutant is not an adequate mimic of phosphorylation status.

Domain structure of PRC1

PRC1 contains multiple α-helical regions with the potential for formation of multicoils that may figure in interprotein linkages (Fig. 1 B). It shares 57% homology with the budding yeast protein Ase1 that localizes to the anaphase spindle midzone and is required for many aspects of mitosis (Juang et al., 1997). Together with another nonmotor MT-associated protein, Ase1 is required for anaphase B, the elongation of the spindle and separation of spindle poles (Pellman et al., 1995). Loss of Ase1 protein function destabilizes the spindle during telophase (Juang et al., 1997). Significant sequence homology (56%) is also shared with a *Nicotiana tabacum* MT-associated protein, Map65 (GenBank/EMBL/DDBJ accession no. CAC17794, CAC17795, and CAC17796). The homologue of Map65 in carrots has been demonstrated to form regular inter-MT linkages, thus generating MT bundles (Chan et al., 1999). Similarly, our data indicate that PRC1 forms bundles of aligned MTs where inter-MT linkage is made through filamentous projections at a constant angle with respect to the longitudinal MT axis. MT bundling may require dimers or higher oligomers of PRC1, a possibility we are currently exploring. In preliminary experiments, we have found that PRC1 runs as a single included peak on sizing columns, with a mass of ~300 kD (unpublished data), suggesting that it forms small oligomers in vitro. The primary se-

quence of PRC1 gives a clear indication that the protein has distinct domains. Truncation mutants confirm this impression, and demonstrate that distinct regions of PRC1 have distinct roles. The central region is clearly implicated in MT binding. In contrast, the NH_2-terminal region does not bind MTs, but is required for association of PRC1 with the Flemming body at the center of the midbody in late cleavage. These results show that association of PRC1 with the Flemming body does not require MT association. In fact, one of the truncation mutants of PRC1, N305, neither associates with MTs in vitro nor with the spindle MTs in vivo, but clearly associates with the Flemming body during cleavage.

Thus, it is possible that PRC1 has two distinct functions in cleavage, one for MT bundling and another relating to association with the Flemming body at the last stages of cleavage. Cleavage has two distinct stages, the first involving the initial cortical contraction, and the second, resolution and final cell separation (Zeitlin and Sullivan, 2001). PRC1 may play a role in each of these distinct events. siRNA experiments show that cleavage can fail at an early stage in the absence of PRC1, but this result does not exclude a further role for PRC1 in the final stage of cleavage.

Potential association with other cleavage proteins

The spindle-associated motor protein MKLP1 has been speculated to play a role in bundling the late mitotic central spindle based on its in vitro capacity to bundle MTs (Nislow et al., 1992). MKLP1 homologues in lower eukaryotes play a role in cytokinesis, as mutants of these homologues, pavarotti (Adams et al., 1998) and ZEN-4 (Raich et al., 1998; Severson et al., 2000), exhibit derangements in cleavage. Our results suggest that MKLP1 alone is not sufficient to maintain the midzone MT bundle. In fact, the role of MKLP1 is complex, as an alternatively spliced form, CHO1, must bind actin to complete the terminal step in cleavage (Kuriyama et al., 2002).

Cyk-4, a Rho GAP, interacts specifically with ZEN-4 in *Caenorhabditis elegans*, and both proteins appear to be required for formation of the midzone spindle in late mitosis (Mishima et al., 2002). A human Cyk-4 orthologue, HsCYK-4, has recently been shown to form a heterotetramer with MKLP-1 and to bundle microtubules in vitro (Mishima et al., 2002).

Additionally, the PRC1 truncation mutant N305 does not bind directly to MTs, but does associate with the spindle midzone. Thus, it is possible that PRC1, in addition to binding directly to MTs, also binds as part of a protein complex at the late mitotic spindle midzone.

Our evidence supports a role for in the formation of midzone MT bundles during anaphase. Further work will establish what proteins PRC1 associates with and, specifically, if there is interaction and cooperation between PRC1, Cyk-4, and MKLP1 in maintaining the spindle midzone, as well as in the terminal stage of cleavage.

Materials and methods

Cloning and mutagenesis

Wild-type PRC1 cDNA in pCL (Jiang et al., 1998) was used to generate different constructs. Using a BamHI internal site, PRC1 cDNA, including the 5′ untranslated region (UTR) up to nucleotide 1836, was subcloned into the EcoRI-BamHI sites of the pEGFP-N1 vector (CLONTECH Laboratories, Inc.). This construct encoded the PRC1 protein, lacking the last 35 amino acids at the COOH terminus, fused upstream to the EGFP protein. To generate a wild-type Histidine-PRC1 (His-PRC1), the entire coding sequence of PRC1 was amplified by PCR and subcloned into the EcoRI-NotI of pHAT2 (Perānen et al., 1996). To generate an EGFP–PRC1 fusion protein, the fragment EcoRI-NotI in pHAT2 was cut with NotI, filled with Klenow (Biolabs) and then ligated into the EcoRI-SmaI sites of pEGFP-C2. The $PRC1^{AA}$ and $PRC1^{EE}$ mutants in which Thr 470 and Thr 481 were respectively substituted by Ala or Glu, were generated by PCR. For $PRC1^{AA}$, two independent PCR reactions were performed using oligonucleotides 5′-CCGGAATTCATGAGGAGAAGTGAGGTGCTG-3′, 5′-TGCTCGAGGAGCGCTGCCATACAG-3′ and 5′-CCTAGCAAGCGGCGAGGACTGGCTCCCAATGCCCC-3′, 5′-TTTATAGCGGCCGCTCAGGACTGGATGTTGGTTG-3′.

These oligonucleotides were designed to substitute both Thr 470 and Thr 481 by Ala along with two silent mutations generating SmaI and XhoI restriction sites. An identical PCR strategy was used to generate the $PRC1^{EE}$. To generate the EGFP–$PRC1^{AA}$ and EGFP–$PRC1^{EE}$ fusions, the fragments EcoRI-NotI in pHAT2 were cut with NotI, filled with Klenow and then ligated into the EcoRI-SmaI sites of pEGFP-C2. To create the truncations PRC1–$EGFP^{AA}$ and PRC1–$EGFP^{EE}$, the fragments EcoRI-BamHI from the pEGFP-C2 constructs were subcloned into the EcoRI-BamHI sites of pEGFP-N1. The different truncations were generated either by PCR, introducing premature stop codons, or by restriction enzymes to cut within the PRC1 coding region. C273 was generated by cutting the wt EGFP-PRC1 construct with BspEI and XhoI followed by mung bean nuclease treatment and ligation. M273 was similarly obtained, starting from the N486 construct. C373 was obtained by cutting the wt EGFP–PRC1 construct with HIndIII followed by mung bean nuclease and ligation. M373 was obtained as described for C373 starting from the N486 construct. N305, M273, C373, and C439 were cloned into pHAT2 for protein expression. All the constructs were verified by DNA sequencing (Eurogentec).

Cell culture and transfection

HeLa cells were grown as a monolayer in DME (GIBCO BRL) supplemented with 10% fetal bovine serum (Hyclone), and maintained in a humid incubator at 37°C in a 5% CO_2 environment. HeLa cells (3×10^6), attached to coverslips in 10-mm dishes, were transfected by Exgen (Euromedex) or Lipofectamine 2000 (GIBCO BRL), with 4 μg of one of the PRC1 fusion constructs, or with a control (pEGFP-N1) plasmid, according to manufacturer's instructions. For the preparation of the cell extracts, in order to obtain a better efficiency of transfection (~70%), cells were transfected with a mixture of 20 μg of each of the plasmids and the Lipofectamine 2000. HeLa cells transfected with the PRC1–EGFP plasmid were selected in 1.5 mg/ml geneticin G418 (GIBCO BRL). Nocodazole was dissolved in DMSO and used at 0.04 μg/ml or 1 μg/ml. For nocodazole treatment, HeLa cells transiently transfected with the PRC1–EGFP plasmid were exposed to 0.04 or 1 μg/ml nocodazole for 4 h before fixation.

siRNA oligonucleotides and transfection

To generate single-stranded, gene-specific annealed RNA oligomers (Dharmacon Research), we used 5′-AAATATGGGAGCTAATTGGGA-3′ as the human PRC1 cDNA sequence to be targeted by the oligonucleotides. Transfection conditions were as described by Elbashir and colleagues (2001). HeLa cells were plated on coverslips in a 24-well plate and transfected using oligofectamine (GIBCO BRL). Cells were fixed at different time points after transfection and processed for immunofluorescence. For Western blots, cells were harvested with trypsin and washed in PBS before adding SDS-PAGE sample buffer.

Immunofluorescence microscopy

Cells grown on poly-D-lysine–coated glass coverslips for immunofluorescence microscopy were fixed with 2% paraformaldehyde-PBS, or alternatively, with cold methanol, followed by a step of rehydration in PBS. Cells were then processed with primary and secondary antibodies and counterstained with propidium iodide. For protocol detail see Martineau-Thuillier et al. (1998). Affinity-purified PRC1 COOH-terminal antibody (Jiang et al., 1998), anti–β-tubulin monoclonal antibody (T4026; Sigma-Aldrich), anti-tyrosinated α-tubulin rat monoclonal antibody (Lafanechere et al., 1998) (YL 1/2), and JH human autoimmune serum, used to detect TD-60 (Andreassen et al., 1991), were diluted 500, 400, 500 and 300×, respectively. Secondary antibodies, including FITC-conjugated affinity-purified goat anti–rabbit IgG, rhodamine-conjugated

anti–human IgG (Jackson Laboratories), Texas red–conjugated sheep anti–mouse IgG, and rhodamine-conjugated goat anti–rat IgG (Cappel), were used at 2.5 μg/ml. Images were collected with a MRC-600 Laser Scanning Confocal Apparatus (Bio-Rad Laboratories) coupled to Nikon Optiphot microscope.

Cell extracts and immunoblotting

24 h after transfection, cells were trypsinized, collected by centrifugation, and washed in PBS before the addition of SDS-PAGE loading buffer. After a short sonication, 10 μg/lane of cell extract was resolved on 8 or 10% polyacrylamide gels using a minigel apparatus (Bio-Rad Laboratories) and transferred to nitrocellulose. Affinity-purified rabbit antibodies against PRC1 (Jiang et al., 1998) were diluted 1,000-fold to detect the endogenous and the overexpressed fusion proteins. Anti-EGFP polyclonal antibody (CLONTECH Laboratories, Inc.), diluted 500-fold, was used to detect expression of the fusion proteins. The anti–β-tubulin monoclonal antibody was diluted 1,000-fold. Blots were then exposed to HRP-conjugated goat anti–rabbit IgG (TAGO), diluted 2,500-fold, for 1 h, and then developed by ECL (Pierce Chemical Co.).

Antibody microinjection

For microinjection, HeLa cells were grown on glass coverslips as previously described (Jiang et al., 1998). Interphase cells were injected in the cytoplasm with affinity-purified anti-PRC1 antibodies (3.8 mg/ml), using a semiautomatic microinjector (Eppendorf). After a 21-h incubation, coverslips were fixed and stained with FITC-conjugated goat anti–rabbit IgG, along with anti–β-tubulin monoclonal antibody.

Nickel affinity chromatography

All the constructs in pHAT2 were expressed in BL21 DE3. Bacteria were induced at 37°C for 4 h in the presence of 0.5 mM isopropylthio-β-D-galactoside (IPTG). Lysis and binding to nickel-Sepharose beads (Hitrap chelating; Amersham Pharmacia Biotech) was performed in a phosphate buffer (50 mM NaH_2PO_4, pH 7.6, 300 mM NaCl, 5 mM imidazole, 0.1 mM PMSF, and 10 mg/ml aprotinin). The proteins were eluted with 250 mM imidazole, analyzed by SDS-PAGE, and used for further MT binding assays.

In vitro MT binding assays and electron microscopy

The His-PRC1 constructs from nickel-Sepharose purification were diluted to <0.2 μg/μl in 20 μM Taxol-PEM (80 mM Pipes, pH.6.8, 1 mM EGTA, 1 mM $MgCl_2$). Pure tubulin MTs (6.4 mg/ml; provided by Dr. L. Wilson [University of California, Santa Barbara, CA]), isolated from bovine brain (Farrell et al., 1987), were assembled at 37°C, stabilized with 5 μM Taxol, and then mixed with His-PRC1 to a final concentration of 0.6 μg/μl in a total volume of 20 μl. The mixture was then incubated 10 min at 37°C. For SDS-PAGE and Western blot analysis of MT bundles, PRC1 constructs were cosedimented with MTs in a short centrifugation step at 16,000 *g* (cold, 5 min). The pellets were rinsed twice in PEM, both pellets and supernatants were recovered in equal volumes of SDS-PAGE loading buffer, and samples subjected to electrophoresis.

For immunofluorescence studies, 1 vol of the incubated MTs/PRC1 (wild-type His-PRC1 or mutant His-$PRC1^{EE}$) mix was diluted in 60 vol of prewarmed PEM-Taxol containing 0.05% glutaraldehyde. The solution was deposited on a polylysine-coated glass coverslip, and then fixed in 100% methanol and prepared as for immunofluorescence microscopy. A control MT preparation without PRC1 was treated identically.

For electron microscopy, protein samples at 0.05 μg/μl, prepared as described above, were applied to the clean side of carbon on mica (carbon/mica interface) and negatively stained with 2% uranyl acetate. Micrographs were taken under low-dose conditions with a JEOL 1200 EX II microscope at 100 kV at a nominal magnification of 40,000×.

We thank Dr. R. Wade and Dr. R.W.H. Ruigrok for assistance with electron microscopy. We also thank Dr. L. Wilson for providing bovine brain PC-tubulin.

This work was supported by funding from La Ligue Nationale Contre le Cancer (Laboratoire Labelliseé), and Association pour la Recherche contre le Cancer (5338; R.L. Margolis). T. Hunter is a Frank and Else Schilling American Cancer Society Research Professor. C. Mollinari is supported by a Telethon fellowship (Telethon Fondazione Onlus, Rome, Italy). J.P Kleman is a researcher of the Commissariat à l'Energie Atomique. W. Jiang is a scholar of Mallinckrodt Foundation.

Submitted: 13 November 2001
Revised: 3 May 2002
Accepted: 8 May 2002

References

Adams, R.R., A.A. Tavares, A. Salzberg, H.J. Bellen, and D.M. Glover. 1998. Pavarotti encodes a kinesin-like protein required to organize the central spindle and contractile ring for cytokinesis. *Genes Dev.* 12:1483–1494.

Andreassen, P.R., D.K. Palmer, M.H. Wener, and R.L. Margolis. 1991. Telophase disc: a new mammalian mitotic organelle that bisects telophase cells with a possible function in cytokinesis. *J. Cell Sci.* 99:523–534.

Barlow, S., M.L. Gonzalez-Garay, R.R. West, J.B. Olmsted, and F. Cabral. 1994. Stable expression of heterologous microtubule-associated proteins (MAPs) in Chinese hamster ovary cells: evidence for differing roles of MAPs in microtubule organization. *J. Cell Biol.* 126:1017–1029.

Cao, L.G., and Y.L. Wang. 1990. Mechanism of the formation of contractile ring in dividing cultured animal cells. I. Recruitment of preexisting actin filaments into the cleavage furrow. *J. Cell Biol.* 110:1089–1095.

Cao, L.G., and Y.L. Wang. 1996. Signals from the spindle midzone are required for the stimulation of cytokinesis in cultured epithelial cells. *Mol. Biol. Cell.* 7:225–232.

Carmena, M., M.G. Riparbelli, G. Minestrini, A.M. Tavares, R. Adams, G. Callaini, and D.M. Glover. 1998. *Drosophila* polo kinase is required for cytokinesis. *J. Cell Biol.* 143:659–671.

Chan, J., C.G. Jensen, L.C. Jensen, M. Bush, and C.W. Lloyd. 1999. The 65-kDa carrot microtubule-associated protein forms regularly arranged filamentous cross-bridges between microtubules. *Proc. Natl. Acad. Sci. USA.* 96:14931–14936.

Drechsel, D.N., A.A. Hyman, A. Hall, and M. Glotzer. 1997. A requirement for Rho and Cdc42 during cytokinesis in *Xenopus* embryos. *Curr. Biol.* 7:12–23.

Elbashir, S.M., J. Harborth, W. Lendeckel, A. Yalcin, K. Weber, and T. Tuschl. 2001. Duplexes of 21-nucleotide RNAs mediate RNA interference in cultured mammalian cells. *Nature.* 411:494–498.

Farrell, K.W., M.A. Jordan, H.P. Miller, and L. Wilson. 1987. Phase dynamics at microtubule ends: the coexistence of microtubule length changes and treadmilling. *J. Cell Biol.* 104:1035–1046.

Glotzer, M. 1997. The mechanism and control of cytokinesis. *Curr. Opin. Cell Biol.* 9:815–823.

Glotzer, M., A.W. Murray, and M.W. Kirschner. 1991. Cyclin is degraded by the ubiquitin pathway. *Nature.* 349:132–138.

Hill, E., M. Clarke, and F.A. Barr. 2000. The Rab6-binding kinesin, Rab6-KIFL, is required for cytokinesis. *EMBO J.* 19:5711–5719.

Jantsch-Plunger, V., P. Gonczy, A. Romano, H. Schnabel, D. Hamill, R. Schnabel, A.A. Hyman, and M. Glotzer. 2000. CYK-4: a Rho family GTPase activating protein (GAP) required for central spindle formation and cytokinesis. *J. Cell Biol.* 149:1391–1404.

Jiang, W., G. Jimenez, N.J. Wells, T.J. Hope, G.M. Wahl, T. Hunter, and R. Fukunaga. 1998. PRC1: a human mitotic spindle-associated CDK substrate protein required for cytokinesis. *Mol. Cell.* 2:877–885.

Juang, Y.L., J. Huang, J.M. Peters, M.E. McLaughlin, C.Y. Tai, and D. Pellman. 1997. APC-mediated proteolysis of Ase1 and the morphogenesis of the mitotic spindle. *Science.* 275:1311–1314.

Kishi, K., T. Sasaki, S. Kuroda, T. Itoh, and Y. Takai. 1993. Regulation of cytoplasmic division of *Xenopus* embryo by rho p21 and its inhibitory GDP/GTP exchange protein (rho GDI). *J. Cell Biol.* 120:1187–1195.

Koonce, M.P., J. Kohler, R. Neujahr, J.M. Schwartz, I. Tikhonenko, and G. Gerisch. 1999. Dynein motor regulation stabilizes interphase microtubule arrays and determines centrosome position. *EMBO J.* 18:6786–6792.

Kuriyama, R., C. Gustus, Y. Terada, Y. Uetake, and J. Matuliene. 2002. CHO1, a mammalian kinesin-like protein, interacts with F-actin and is involved in the terminal phase of cytokinesis. *J. Cell Biol.* 156:783–790.

Lafanechere, L., C. Courtay-Cahen, T. Kawakami, M. Jacrot, M. Rudiger, J. Wehland, D. Job, and R.L. Margolis. 1998. Suppression of tubulin tyrosine ligase during tumor growth. *J. Cell Sci.* 111:171–181.

Lee, K.S., Y.L. Yuan, R. Kuriyama, and R.L. Erikson. 1995. Plk is an M-phase-specific protein kinase and interacts with a kinesin-like protein, CHO1/MKLP-1. *Mol. Cell. Biol.* 15:7143–7151.

Mackay, A.M., A.M. Ainsztein, D.M. Eckley, and W.C. Earnshaw. 1998. A dominant mutant of inner centromere protein (INCENP), a chromosomal protein, disrupts prometaphase congression and cytokinesis. *J. Cell Biol.* 140:991–1002.

Madaule, P., M. Eda, N. Watanabe, K. Fujisawa, T. Matsuoka, H. Bito, T. Ishizaki, and S. Narumiya. 1998. Role of citron kinase as a target of the small GTPase Rho in cytokinesis. *Nature.* 394:491–494.

Mandelkow, E.M., O. Schweers, G. Drewes, J. Biernat, N. Gustke, B. Trinczek, and E. Mandelkow. 1996. Structure, microtubule interactions, and phosphorylation of tau protein. *Ann. NY Acad. Sci.* 777:96–106.

Martineau-Thuillier, S., P.R. Andreassen, and R.L. Margolis. 1998. Colocalization

of TD-60 and INCENP throughout G2 and mitosis: evidence for their possible interaction in signaling cytokinesis. *Chromosoma.* 107:461–470.

Mastronarde, D.N., K.L. McDonald, R. Ding, and J.R. McIntosh. 1993. Interpolar spindle microtubules in PTK cells. *J. Cell Biol.* 123:1475–1489.

Mishima, M., S. Kaitna, and M. Glotzer. 2002. Central spindle assembly and cytokinesis requires a kinesin-like protein/RhoGAP complex with microtubule bundle activity. *Dev. Cell.* 2:41–54.

Nislow, C., V.A. Lombillo, R. Kuriyama, and J.R. McIntosh. 1992. A plus-end-directed motor enzyme that moves antiparallel microtubules in vitro localizes to the interzone of mitotic spindles. *Nature.* 359:543–547.

O'Connell, C.B., S.P. Wheatley, S. Ahmed, and Y.L. Wang. 1999. The small GTP-binding protein rho regulates cortical activities in cultured cells during division. *J. Cell Biol.* 144:305–313.

Ohkura, H., T. Torok, G. Tick, J. Hoheisel, I. Kiss, and D.M. Glover. 1997. Mutation of a gene for a *Drosophila* kinesin-like protein, Klp38B, leads to failure of cytokinesis. *J. Cell Sci.* 110:945–954.

Pellman, D., M. Bagget, Y.H. Tu, G.R. Fink, and H. Tu. 1995. Two microtubule-associated proteins required for anaphase spindle movement in *Saccharomyces cerevisiae. J. Cell Biol.* 130:1373–1385.

Peränen, J., M. Rikkonen, M. Hyvönen, and L. Kääriäinen. 1996. T7 vectors with a modified T7lac promoter for expression of proteins in *Escherichia coli. Anal. Biochem.* 236:371–373.

Pfleger, C.M., and M.W. Kirschner. 2000. The KEN box: an APC recognition signal distinct from the D box targeted by Cdh1. *Genes Dev.* 14:655–665.

Prokopenko, S.N., A. Brumby, L. O'Keefe, L. Prior, Y. He, R. Saint, and H.J. Bellen. 1999. A putative exchange factor for Rho1 GTPase is required for initiation of cytokinesis in *Drosophila. Genes Dev.* 13:2301–2314.

Raich, W.B., A.N. Moran, J.H. Rothman, and J. Hardin. 1998. Cytokinesis and midzone microtubule organization in *Caenorhabditis elegans* require the kinesin-like protein ZEN-4. *Mol. Biol. Cell.* 9:2037–2049.

Robinson, D.N., and J.A. Spudich. 2000. Towards a molecular understanding of cytokinesis. *Trends Cell Biol.* 10:228–237.

Sellitto, C., and R. Kuriyama. 1988. Distribution of a matrix component of the midbody during the cell cycle in Chinese hamster ovary cells. *J. Cell Biol.* 106:431–439.

Severson, A.F., D.R. Hamill, J.C. Carter, J. Schumacher, and B. Bowerman. 2000. The aurora-related kinase AIR-2 recruits ZEN-4/CeMKLP1 to the mitotic spindle at metaphase and is required for cytokinesis. *Curr. Biol.* 10:1162–1171.

Skoufias, D.A., C. Mollinari, F.B. Lacroix, and R.L. Margolis. 2000. Human survivin is a kinetochore-associated passenger protein. *J. Cell Biol.* 151:1575–1582.

Smith, D.S., M. Niethammer, R. Ayala, Y. Zhou, M.J. Gambello, A. Wynshaw-Boris, and L.H. Tsai. 2000. Regulation of cytoplasmic dynein behaviour and microtubule organization by mammalian Lis1. *Nat. Cell Biol.* 2:767–775.

Takada, M., N. Morii, S. Kumagai, and R. Ryo. 1996. The involvement of the rho gene product, a small molecular weight GTP-binding protein, in polyploidization of a human megakaryocytic cell line, CMK. *Exp. Hematol.* 24:524–530.

Tatsumoto, T., X. Xie, R. Blumenthal, I. Okamoto, and T. Miki. 1999. Human ECT2 is an exchange factor for Rho GTPases, phosphorylated in G2/M phases, and involved in cytokinesis. *J. Cell Biol.* 147:921–928.

Terada, Y., M. Tatsuka, F. Suzuki, Y. Yasuda, S. Fujita, and M. Otsu. 1998. AIM-1: a mammalian midbody-associated protein required for cytokinesis. *EMBO J.* 17:667–676.

Togel, M., G. Wiche, and F. Propst. 1998. Novel features of the light chain of microtubule-associated protein MAP1B: microtubule stabilization, self interaction, actin filament binding, and regulation by the heavy chain. *J. Cell Biol.* 143:695–707.

Uren, A.G., L. Wong, M. Pakusch, K.J. Fowler, F.J. Burrows, D.L. Vaux, and K.H. Choo. 2000. Survivin and the inner centromere protein INCENP show similar cell-cycle localization and gene knockout phenotype. *Curr. Biol.* 10:1319–1328.

Waterman-Storer, C.M., S. Karki, and E.L. Holzbaur. 1995. The p150Glued component of the dynactin complex binds to both microtubules and the actin-related protein centractin (Arp-1). *Proc. Natl. Acad. Sci. USA.* 92:1634–1638.

Weisshaar, B., T. Doll, and A. Matus. 1992. Reorganisation of the microtubular cytoskeleton by embryonic microtubule-associated protein 2 (MAP2c). *Development.* 116:1151–1161.

Wheatley, S.P., and Y. Wang. 1996. Midzone microtubule bundles are continuously required for cytokinesis in cultured epithelial cells. *J. Cell Biol.* 135:981–989.

Williams, B.C., M.F. Riedy, E.V. Williams, M. Gatti, and M.L. Goldberg. 1995. The *Drosophila* kinesin-like protein KLP3A is a midbody component required for central spindle assembly and initiation of cytokinesis. *J. Cell Biol.* 129:709–723.

Yasui, Y., M. Amano, K. Nagata, N. Inagaki, H. Nakamura, H. Saya, K. Kaibuchi, and M. Inagaki. 1998. Roles of Rho-associated kinase in cytokinesis; mutations in Rho-associated kinase phosphorylation sites impair cytokinetic segregation of glial filaments. *J. Cell Biol.* 143:1249–1258.

Yen, T.J., G. Li, B.T. Schaar, I. Szilak, and D.W. Cleveland. 1992. CENP-E is a putative kinetochore motor that accumulates just before mitosis. *Nature.* 359:536–539.

Zeitlin, S.G., and K.F. Sullivan. 2001. Animal cytokinesis: breaking up is hard to do. *Curr. Biol.* 11:R514–R516.

Developmental Cell, Vol. 5, 1–20, August, 2003, Copyright ©2003 by Cell Press

The Mammalian Passenger Protein TD-60 Is an RCC1 Family Member with an Essential Role in Prometaphase to Metaphase Progression

Cristiana Mollinari,[1,5] Caroline Reynaud,[1,5] Stephanie Martineau-Thuillier,[1] Solange Monier,[2] Sylvie Kieffer,[3] Jerome Garin,[3] Paul R. Andreassen,[4] Annick Boulet,[2] Bruno Goud,[2] Jean-Philippe Kleman,[1] and Robert L. Margolis[1,*]

[1]Institut de Biologie Structurale J-P Ebel
CEA-CNRS
41 rue Jules Horowitz
38027 Grenoble Cedex 1
[2]Institut Curie
26 rue d'Ulm
75248 Paris Cedex 5
[3]Département Réponse et Dynamique Cellulaires
CEA Grenoble
38054 Grenoble Cedex 9
France
[4]Dana-Farber Cancer Institute
M640
44 Binney Street
Boston, Massachusetts 02115

Summary

Passenger proteins migrate from inner centromeres to the spindle midzone during late mitosis, and those described to date are essential both for proper chromosome segregation and for completion of cell cleavage. We have purified and cloned the human passenger protein TD-60, and we here report that it is a member of the RCC1 family and that it binds preferentially the nucleotide-free form of the small G protein Rac1. Using siRNA, we further demonstrate that the absence of TD-60 substantially suppresses overall spindle assembly, blocks cells in prometaphase, and activates the spindle assembly checkpoint. These defects suggest TD-60 may have a role in global spindle assembly or may be specifically required to integrate kinetochores into the mitotic spindle. The latter is consistent with a TD-60 requirement for recruitment of the passenger proteins survivin and Aurora B, and suggests that like other passenger proteins, TD-60 is involved in regulation of cell cleavage.

Introduction

The passenger proteins are important to the control of cell cleavage. They undergo redistribution during mitosis, first associating with inner centromeres from G2 until the metaphase to anaphase transition, then migrating to the equator of the midzone spindle bundle (Earnshaw and Bernat, 1991) where they are critical to the generation of cleavage (Martineau et al., 1995). Orthologs of the mammalian passenger proteins play parallel roles in cell cleavage in *C. elegans* and in *D. melanogaster* (for review, see Adams et al., 2001a).

In addition to their roles in cell cleavage, it is increasingly apparent that passenger proteins also play important roles in the proper congression of chromosomes at prometaphase and in their proper segregation during anaphase (Mackay et al., 1998; Speliotes et al., 2000; Murata-Hori et al., 2002).

The passenger proteins identified to date include INCENP (Cooke et al., 1987), survivin (Skoufias et al., 2000; Uren et al., 2000), Aurora B (Adams et al., 2000), and ORC6 (Prasanth et al., 2002). At least three of these proteins, survivin, Aurora B, and INCENP, interact as a complex (Adams et al., 2000, 2001b; Speliotes et al., 2000; Wheatley et al., 2001a). Mutation or suppression of known passenger proteins can cause cleavage failure as well as chromosome misalignment at metaphase (Mackay et al., 1998; Schumacher et al., 1998; Speliotes et al., 2000; Terada et al., 1998; Uren et al., 2000). In the case of overexpression of Aurora B dead kinase mutant, the mitotic defect can be severe, suppressing the spindle assembly checkpoint and leading to mitotic exit without an intervening metaphase (Murata-Hori et al., 2002).

We have previously identified an additional candidate passenger protein, TD-60, based on its distribution in mitosis as determined by immunofluorescence analysis with JH human autoimmune antiserum (Andreassen et al., 1991). Like the other passenger proteins, TD-60 is associated with the inner centromere of metaphase chromosomes (Martineau-Thuillier et al., 1998). The distribution of TD-60 corresponds precisely with the distribution of INCENP, Aurora B (Martineau-Thuillier et al., 1998), and survivin (Skoufias et al., 2000) through all phases of mitosis.

We have now obtained the full-length cDNA sequence of human TD-60. Sequence analysis reveals that TD-60 is a member of the RCC1 family of guanine nucleotide exchange factors (GEFs). The original member of the family, RCC1, regulates spindle aster dynamics (Kalab et al., 2002; Ohba et al., 1999) and is important for the reformation of the nuclear envelope during the transition from mitosis to G1 (Hetzer et al., 2000; Zhang and Clarke, 2000), in addition to a role in controlled nuclear import (for review, see Nakielny and Dreyfuss, 1999). Another RCC1 family member, Nercc1 may play a role in metaphase checkpoint control (Roig et al., 2002). Unlike RCC1 and Nercc1, which are expressed throughout the cell cycle, TD-60 expression, as recognized by the human autoimmune antiserum JH, is specific to late G2 and mitosis, and its localization is confined to the inner centromere until it migrates to the spindle midzone in anaphase (Andreassen et al., 1991; Martineau et al., 1995). Our results also indicate that TD-60 binds selectively to the small G protein Rac1 in its nucleotide-free form, suggesting it might act as a specific GEF for Rac1 during mitosis.

*Correspondence: margolis@ibs.fr
[5]These authors contributed equally to this work.

Developmental Cell
2

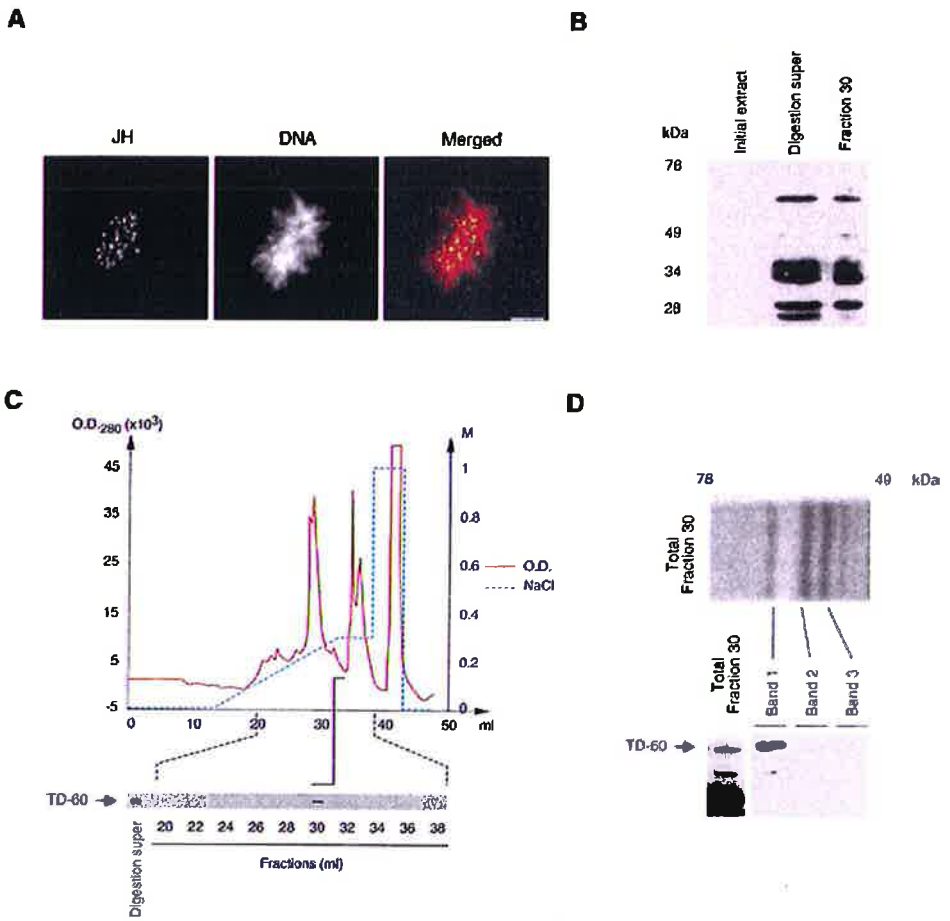

Figure 1. Purification of TD-60 from Manca Chromosomes

(A) JH human autoimmune antiserum demonstrates TD-60 specifically localizes to inner centromeres of mitotic Manca cells. JH antigen (green) is merged with DNA (red) stained with propidium iodide (right); bar = 10 μm.

(B) Presence of 60 kDa TD-60 antigen and its proteolytic fragments in different stages of purification. The antigen is not detectable by Western blot in initial chromosome isolates, but is evident in the chromosome preparation supernatant following the step of DNA digestion (digestion super). The same pattern is recovered in fraction 30 following FPLC S-HyperD column separation of the digestion supernatant.

(C) S-HyperD column profile (OD at 280 nm, red) compared with Western blot assay of the elution position of TD-60.

(D) The concentrated TD-60 peak was run on SDS-PAGE and discrete bands excised for Western blot analysis with JH antiserum. Band 1 is reactive, while bands 2 and 3 are not. All three bands, digested in-gel by trypsin, gave the same profile when subjected to MALDI analysis.

siRNA suppression shows that TD-60 is absolutely required for progression from prometaphase to metaphase. Indeed, its suppression activates the spindle assembly checkpoint, indefinitely blocking cells in mitosis. This result contrasts with results in which suppression of other passenger proteins leads to suppression of the spindle assembly checkpoint and mitotic exit despite misalignment of chromosomes at the metaphase plate, missegregation of chromosomes during anaphase, or cleavage failure. The effect of TD-60 suppression is striking with respect to kinetochore function, suggesting it plays a key role in the integration of the kinetochore into the mitotic spindle. Additionally, TD-60 suppression leads to a general inhibition of spindle assembly, suggesting it may play a global role in mitotic spindle formation and function.

Results

Purification of Human TD-60 and Identification of Its Sequence

To purify TD-60, we took advantage of its presence on inner centromeres of mitotic chromosomes (Figure 1A) (Martineau-Thuillier et al., 1998), and followed its purification with the JH human autoimmune serum. A suspension culture of human Manca cells was blocked in prometaphase with nocodazole, collected by centrifugation, and lysed. The lysate supernatant was centrifuged in a glycerol gradient from which the chromosome-rich fractions were collected, concentrated by centrifugation, and subjected to two extraction steps. The first step was a detergent extraction. Despite the release of the majority of chromosomal proteins at this

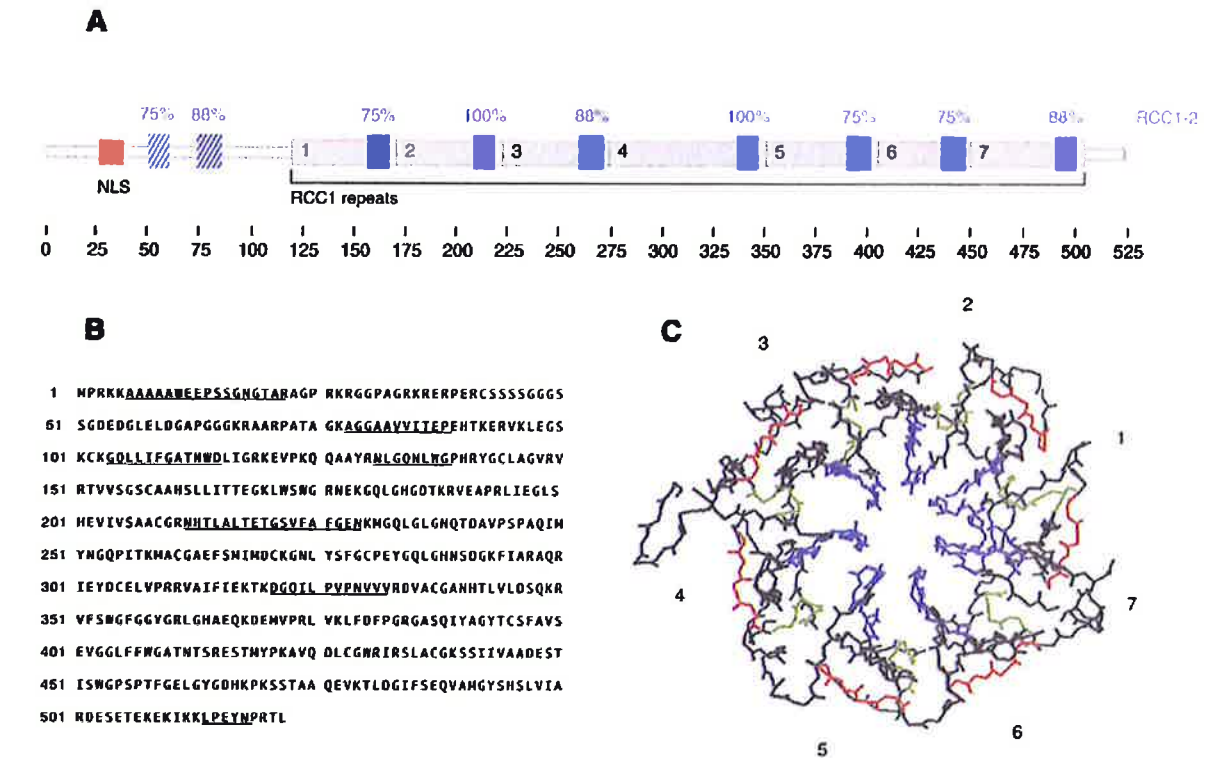

Figure 2. Comparison of TD-60 Sequence and Structure with RCC1

(A) Schematic representation of TD-60 primary sequence. The RCC1-like repeats are boxed in green. The RCC1-2 motifs are represented as blue boxes, with the Identity score shown relative to the PROSITE PS00626. The putative NLS is represented in orange.
(B) TD-60 amino acid sequence. Underlined sequences are the peptides identified using MS/MS.
(C) The tertiary structure of the RCC1 repeats of TD-60 using Swissmodel based on the 1A12 PDB coordinates of RCC1. The color coding corresponds to the structural motifs within each repeat, as detailed in (D). Numbering corresponds to the RCC1 repeat number.
(D) TD-60 repeat alignments. The top sequence is the RCC1-3 consensus (PROSITE PS50012). The scale corresponds to this entry. Red letters indicate residues matching "functional groups": DE (acid), HKR (basic), AGILV (aliphatic), NQ (amide), FWY (aromatic), ST (hydroxyl), CM (sulfur), P (imide). Gray boxes: residues matching "structural groups" DEHKNQR (external), FILMV (internal), ACGPSTWY (random). Italics: putative loops. Green boxes: GLQG structural motif. Red boxes: external β strands. Blue boxes: residues matching the RCC1-2 motif.

stage, including most of the histones (data not shown), TD-60 was not released (Figure 1B, initial extract). Following this step, the residual chromosomal material was digested with nucleases, which released TD-60 to the supernatant fraction (Figure 1B, digestion super).

The JH antiserum recognizes a characteristic pattern of several bands in the chromosomal extract containing TD-60, with a band of 60 kDa the largest. Bands smaller than 60 kDa appear to be cleavage products that arise during the purification procedure. Prior to the step of chromosome extraction, no antigen is detectable with JH antiserum using ECL detection procedures. Only the largest protein is likely to be a translation product. For further purification of TD-60, the chromosome digestion supernatant was subjected to cation exchange chromatography. Fraction 30 contained the 60 kDa TD-60 antigen, as well as the characteristic pattern of apparent degradation products (Figures 1B and 1C). Fraction 30 was concentrated and separated by PAGE, where Coomassie stain showed three major protein bands above

Developmental Cell
4

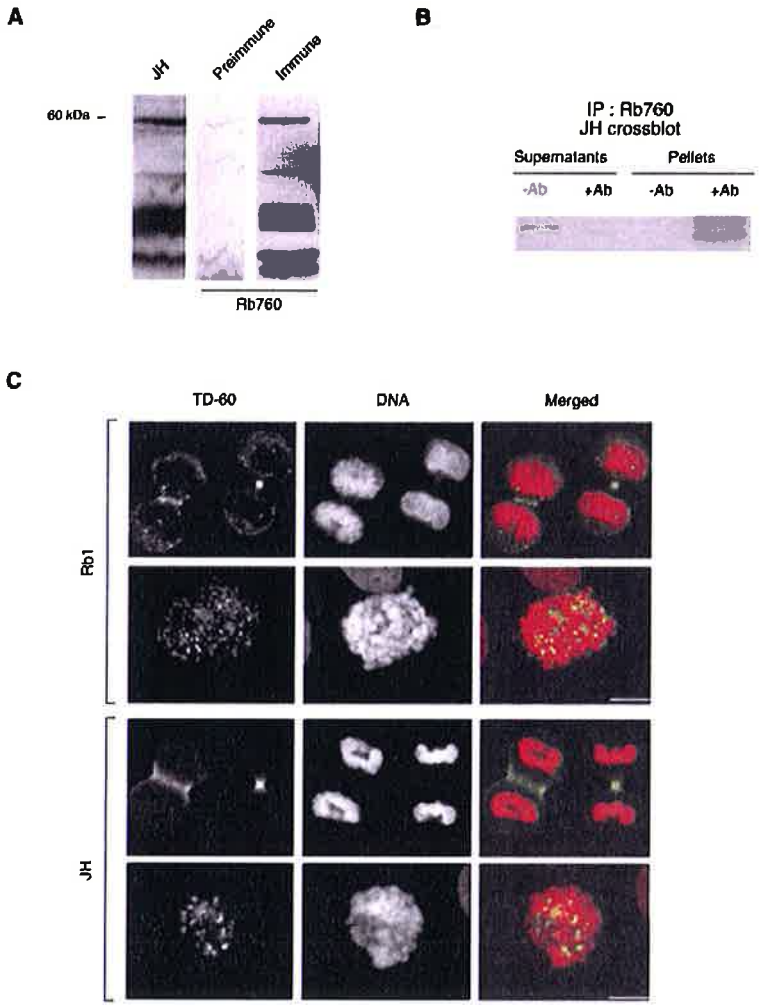

Figure 3. The TD-60 JH Antigen and the RCC1-like Protein Are Identical

(A) Rabbit polyclonal antibody Rb760 and JH antiserum recognize a similar pattern of proteolytic fragments of TD-60, as well as a protein of 60 kDa, in the digestion supernatant obtained from a Manca cell chromosome preparation. Western blots were probed with JH antiserum (left) or with either preimmune (middle) or immune serum Rb760, raised against peptide sequence from TD-60.

(B) Immunoprecipitation and crossblot analysis shows that JH antiserum recognizes the 60 kDa protein immunoprecipitated by rabbit polyclonal antibody Rb760. Lanes marked "−Ab" were immunoprecipitations performed in the absence of the primary antibody.

(C) Antibody raised against TD-60 sequence (Rb 1) localizes to the spindle midzone in anaphase and to midbodies in late telophase (upper TD-60 panel) and to centromeres in prometaphase (lower TD-60 panel). Staining with JH antiserum (green) is shown for comparison (lower panels). The counterstain for DNA (red) is propidium iodide. Bar = 10 μm.

the 49 kDa marker. Of these bands, only the highest, band 1, reacted with the JH antiserum (Figure 1D). Following in-gel digestion, trypsin fragments of all three bands were analyzed by MALDI-TOF mass spectrometry. Peptide mass fingerprints were identical for all three bands. Therefore, it is clear that all of the copurifying bands of highest mass derive from the same protein, although the antiserum recognizes only one band in this gel region.

TD-60 tryptic peptides were further analyzed by tandem mass spectrometry, yielding several amino acid sequences that were identified by BLAST searches against human ESTs. All sequences were present in a single entry (gi:7959200). We then completed the cDNA sequence by 5′RACE. We have deposited the sequence of the full-length TD-60 at EMBL under reference AJ421269.

TD-60 Sequence and Structure

Sequence analysis revealed that TD-60 has seven RCC1 repeats, shown as green boxes in the schematic representation of the primary sequence (Figure 2A). Within these repeats there is a repeated RCC1-2 motif (PROSITE PS00626), shown as blue boxes in Figure 2A. The identity scores relative to the canonical sequence are shown above the boxes. The peptide sequence of the full-length TD-60 is shown in Figure 3B. Underlined sequences are the peptides obtained by MS/MS, which are present throughout the primary sequence. In addition, there are two RCC1-2 motifs upstream of the major repeats that are not embedded within the usual RCC1 fold motifs. The TD-60 RCC1 domain has 20% identity and 38% strong similarity with RCC1. Among hypothetical TD-60 orthologs (EGO 187927), the *Drosophila* ortholog (CG9135) shares 61% strong similarity to human TD-60, and 43% identity.

We have modeled the tertiary structure using Swissmodel (Guex and Peitsch, 1997), based on the 1A12 PDB coordinates of RCC1 (Figure 2C). The numbering corresponds to the repeats (Figure 2A). Alignment of TD-60 repeats with the consensus PROSITE RCC1-3 sequence (PS50012) shows a good correspondence of each of the TD-60 repeats with the hinge (green), external (red), and RCC1-2 (blue) regions of the model RCC1 repeat (Figure 2D). The colored regions corresponding to the structural motifs of each repeat are shown in the tertiary structure model (Figure 2C).

A BLAST search of the human genome database revealed a single site on chromosome 1 (map locus 55920,

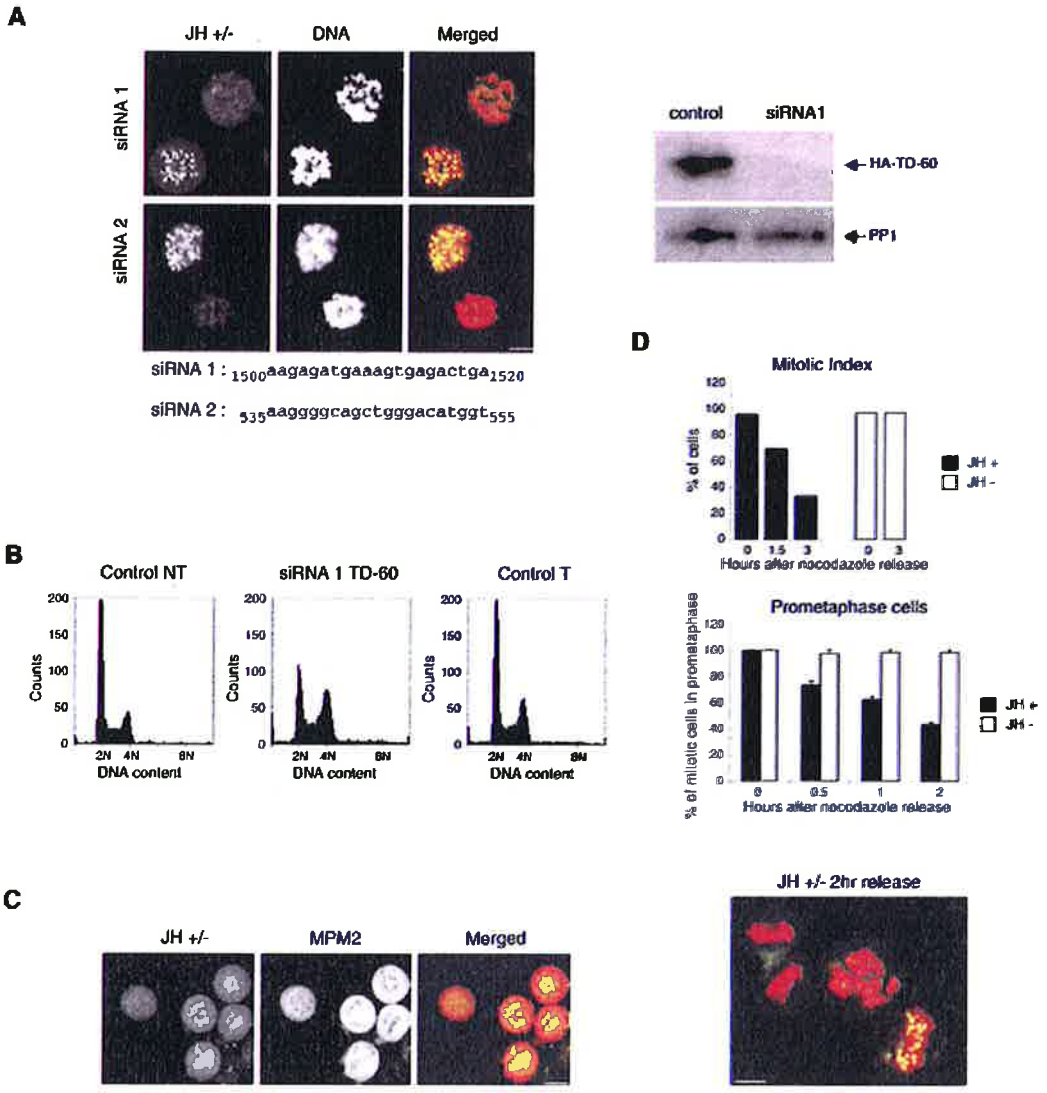

Figure 4. Suppression of TD-60 with siRNA Arrests HeLa Cells in Prometaphase

(A) siRNA suppresses the JH antigen in mitotic cells. Cells were transfected with two different siRNA double-stranded probes targeting the TD-60 sequences shown. Both suppress JH signal in mitotic HeLa cells following accumulation in mitosis with nocodazole for 16 hr. The counterstain for DNA (red) is propidium iodide. Bar = 10 μm. Western blots of extracts from cells cotransfected with siRNA1 and HA-TD-60 demonstrate that the siRNA effectively suppresses the translation of the tagged TD-60. Protein phosphatase-1, probed with pan PP-1 antibody, serves as a loading control.

(B) HeLa were transfected with siRNA1 and harvested 48 hr later. Control nontransfected cells show a normal cell cycle profile (Control NT), as do sham transfected cells, exposed to Oligofectamine without siRNA (Control T). In contrast, cells transfected with siRNA1 (siRNA1 TD-60) accumulate with a 4N DNA content.

(C) Cells with suppressed TD-60 signal, as recognized by JH antiserum, enter mitosis during treatment with nocodazole. HeLa were transfected with siRNA1, then exposed 48 hr later to 0.04 μg/ml nocodazole for 16 hr to induce mitotic arrest. Transfected cells enter mitosis by the criterion of MPM2 staining. Consistently, although JH-negative cells are positive for MPM2, they have reduced MPM2 staining relative to nontransfected neighbors. Bar = 10 μm.

(D) HeLa cells were arrested in mitosis with 0.04 μg/ml nocodazole and collected by shake off. After replating, cells were released from nocodazole block and quantitated for mitotic index by the criterion of being MPM2 antigen positive. JH-positive cells exit mitosis (upper bar graph), while JH-negative cells remain quantitatively in mitosis. Note that more than 20% of JH-positive cells remain mitotic at 3 hr. The retardation of mitotic exit results from the transfection procedure, even in untransfected cells. Cells were also scored for percentage in prometaphase by visual analysis of chromosome distribution (lower bar graph). Of the remaining mitotic cells, progressively fewer JH-positive cells were in prometaphase with time, while JH-negative cells remained quantitatively in prometaphase. A typical field of cells at 2 hr release (bottom) shows JH-positive cells in later stages of mitosis, while a JH-negative cell remains in prometaphase. JH is green; DNA (propidium iodide) is red. Bar = 10 μm.

chromosome 1p36.13) that yielded multiple BLAST hits with the TD-60 query sequence, the best alignment (KIA001470) being 100% identical to the query sequence. No other genomic sequences had equivalent identity, although we found a 30 kDa homolog (LOC221341) of TD-60 on chromosome 6, with 40% identity and 44% strong similarity to TD-60.

Demonstration that the RCC1 Protein Is TD-60

We have taken two approaches to demonstrate that the sequence obtained represents the passenger protein TD-60: analysis of antigenicity of TD-60 with antibodies raised against the database sequence, and demonstration that TD-60 signal from the original human autoimmune antiserum is suppressed in cells by transfection with siRNA targeting the database sequence.

We raised rabbit polyclonal antibodies against oligopeptides unique to TD-60 and not related to RCC1. In Western blots of the digestion supernatant from a Manca chromosome preparation (Figure 1B), one such antibody, Rb760, recognizes a protein "fingerprint" pattern similar to that recognized by JH human antiserum (Figure 3A), whereas preimmune serum from the rabbit shows no specific reaction. Further, immunoprecipitation of the same chromosome fraction with Rb760 and crossblotting with JH antiserum shows that JH recognizes the 60 kDa protein in the immunoprecipitate (Figure 3B).

While Rb760 gave no immunofluorescence signal, another polyclonal antibody, Rb1, which recognizes the same "fingerprint" pattern on Western blots (data not shown), gave the same pattern of localization to chromosomes at prometaphase and to the spindle midzone during early cleavage as observed with JH antiserum (Figure 3C), confirming that the protein sequenced is indeed a passenger protein.

We obtained further confirmation that the cDNA sequence codes for TD-60 by transfection of two distinct siRNA probes directed against two separate sequences of TD-60. Both probes extinguished JH antigen staining at the inner centromere region in early mitotic cells. We show, for each siRNA transfection, two cells in early mitosis. In both cases, one cell has no JH staining at inner centromeres (Figure 4A). By contrast, in untransfected cell cultures, all cells in early mitosis are positive for JH antigen (data not shown). Thus, transfections with both siRNAs were successful at suppressing the expression of TD-60 cDNA. When cells were cotransfected with siRNA1 to TD-60, along with cDNA for HA-tagged TD-60, Western blots showed no HA-tagged TD-60 present. By contrast, transfection with HA-tagged TD-60 cDNA alone yielded a strong HA antibody reactive signal (Figure 4A). HA-tagged coexpression of TD-60 was used because endogenous TD-60 levels are insufficient for detection on Western blots in whole-cell extracts. In contrast to extinction of TD-60, the siRNA had no effect on levels of the control, protein phosphatase-1 (PP-1).

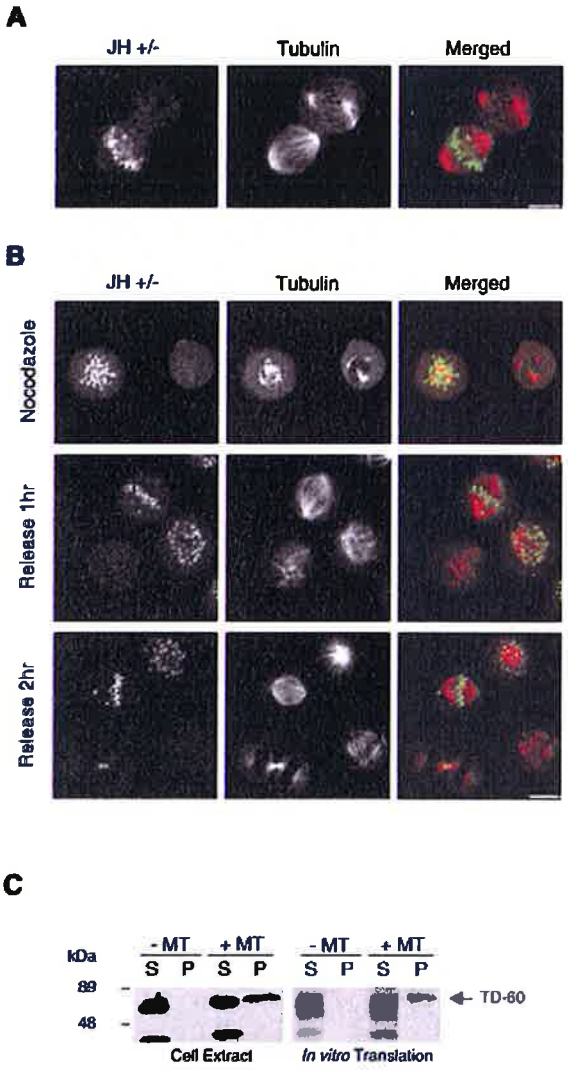

Figure 5. TD-60 Is Required for Kinetochore Integration into the Mitotic Spindle and Binds Microtubules

(A) HeLa were transfected with siRNA1, then stained 48 hr later with JH antiserum and tubulin antibody. Of two randomly cycling mitotic HeLa cells, the cell without JH signal shows separated centrosomes in the absence of TD-60, but a robust bipolar spindle is absent. By comparison, the JH-positive cell has a well-formed bipolar spindle.

(B) Transfected cells were observed following 16 hr in 0.04 μg/ml nocodazole. In the continued presence of 0.04 μg/ml nocodazole, JH-negative mitotic cells exhibit a lower microtubule assembly state and lack satellite asters normally associated with kinetochores at low nocodazole concentrations (see Andreassen and Margolis, 1994), evident as microtubules in close association with JH signal in JH-positive cells. At 1 and 2 hr release, JH-negative cells have poorly developed spindle asters compared to JH-positive cells. Bars = 10 μm.

(C) In vitro microtubule binding assay shows that full-length TD-60, isolated by extraction from chromosomes (Cell Extract, left), pellets with microtubules whereas TD-60 fragments of lower mass do not. In vitro-translated TD-60 similarly associates with microtubules (In vitro Translation, right) as determined by autoradiograph, indicating the binding is direct.

Suppression of TD-60 Expression Blocks HeLa Cells in Prometaphase

Suppression of TD-60 expression resulted in a dramatic phenotype. Forty-eight hours after transfection with siRNA1, 48% of the HeLa population was in 4N compared with 20% of untransfected and 27% of sham-transfected (Oligofectamine alone) controls (Figure 4B).

Given that approximately 50% of HeLa are transfected by these procedures (data not shown), these results are compatible with the possibility that loss of TD-60 creates an effective G2/M arrest.

Cells in which TD-60 was suppressed by siRNA were arrested in prometaphase. The arrested population contained condensed chromosomes in a prometaphase array, lamin B stain showed the nuclear envelope had dispersed (data not shown), and spindle asters had formed (see Figure 5). In randomly cycling cells at 48 hr after transfection, apparently mitotic cells that were TD-60 negative were never seen in a metaphase or anaphase configuration. When the population was arrested in mitosis with nocodazole, the apparently mitotic cells that were negative for JH antigen were also positive for MPM-2, a mitosis-specific phosphoantigen (Figure 4C). Interestingly, the intensity of MPM-2 stain was uniformly lower in TD-60-suppressed cells than in adjacent cells expressing TD-60.

We then assayed for the capacity of TD-60-suppressed cells to recover from nocodazole arrest, compared to normal controls. Cells were arrested in nocodazole for 16 hr, the mitotic subpopulation was purified by shake-off, and cells were then released from the nocodazole block. Mitotic exit was determined by loss of MPM-2 stain (Figure 4D) and by restoration of nuclei with lamin B-labeled borders (data not shown), with equivalent results. Within 3 hr of release, the majority of cells containing TD-60 had exited mitosis, while those that did not contain TD-60 remained quantitatively in mitosis. Further, the TD-60-negative cells remained quantitatively in prometaphase as scored by the absence of metaphase chromosome alignment or of anaphase figures. By contrast, those TD-60-expressing cells that were still in mitosis at 2 hr following release were in prometaphase, metaphase, and anaphase, and hence showed less than 50% remaining in prometaphase (Figure 4D). A typical field of cells (Figure 4D, bottom) shows two JH-positive cells in metaphase and telophase, and a JH-negative cell in prometaphase, at 2 hr of release from nocodazole block. We conclude that TD-60 is required for progression from prometaphase to metaphase.

TD-60 Is Important for Spindle Association with Kinetochores

HeLa cells in which TD-60 is suppressed contained reduced and aberrant spindles compared to control cells in mitosis. Typically, mitotic cells that were TD-60 negative contained well-separated spindle poles, but the spindles were not organized compared to controls containing TD-60. Two mitotic cells in a randomly cycling population are shown, one positive for TD-60 and at metaphase, the other negative for TD-60 and containing a disorganized spindle (Figure 5A). We then enriched the transfected population for mitotic cells by release from nocodazole arrest. TD-60-suppressed cells accumulated in mitosis in the presence of nocodazole. Following 1 or 2 hr release from nocodazole, mitotic cells lacking JH antigen contained smaller asters than controls (Figure 5B). When HeLa were arrested in mitosis with 0.04 μg/ml nocodazole, JH antigen-positive cells contained multiple asters, and some focused on kinetochores (Figure 5B), as we have previously reported (Andreassen and Margolis, 1994). In contrast, asters were

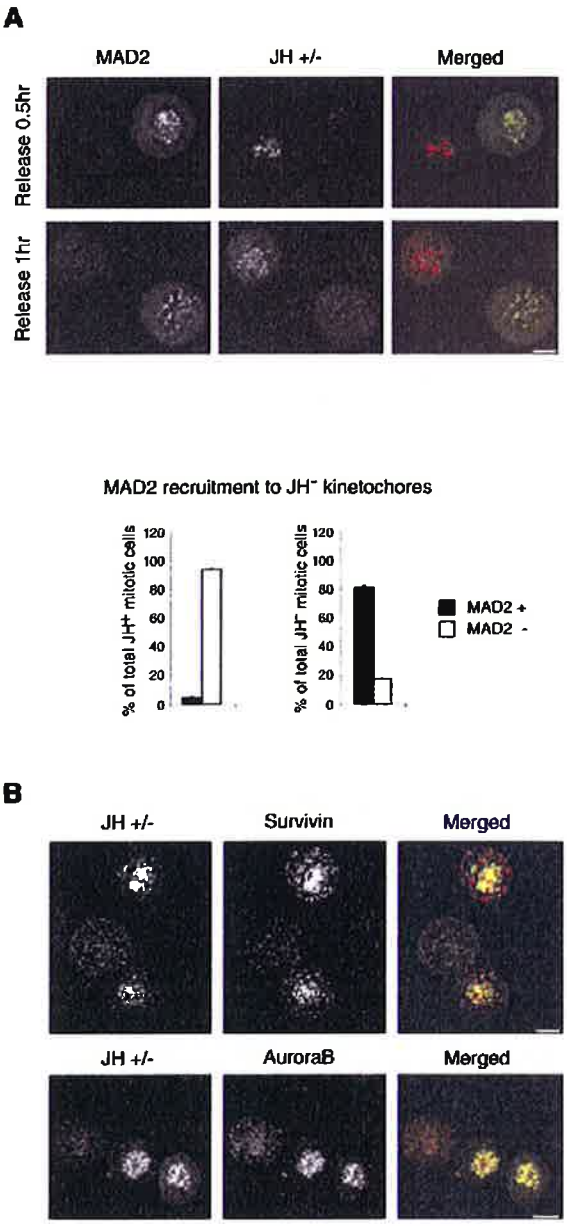

Figure 6. Effect of Loss of TD-60 on Mad2 and Passenger Protein Recruitment to Kinetochores

(A) The absence of JH recruits Mad2 to kinetochores. JH-negative cells released from 16 hr arrest with 0.04 μg/ml nocodazole for either 0.5 or 1 hr are strongly Mad2 positive while JH-positive cells are largely Mad2 negative. There is no change in Mad2 staining at kinetochores with time. The bar-graph quantitates mitotic JH-positive (left) or JH-negative (right) cells in a HeLa population transfected with siRNA1 that are Mad2 positive or negative at kinetochores after 1 hr release from nocodazole arrest. Only 5% of JH-positive cells are positive for Mad2 on kinetochores, while more than 80% of JH-negative cells are Mad2 positive. For this analysis, a GFP-Mad2 expressing HeLa cell line was used.

(B) Absence of TD-60 prevents survivin and Aurora B recruitment to kinetochores. HeLa cells were arrested in mitosis with 0.04 μg/ml nocodazole for 16 hr, then stained with JH antiserum and with survivin antibody, or with AIM-1 antibody to Aurora B. The two panels show clusters of prometaphase cells. JH-negative cells uniformly have no survivin or Aurora B localized to inner centromeres. Bars = 10 μm.

Developmental Cell
8

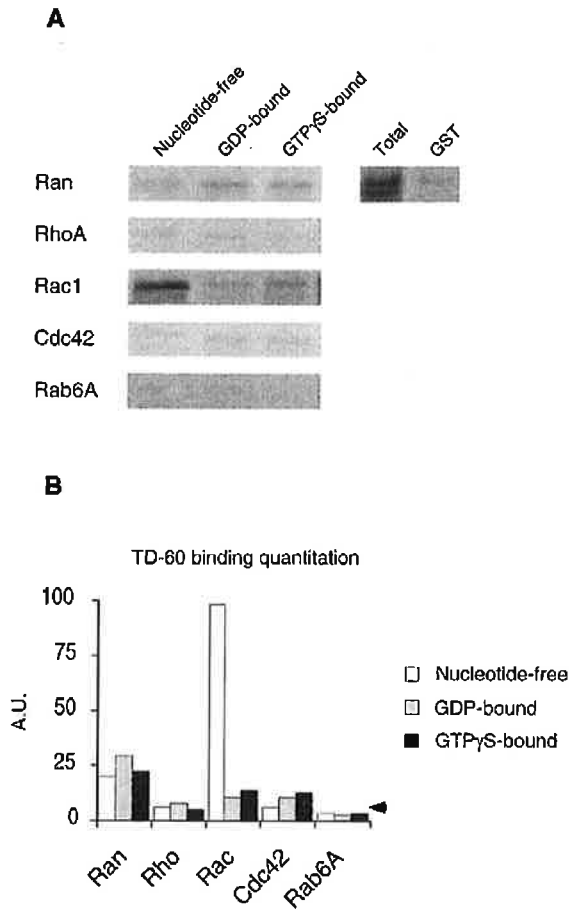

Figure 7. TD-60 Binds the Nucleotide-free Rac1

(A) In vitro-translated TD-60 (TNT) was subjected to autoradiographic analysis in GST pull-down assays of glutathione beads loaded with relevant GTPases. In these assays, the nucleotide-free form of Rac1 bound to TD-60, yielding a strong signal, whereas both GDP- and GTPγS-loaded Rac1 did not bind. In the same assay, GST fusions of Rab6A, Ran, RhoA, and cdc42 were negative for TD-60 pull-down when compared to controls in the presence of GST alone (right).

(B) Bar graph showing quantification, in arbitrary units (A.U.), of the Phosphoimager scans obtained from the autoradiographs shown in (A). Arrowhead shows the level of the nonspecific TD-60 binding on GST alone.

few in number, small, and not associated with chromosomes in JH-negative cells (Figure 5B).

Coupled with the observed failure of JH antigen-negative cells to progress to metaphase, these results suggested that TD-60 is critical to the integration of kinetochores into the mitotic spindle, and additionally may be required for overall spindle assembly. We therefore tested for the possibility that TD-60 can associate with microtubules in vitro. In an in vitro microtubule binding assay, full-length TD-60 isolated from human chromosomes pelleted in the presence, but not in the absence, of microtubules (Figure 5C). Interestingly, only full-lengthTD-60 pelleted in the presence of microtubules, while its fragments did not. This suggests that the correct folding of TD-60 may be important to its association with microtubules, and that association is thus possibly of physiological importance. Direct binding of TD-60 to microtubules was confirmed by assay of microtubule association following in vitro translation of TD-60 (Figure 5C).

Mad2 is a spindle assembly checkpoint protein that is recruited to kinetochores when they have not engaged into the mitotic spindle (Skoufias et al., 2001). A consequence of the failure of chromosomes to associate with microtubules during mitosis should thus be the continued presence of Mad2 on kinetochores. To assay for this possibility, HeLa cells selected to express GFP-Mad2 were transfected with siRNA1 to suppress TD-60 translation. Cells were then blocked with nocodazole and released 0.5 or 1 hr to allow kinetochore association with microtubules in control cells (Figure 5B) (Andreassen and Margolis, 1994).

Cells positive for TD-60 were largely negative for Mad2 during drug-released prometaphase, indicating microtubule association with the kinetochores. In contrast, cells that were negative for TD-60 were largely positive for Mad2 on kinetochores, and the extent of Mad2 association with kinetochores did not visibly vary with time of nocodazole release (Figure 6A, images). The results were consistent with a TD-60 requirement for the association of kinetochores with spindle microtubules during prometaphase. To quantitate the correlation between TD-60 absence and Mad2 presence on kinetochores, HeLa cells, transfected with siRNA1, were released from nocodazole arrest for 1 hr and scored for the presence or absence of Mad2 on kinetochores as a function of the presence of TD-60. As shown in the bar graph (Figure 6A), kinetochores were Mad2 positive in virtually all TD-60-negative cells, while the majority of TD-60-positive cells were Mad2 negative.

Previous work has demonstrated that several passenger proteins are interdependent for recruitment to the inner centromere (for review, see Adams et al., 2001a). We therefore tested for the effect of suppression of TD-60 on the presence of other passenger proteins, survivin and Aurora B, at inner centromeres in mitosis. HeLa cells were transfected with siRNA1 and blocked in mitosis with nocodazole. Those mitotic cells that contained JH antigen were also positive for survivin and Aurora B at inner centromeres, while cells in which JH antigen was suppressed also showed loss of survivin and Aurora B (Figure 6B). The presence of TD-60 is therefore critical for the recruitment of other passenger proteins to inner centromeres in mitosis.

TD-60 Is a Potential Exchange Factor for the Small GTPase Rac1

TD-60 is highly related to the guanine exchange factor (GEF) for the Ras-like small GTPase Ran. We have thus screened a panel of GTPases for putative binding to TD-60 in a yeast two-hybrid assay using histidine auxotrophy and β-galactosidase activity as readout (Janoueix-Lerosey et al., 1995). Dominant-negative, dominant-active, or wild-type forms of Ran, Rab6A, Rab6A′, RhoA, cdc42, and Rac1 have been tested. Among them, the dominant-negative form of Rac1 (T17N), and to a lesser extent the dominant-negative forms of Rab6A (T27N) and cdc42 (T17N), grew on histidine, while all three forms of Ran and RhoA were unable to grow (data

not shown). We then tested the ability of in vitro-translated TD-60 to bind these GTPases in pull-down assays in the presence of GDP, GTPγS, or in the absence of nucleotide (Figure 7). As expected from the two-hybrid screen, Ran and RhoA are unable to bind TD-60 in all conditions tested (Figure 7A). TD-60 is pulled down neither by Rab6A nor by cdc42 regardless of their nucleotide state, despite their weakly positive growth in two-hybrid tests. In contrast, TD-60 is effectively pulled down by Rac1, and the pull-down is ten times more efficient in the absence of added nucleotide than in the presence of nonhydrolyzable GTP or in the presence of GDP (Figure 7B). This result is consistent with the expected behavior of a guanine exchange factor, which stabilizes the nucleotide-free form of the target GTPase (Vetter and Wittinghofer, 2001). Unfortunately, inability to produce active recombinant TD-60 prevented a direct test of its GEF activity on Rac1.

Discussion

The Passenger Protein TD-60 Is an RCC1 Protein

We have purified and sequenced the human passenger protein TD-60 and have demonstrated that it is a member of the RCC1 family, with a strong conservation of RCC1 motif repeats. Alignment of its sequence with RCC1 reveals it is also likely to fold as a seven propeller protein, with proper alignment of its hinge, external β strand, and RCC1-2 motifs superimposable on the structure of RCC1. The protein that we have cloned is identical with the JH antigen by several criteria. First, in Western blots of chromosome extracts, an antibody raised against the sequenced protein recognizes the same pattern of proteolytic fragments of TD-60 as the human autoimmune antiserum JH, which was originally used for identification of the antigen. Second, immunoprecipitation and cross-blot analysis shows that the rabbit antibody pulls down the JH antigen. Third, a polyclonal antibody raised against TD-60 sequence shows the typical passenger protein staining pattern in mitosis. Fourth, two independent siRNA sequences both suppress the JH antigen signal at inner centromeres of transfected cells.

Significantly, by suppressing TD-60 with siRNA transfection, we have also demonstrated that TD-60 is required for cell cycle progression from prometaphase to metaphase. TD-60 is unique among the passenger proteins in that its suppression activates the spindle assembly checkpoint and prevents progression to metaphase, leading to indefinite mitotic arrest. These results suggest an important role for TD-60 in kinetochore integration into the mitotic spindle. Our results can be compared with the severe phenotype reported following overexpression of Aurora B dead kinase in mammalian cells (Murata-Hori et al., 2002). In that case, chromosomes failed to align on a metaphase plate, but the spindle assembly checkpoint was suppressed and cells were not inhibited from exiting mitosis. On the whole, the other passenger proteins, Aurora B, INCENP, and survivin, have been demonstrated to play a role in proper chromosome alignment, segregation during anaphase, and in cell cleavage. In contrast, TD-60 is uniquely required for integration of kinetochores into the mitotic spindle and satisfaction of the spindle assembly checkpoint.

The fact that TD-60 is required for proper integration of kinetochores into the mitotic spindle suggests a role for TD-60 in microtubule association with the kinetochores in early mitosis. It is interesting in this light that we have found that TD-60 can associate with microtubules in vitro. The association is probably direct, as the in vitro-translated protein retains microtubule binding behavior. Direct microtubule binding has also been reported for INCENP (Wheatley et al., 2001b), another passenger protein. Interestingly, both TD-60 and INCENP associate with the mitotic spindle only during anaphase, suggesting microtubule association is tightly controlled. It remains to be determined whether the microtubule association of TD-60 is essential to its function in the cell.

The role of TD-60 in cell cleavage has been obscured by the strong epistatic effect of its suppression on progression to metaphase. However, loss of TD-60 causes survivin and Aurora B to disperse from inner centromeres of mitotic cells, and as survivin and Aurora B have been shown to be essential for cell cleavage (Terada et al., 1998; Uren et al., 2000), it is likely that TD-60 is required for the cell cleavage mechanism. Further support for a role of TD-60 in cleavage comes from our previous demonstration of a strong correlation between TD-60 localization to the cell cortex and actin recruitment for cleavage induction (Martineau et al., 1995).

The RCC1 Family and Mitotic Regulation

The effect of TD-60 on mitotic spindle function is of interest in light of its identity as a member of the RCC1 family. RCC1 is a GEF for Ran-GTPase (Bischoff and Ponstingl, 1991). The strongest evidence of a function for RCC1 in spindle formation comes from work on spindle reconstruction in *Xenopus* oocyte mitotic extracts. Following the depletion of RCC1 or introduction of mutant Ran (Carazo-Salas et al., 1999; Kalab et al., 1999; Ohba et al., 1999; Wilde and Zheng, 1999), a bipolar spindle does not form and chromosomes do not become engaged in the astral microtubules. In contrast, suppression of RCC1 in mutant cell lines has shown that loss of RCC1 function does not affect the formation of a bipolar spindle in mammalian cells (Nishitani et al., 1991).

TD-60 binds the small G protein Rac1 and is unique among the RCC1 family in this respect, although there is precedence for a RCC1 protein binding to small G-proteins other than Ran, as the RCC1 domain protein p619 stimulates GTP exchange on ARF1 and Rab proteins (Rosa et al., 1996). Further, it is likely that TD-60 is an exchange factor for Rac1, as it has the characteristic signature of a GEF, binding preferentially to the unloaded form of the GTPase (Vetter and Wittinghofer, 2001).

It is noteworthy that Rac1 mutants have been reported to arrest mammalian cells in G2/M (Moore et al., 1997), and it will be of great interest to determine if this effect occurs in prometaphase, with TD-60 involvement. Rac1 is key to activation of p65PAK, which in turn regulates

stathmin activity (Daub et al., 2001). As stathmin regulates microtubule dynamics in the mitotic spindle (Belmont and Mitchison, 1996), TD-60 may be directly involved in this pathway of microtubule regulation at prometaphase. We note with interest, in light of the possibility that TD-60 may thus act globally on microtubule dynamics, since cells in which siRNA has suppressed TD-60 exhibit generally smaller spindles than controls (Figure 5).

Rac1 has been also recently reported to participate in CLIP170-dependent microtubule plus-end capture through IQGAP1, a GTPase-activating protein for Rac1 and cdc42 (Fukata et al., 2002). CLIP170 is also known to participate in kinetochore function in prometaphase (Dujardin et al., 1998), raising the intriguing possibility that TD60 may act as a GEF for Rac1 in the prometaphase to metaphase transition.

Further, there is suggestive evidence that Rac1 may have a role in cytokinesis. MgcRacGAP/Cyk4 (Toure et al., 1998) localizes to the mitotic spindle and the midbody during mitosis, and both dominant mutants and siRNA depletion cause cleavage failure (Hirose et al., 2001). While it has been suggested that MgcRacGAP/Cyk4 acts on RhoA during cytokinesis, Rac1 is a far better substrate for MgcRacGAP/Cyk4 than is RhoA (Jantsch-Plunger et al., 2000; Toure et al., 1998). Further, the Rho dissociation inhibitor, GDI1, which is required for cytokinesis in *Dictyostelium*, was recently shown to bind members of the Rac family (Rivero et al., 2002), and members of the Rac family have been shown essential for cytokinesis in this species (Dumontier et al., 2000).

TD-60 Function as a Passenger Protein

Passenger proteins (Earnshaw and Bernat, 1991) play a key role in the proper completion of cytokinesis in mammalian cells (Mackay et al., 1998; Martineau et al., 1995; Terada et al., 1998). They are present on inner centromeres until the onset of anaphase. They then associate with the mitotic spindle and relocate to the midzone position of the mitotic spindle where they spread laterally from the spindle equator late in anaphase just prior to cleavage (Andreassen et al., 1991; Earnshaw and Bernat, 1991), finally ending in the midbody that links the two daughter cells upon completion of cell cleavage. Several members of the mammalian passenger protein family have been identified, including INCENP (Cooke et al., 1987), survivin (Skoufias et al., 2000; Uren et al., 2000), Aurora B (Terada et al., 1998), and ORC6 (Prasanth et al., 2002). The identity is known for all these proteins. We have now added TD-60 to the list of passenger proteins with known sequence.

Among the passenger proteins, the only one to date with an identifiable function in mitosis is Aurora B, a protein kinase. TD-60 is likely to have a distinct function as a GEF. An understanding of its detailed function in cell cleavage will greatly help to elucidate the molecular detail of the cleavage control mechanism.

INCENP, survivin, and Aurora B form a complex in vivo (Adams et al., 2000; Wheatley et al., 2001a). Since TD-60 shows an entirely coincident localization throughout mitosis with INCENP, survivin, and Aurora B (Martineau-Thuillier et al., 1998; Skoufias et al., 2000), it will now be of substantial interest to establish whether TD-60 forms a complex with these other passenger proteins. However, the role of TD-60 in prometaphase progression suggests a function that is at least partially independent of the other passenger proteins.

Experimental Procedures

Cell Culture

Manca (human leukemia) cells were maintained in suspension in RPMI 1640 medium (Roswell Park Memorial Institute, GIBCO) containing 5% bovine serum (Hyclone). HeLa and GFP-Mad2 cells were grown in DMEM (Dulbecco's modified Essential medium; GIBCO) containing 10% Fetal Calf Serum (Biological Industries). When specified, cells were treated with 0.04 μg/ml nocodazole for 16 hr, and released as mentioned in figure legends, in drug-free medium.

To derive HeLa cells constitutively expressing GFP-Mad2, we subcloned human Mad2 cDNA, a generous gift from Dr. Benezra (Sloan-Kettering, NY), into pEGFP-C2 (Clontech). HeLa cells were transfected using Lipofectamine 2000 (InVitrogen) and selected after 48 hr with G418 (GIBCO). Cells positive for nuclear envelope signal were selected (Campbell et al., 2001) and further screened using as a final criterion the kinetochore labeling of cells arrested in mitosis with nocodazole.

Chromosome Extraction of TD-60

The protocol used for the mitotic chromosome isolation is a modification of the procedure of Gasser and Laemmli (Gasser and Laemmli, 1987). 3 liters of Manca cells (6×10^5 cells/ml), were blocked in mitosis with 0.08 μg/ml nocodazole for 12 hr, harvested by centrifugation (10 min, 750 × g), rinsed in 100 ml of cold PBS, resuspended in 44 ml of lysis buffer (buffer A: Tris 7.5 mM, pH 7.4, 1 mM EDTA, 40 mM KCl, 0.1 mM spermine, 0.25 mM spermidine, 0.1%; plus thiodiglycol, 0.1% Triton X 100, 1 mM PMSF, 10 μg/ml aprotinin, 10% glycerol) and lysed by Dounce homogenization. At the end of homogenization, the presence of intact interphase nuclei was verified by microscopy. The lysate (11 ml/tube) was layered onto glycerol gradients (20 ml 25% glycerol and 5 ml 70% glycerol, in lysis buffer) and centrifuged 20 min at 4°C, 1000 × g. The pellet, containing purified chromosomes, was resuspended, washed, and centrifuged twice in lysis buffer (minus glycerol). For the first extraction step, each chromosome pellet was resuspended in 1 ml of extraction buffer (buffer A plus NaCl 150 mM, 1% deoxycholic acid, 1% NP40, 1 mM PMSF, 2 μg/ml aprotinin, 2 μg/ml leupeptin), agitated 30 min at 4°C, and centrifuged (10 min, 1000 × g). The pellet was resuspended in 1 ml digestion buffer (Tris 10 mM, pH 8, 1 mM $CaCl_2$, 10 mM $MgCl_2$, Dnase I 2000 UA_{260}/ml, 3000 UA_{260}/ml micrococcal nuclease, 1 mM PMSF, 10 μg/ml aprotinin, 10 μg/ml leupeptin) and agitated 1 hr at 37°C. Finally, the chromosome preparation was centrifuged 45 min at 4°C, 17,000 × g. TD-60 was in the supernatant fraction.

Column Purification of TD-60

The digestion supernatant, derived from several Manca cell purification runs of 30 liters each, was loaded onto a S-HyperD 10 column (Biosepra) and eluted with a 20 ml linear gradient of 0–400 mM NaCl in 50 mM Tris (pH 8) buffer. Fractions were assayed for the presence of TD-60 by Western blot using JH antiserum, pooled, concentrated using a Centricon, and then run on 8% SDS-PAGE. Coomassie blue stained bands were recovered and a portion of each was used for blotting or for in-gel digestion by trypsin.

TD-60 Cloning, In Vitro Translation, and Microtubule Assay

TD-60 coding region was amplified by PCR with the Pfx Platinum (InVitrogen) using oligonucleotides 5′CTCATCACTCCAACCAGCC GCGCATATGCCCAGGA3′ and 5′CGCGGATCCTCAGAGGGTTCG GGGGTTGTATTC3′. The NdeI-BamHI fragment (1.5 kb) was then filled in by Klenow and subcloned into EcoRV of HA-pCDNA3(+) (InVitrogen). The resulting HA tag resides at the NH_2-terminal region of TD-60 protein.

This construct has been used as template for in vitro translation

using TNT with Transcend (Promega) or Translabel (Amersham) labeling systems, according to manufacturers' specifications.

TD-60 purified from extract or from TNT was assayed for microtubule affinity as described elsewhere (Mollinari et al., 2002). After ultracentrifugation, pellet and supernatant fractions were loaded on 10% SDS-PAGE, blotted, stained using Ponceau, and then probed with JH antiserum. Tubulin obtained from bovine brain by standard purification protocols (Farrell et al., 1987) was the kind gift of Dr. L. Wilson.

Mass Spectrometry Analysis

MALDI mass spectra of peptide mixtures were obtained using a Biflex (Bruker Daltonik, Bremen, Germany) matrix-assisted laser desorption/ionization time-of-flight (MALDI-TOF) mass spectrometer. Tandem mass spectrometry experiments were carried out on a Q-TOF hybrid mass spectrometer (Micromass, Manchester, UK) working in the nanospray mode, essentially as described (Garin et al., 2001). The cDNA clone (AB040903, EMBL), was obtained from the HUGE database.

GTPase Pull-Down Assays

TD-60 binding assays have been performed using in vitro-translated TD-60 obtained as described above, employing a procedure described elsewhere (Monier et al., 2002). Briefly, 50 μg of the different GST-GTPases were coupled to 150 μl of glutathione beads and then divided in three equal parts: loaded with either GDP, GTPγS, or without added nucleotide. The interaction assay was performed in the presence of 35 μl of ^{35}S-labeled TNT mix. After exhaustive rinses, bound proteins were separated by SDS gel electrophoresis and analyzed by gel autoradiography or using Phosphoimager (Molecular Dynamics) for quantitation.

Antibodies, Immunoprecipitation, and Western Blots

Rabbit polyclonal antibodies were raised commercially (Eurogentec) against peptides 178-EKGQLGHGDTKRVEA-192 (Rb760) and a mix of 22-RAGPRKRGGPAGRKRE-37 and 311-RVAIFIEKTKDGQILP-326 (Rb1), using conventional protocols. The IgG fraction was obtained from whole serum prior to use, by Caprylic acid precipitation (Habeeb and Francis, 1984). Immunoprecipitations were performed as described (Skoufias et al., 2001). For Western blots, JH human autoimmune serum was used at 1:10000, Rb760 polyclonal antibody, anti-HA monoclonal antibody (Babco), and anti-PP1 monoclonal antibody (E-9; Santa Cruz) were used at 1:1000.

siRNA Oligonucleotides and Transfection

To suppress TD-60 expression by RNA interference technique, two sequences of TD-60 cDNA were chosen and corresponding duplexes were synthetized, siRNA1: 1500-1520 (Dharmacon), and siRNA2: 535-555 (Xeragon). Transfection conditions using Oligofectamine (InVitrogen) were as described (Elbashir et al., 2001). Cells were directly collected or nocodazole treated 48 hr after transfection. HeLa cells were also transfected by Lipofectamine 2000 with 10 μg of HA-TD-60 plasmid according to manufacturer's instructions. 24 hr after transfection, cells were treated with siRNA1 as described above.

Flow Cytometry

Randomly cycling cells, or cells transfected with siRNA1 oligonucleotide for 48 hr, were harvested, fixed, and labeled with MPM2 antibodies and propidium iodide as previously described (Andreassen and Margolis, 1994). Data were collected using a FACScan flow cytometer (Becton Dickinson). For each sample, 10,000 events were collected, and aggregated cells were gated out.

Immunofluorescence

HeLa cells were grown and fixed with 2% paraformaldehyde as described (Mollinari et al., 2002). Nocodazole-treated cells were pelleted at low speed, fixed, and, after permeabilization, applied to treated coverslips by a short spin. Cells were then processed using conventional methods (Mollinari et al., 2002). In this study we used anti-survivin polyclonal antibody (Novus Biological, 1:500), anti-MPM2 and AIM-1 (anti Aurora B) monoclonal antibodies (Transduction Laboratories, 1:100), and Rb1 (anti TD-60). Secondary antibodies, including FITC-conjugated affinity-purified goat anti-human IgG, Alexafluor-568-conjugated goat anti-rabbit IgG (Molecular Probes) and Cyanin3-conjugated goat anti-mouse IgG (Pierce) were used at 2.5 μg/ml.

Acknowledgments

We thank D. Skoufias for the GFP-Mad2 HeLa cells, and P. Gans for help in sequence analysis. We are grateful to Drs. Shuh Narumiya, Philippe Fort, Philippe Chavrier, Gérard Gacon, and Anne-Marie Tassin for providing us with two-hybrid plasmid vectors and GST-fusion constructs of small GTPases. This work was supported by La Ligue Nationale Contre le Cancer (Laboratoire Labelisé) and Association pour la Recherche contre le Cancer (ARC #4666) (R.L.M.). C.M. was supported by a Telethon fellowship (Telethon Fondazione Onlus, Italy). C.R. was supported by a fellowship from La Ligue Nationale Contre le Cancer. J.P.K. is a researcher of the Commissariat à l'Energie Atomique.

Received: December 16, 2002
Revised: April 1, 2003
Accepted: May 27, 2003
Published: August 11, 2003

References

Adams, R.R., Carmena, M., and Earnshaw, W.C. (2001a). Chromosomal passengers and the (aurora) ABCs of mitosis. Trends Cell Biol. *11*, 49–54.

Adams, R.R., Maiato, H., Earnshaw, W.C., and Carmena, M. (2001b). Essential roles of Drosophila inner centromere protein (INCENP) and aurora B In hIstone H3 phosphorylation, metaphase chromosome alignment, kinetochore disjunction, and chromosome segregation. J. Cell Biol. *153*, 865–880.

Adams, R.R., Wheatley, S.P., Gouldsworthy, A.M., Kandels-Lewis, S.E., Carmena, M., Smythe, C., Gerloff, D.L., and Earnshaw, W.C. (2000). INCENP binds the Aurora-related kinase AIRK2 and is required to target it to chromosomes, the central spindle and cleavage furrow. Curr. Biol. *10*, 1075–1078.

Andreassen, P.R., and Margolis, R.L. (1994). Microtubule dependency of p34cdc2 inactivation and mitotic exit in mammalian cells. J. Cell Biol. *127*, 789–802.

Andreassen, P.R., Palmer, D.K., Wener, M.H., and Margolis, R.L. (1991). Telophase disc: a new mammalian mitotic organelle that bisects telophase cells with a possible function in cytokinesis. J. Cell Sci. *99*, 523–534.

Belmont, L.D., and Mitchison, T.J. (1996). Identification of a protein that interacts with tubulin dimers and increases the catastrophe rate of microtubules. Cell *84*, 623–631.

Bischoff, F.R., and Ponstingl, H. (1991). Mitotic regulator protein RCC1 is complexed with a nuclear ras-related polypeptide. Proc. Natl. Acad. Sci. USA *88*, 10830–10834.

Campbell, M.S., Chan, G.K., and Yen, T.J. (2001). Mitotic checkpoint proteins HsMAD1 and HsMAD2 are associated with nuclear pore complexes in interphase. J. Cell Sci. *114*, 953–963.

Carazo-Salas, R.E., Guarguaglini, G., Gruss, O.J., Segref, A., Karsenti, E., and Mattaj, I.W. (1999). Generation of GTP-bound Ran by RCC1 is required for chromatin-induced mitotic spindle formation. Nature *400*, 178–181.

Cooke, C.A., Heck, M.M., and Earnshaw, W.C. (1987). The inner centromere protein (INCENP) antigens: movement from inner centromere to midbody during mitosis. J. Cell Biol. *105*, 2053–2067.

Daub, H., Gevaert, K., Vandekerckhove, J., Sobel, A., and Hall, A. (2001). Rac/Cdc42 and p65PAK regulate the microtubule-destabilizing protein stathmin through phosphorylation at serine 16. J. Biol. Chem. *276*, 1677–1680.

Dujardin, D., Wacker, U.I., Moreau, A., Schroer, T.A., Rickard, J.E., and De Mey, J.R. (1998). Evidence for a role of CLIP-170 in the

establishment of metaphase chromosome alignment. J. Cell Biol. *141*, 849–862.

Dumontier, M., Hocht, P., Mintert, U., and Faix, J. (2000). Rac1 GTPases control filopodia formation, cell motility, endocytosis, cytokinesis and development in Dictyostelium. J. Cell Sci. *113*, 2253–2265.

Earnshaw, W.C., and Bernat, R.L. (1991). Chromosomal passengers: toward an integrated view of mitosis. Chromosoma *100*, 139–146.

Elbashir, S.M., Harborth, J., Lendeckel, W., Yalcin, A., Weber, K., and Tuschl, T. (2001). Duplexes of 21-nucleotide RNAs mediate RNA interference in cultured mammalian cells. Nature *411*, 494–498.

Farrell, K.W., Jordan, M.A., Miller, H.P., and Wilson, L. (1987). Phase dynamics at microtubule ends: the coexistence of microtubule length changes and treadmilling. J. Cell Biol. *104*, 1035–1046.

Fukata, M., Watanabe, T., Noritake, J., Nakagawa, M., Yamaga, M., Kuroda, S., Matsuura, Y., Iwamatsu, A., Perez, F., and Kaibuchi, K. (2002). Rac1 and Cdc42 capture microtubules through IQGAP1 and CLIP-170. Cell *109*, 873–885.

Garin, J., Diez, R., Kieffer, S., Dermine, J.F., Duclos, S., Gagnon, E., Sadoul, R., Rondeau, C., and Desjardins, M. (2001). The phagosome proteome: insight into phagosome functions. J. Cell Biol. *152*, 165–180.

Gasser, S.M., and Laemmli, U.K. (1987). Improved methods for the isolation of individual and clustered mitotic chromosomes. Exp. Cell Res. *173*, 85–98.

Guex, N., and Peitsch, M.C. (1997). SWISS-MODEL and the Swiss-PdbViewer: an environment for comparative protein modeling. Electrophoresis *18*, 2714–2723.

Habeeb, A.F., and Francis, R.D. (1984). Preparation of human immunoglobulin by caprylic acid precipitation. Prep. Biochem. *14*, 1–17.

Hetzer, M., Bilbao-Cortes, D., Walther, T.C., Gruss, O.J., and Mattaj, I.W. (2000). GTP hydrolysis by Ran is required for nuclear envelope assembly. Mol. Cell *5*, 1013–1024.

Hirose, K., Kawashima, T., Iwamoto, I., Nosaka, T., and Kitamura, T. (2001). MgcRacGAP is involved in cytokinesis through associating with mitotic spindle and midbody. J. Biol. Chem. *276*, 5821–5828.

Janoueix-Lerosey, I., Jollivet, F., Camonis, J., Marche, P.N., and Goud, B. (1995). Two-hybrid system screen with the small GTP-binding protein Rab6. Identification of a novel mouse GDP dissociation inhibitor isoform and two other potential partners of Rab6. J. Biol. Chem. *270*, 14801–14808.

Jantsch-Plunger, V., Gonczy, P., Romano, A., Schnabel, H., Hamill, D., Schnabel, R., Hyman, A.A., and Glotzer, M. (2000). CYK-4: a Rho family GTPase activating protein (GAP) required for central spindle formation and cytokinesis. J. Cell Biol. *149*, 1391–1404.

Kalab, P., Pu, R.T., and Dasso, M. (1999). The ran GTPase regulates mitotic spindle assembly. Curr. Biol. *9*, 481–484.

Kalab, P., Weis, K., and Heald, R. (2002). Visualization of a Ran-GTP gradient in interphase and mitotic Xenopus egg extracts. Science *295*, 2452–2456.

Mackay, A.M., Ainsztein, A.M., Eckley, D.M., and Earnshaw, W.C. (1998). A dominant mutant of inner centromere protein (INCENP), a chromosomal protein, disrupts prometaphase congression and cytokinesis. J. Cell Biol. *140*, 991–1002.

Martineau, S.N., Andreassen, P.R., and Margolis, R.L. (1995). Delay of HeLa cell cleavage into interphase using dihydrocytochalasin B: retention of a postmitotic spindle and telophase disc correlates with synchronous cleavage recovery. J. Cell Biol. *131*, 191–205.

Martineau-Thuillier, S., Andreassen, P.R., and Margolis, R.L. (1998). Colocalization of TD-60 and INCENP throughout G2 and mitosis: evidence for their possible interaction in signalling cytokinesis. Chromosoma *107*, 461–470.

Mollinari, C., Kleman, J.P., Jiang, W., Schoehn, G., Hunter, T., and Margolis, R.L. (2002). PRC1 is a microtubule binding and bundling protein essential to maintain the mitotic spindle midzone. J. Cell Biol. *157*, 1175–1186.

Monier, S., Jollivet, F., Janoueix-Lerosey, I., Johannes, L., and Goud, B. (2002). Characterization of novel Rab6-interacting proteins involved in endosome-to-TGN transport. Traffic *3*, 289–297.

Moore, K.A., Sethi, R., Doanes, A.M., Johnson, T.M., Pracyk, J.B., Kirby, M., Irani, K., Goldschmidt-Clermont, P.J., and Finkel, T. (1997). Rac1 is required for cell proliferation and G2/M progression. Biochem. J. *326*, 17–20.

Murata-Hori, M., Tatsuka, M., and Wang, Y.L. (2002). Probing the dynamics and functions of aurora B kinase in living cells during mitosis and cytokinesis. Mol. Biol. Cell *13*, 1099–1108.

Nakielny, S., and Dreyfuss, G. (1999). Transport of proteins and RNAs in and out of the nucleus. Cell *99*, 677–690.

Nishitani, H., Ohtsubo, M., Yamashita, K., Iida, H., Pines, J., Yasudo, H., Shibata, Y., Hunter, T., and Nishimoto, T. (1991). Loss of RCC1, a nuclear DNA-binding protein, uncouples the completion of DNA replication from the activation of cdc2 protein kinase and mitosis. EMBO J. *10*, 1555–1564.

Ohba, T., Nakamura, M., Nishitani, H., and Nishimoto, T. (1999). Self-organization of microtubule asters induced in Xenopus egg extracts by GTP-bound Ran. Science *284*, 1356–1358.

Prasanth, S.G., Prasanth, K.V., and Stillman, B. (2002). Orc6 involved in DNA replication, chromosome segregation, and cytokinesis. Science *297*, 1026–1031.

Rivero, F., Illenberger, D., Somesh, B.P., Dislich, H., Adam, N., and Meyer, A.K. (2002). Defects in cytokinesis, actin reorganization and the contractile vacuole in cells deficient in RhoGDI. EMBO J. *21*, 4539–4549.

Roig, J., Mikhailov, A., Belham, C., and Avruch, J. (2002). Nercc1, a mammalian NIMA-family kinase, binds the Ran GTPase and regulates mitotic progression. Genes Dev. *16*, 1640–1658.

Rosa, J.L., Casaroli-Marano, R.P., Buckler, A.J., Vilaro, S., and Barbacid, M. (1996). p619, a giant protein related to the chromosome condensation regulator RCC1, stimulates guanine nucleotide exchange on ARF1 and Rab proteins. EMBO J. *15*, 4262–4273.

Schumacher, J.M., Golden, A., and Donovan, P.J. (1998). AIR-2: an Aurora/Ipl1-related protein kinase associated with chromosomes and midbody microtubules is required for polar body extrusion and cytokinesis in Caenorhabditis elegans embryos. J. Cell Biol. *143*, 1635–1646.

Skoufias, D.A., Mollinari, C., Lacroix, F.B., and Margolis, R.L. (2000). Human survivin is a kinetochore-associated passenger protein. J. Cell Biol. *151*, 1575–1582.

Skoufias, D.A., Andreassen, P.R., Lacroix, F.B., Wilson, L., and Margolis, R.L. (2001). Mammalian mad2 and bub1/bubR1 recognize distinct spindle-attachment and kinetochore-tension checkpoints. Proc. Natl. Acad. Sci. USA *98*, 4492–4497.

Speliotes, E.K., Uren, A., Vaux, D., and Horvitz, H.R. (2000). The survivin-like C. elegans BIR-1 protein acts with the Aurora-like kinase AIR-2 to affect chromosomes and the spindle midzone. Mol. Cell *6*, 211–223.

Terada, Y., Tatsuka, M., Suzuki, F., Yasuda, Y., Fujita, S., and Otsu, M. (1998). AIM-1: a mammalian midbody-associated protein required for cytokinesis. EMBO J. *17*, 667–676.

Toure, A., Dorseuil, O., Morin, L., Timmons, P., Jegou, B., Reibel, L., and Gacon, G. (1998). MgcRacGAP, a new human GTPase-activating protein for Rac and Cdc42 similar to Drosophila rotundRacGAP gene product, is expressed in male germ cells. J. Biol. Chem. *273*, 6019–6023.

Uren, A.G., Wong, L., Pakusch, M., Fowler, K.J., Burrows, F.J., Vaux, D.L., and Choo, K.H. (2000). Survivin and the inner centromere protein INCENP show similar cell-cycle localization and gene knockout phenotype. Curr. Biol. *10*, 1319–1328.

Vetter, I.R., and Wittinghofer, A. (2001). The guanine nucleotide-binding switch in three dimensions. Science *294*, 1299–1304.

Wheatley, S.P., Carvalho, A., Vagnarelli, P., and Earnshaw, W.C. (2001a). INCENP is required for proper targeting of Survivin to the centromeres and the anaphase spindle during mitosis. Curr. Biol. *11*, 886–890.

Wheatley, S.P., Kandels-Lewis, S.E., Adams, R.R., Ainsztein, A.M., and Earnshaw, W.C. (2001b). INCENP binds directly to tubulin and requires dynamic microtubules to target to the cleavage furrow. Exp. Cell Res. *262*, 122–127.

Wilde, A., and Zheng, Y. (1999). Stimulation of microtubule aster formation and spindle assembly by the small GTPase Ran. Science *284*, 1359–1362.

Zhang, C., and Clarke, P.R. (2000). Chromatin-independent nuclear envelope assembly induced by Ran GTPase in Xenopus egg extracts. Science *288*, 1429–1432.

Accession Numbers

The EMBL accession number for the TD-60 sequence reported in this paper is AJ421269

Molecular Cell, Vol. 6, 1831 89, July, 2000, Copyright ©2000 by Cell Press

Crystal Structure of Human Survivin Reveals a Bow Tie Shaped Dimer with Two Unusual α-Helical Extensions

Laurent Chantalat,*‖ Dimitrios A. Skoufias, ‖ Jean-Philippe Kleman, Barbara Jung, Otto Dideberg,*‖ and Robert L. Margolis ‖
*Laboratoire de Cristallographie Macromoléculaire and Laboratoire des Protéines du Cytosquelette
Institut de Biologie Structurale Jean-Pierre Ebel (CEA-CNRS)
41 rue Jules Horowitz
38027 Grenoble cedex 1
France
Sidney Kimmel Cancer Center
10835 Altman Row
San Diego, California 92121

Summary

Survivin is a mitotic spindle-associated protein involved in linking mitotic spindle function to activation of apoptosis in mammalian cells. The structure of the full-length human survivin has been determined by X-ray crystallography to 2.7 A. Strikingly, the structure forms a very unusual bow ties haped dimer. It does not dimerize through a C-terminal coiled-coil, contrary to sequence analysis prediction. The C-terminal helices contain hydrophobic clusters with the potential for proteinp rotein interactions. The unusual shape and dimensions of survivin suggest it serves an adaptor function through its α-helical extensions.

Introduction

Survivin, a recently described BIR motif protein (Ambrosini et al., 1997), has widespread tissue distribution and is overexpressed in many solid tumors (Ambrosini et al., 1997; Lu et al., 1998). It has several singular features that give it the potential to link between mitotic spindle function, checkpoint controls, and apoptotic activation. Survivin is expressed only in the G2/M phase of the cell cycle (Li et al., 1998), where immunofluorescence microscopy shows it associates with the mitotic spindle (Li et al., 1998) and with the centrosomes (Li et al., 1999). The level of expression of survivin in mammalian culture cells, altered either by overexpression following transfection or by antisense expression (Ambrosini et al., 1998 ; Li et al., 1998), correlates strongly with cell survival following mitotic arrest by taxol, an inhibitor of spindle function.

Because of its BIR motif, survivin is a potential member of the inhibitor of apoptosis (IAP) family of proteins, which act at discrete steps to regulate the apoptotic pathway of cell death (Deveraux and Reed, 1999). Proteins in this family all contain one or more signature ~70 residue BIR (baculovirus IAP repeat) motifs. The BIR motifs are essential for interaction of the IAP proteins with proapoptotic proteins, including the caspase family of death proteases. Not all BIR motif proteins act as inhibitors of apoptosis. For example, two BIR motif proteins closely related to survivin, BIR1 in budding yeast (Uren et al., 1999; Yoon and Carbon, 1999; Li et al., 2000) and BIR-1 in *C. elegans* (Fraser et al., 1999), are not involved in suppression of apoptosis but are implicated in spindle function and cell cleavage. Survivin appears to have an IAP function, as it is reported to inhibit caspase-3 activity in vitro (Conway et al., 2000), and its overexpression is reported to suppress caspase-3-dependent product formation and apoptosis (Li et al., 1998; Tamm et al., 1998; Kobayashi et al., 1999) in vivo. Furthermore, in *Drosophila*, loss of function of the survivin-like protein deterin leads to apoptotic cell death (Jones et al., 2000). Although survivin lacks the conserved sequence outside the BIR motif that has been shown essential for inhibition of caspase activity in human XIAP (Sun et al., 1999), it may contain other sequences of similar function.

In addition to a regulatory role in apoptosis, survivin clearly has an independent role in spindle function. Suppression of survivin by antisense expression in HeLa, in addition to inducing apoptosis, causes multiple spindle defects, including generation of multipolar spindles (Li et al., 1999).

Knowledge of survivin structure permits resolution of the first X-ray structure of a BIR motif. Here, we report the crystal structure of human survivin at 2.7 A resolution. It is a bow ties haped dimer that, in addition to its paired BIR motifs, contains two unusual C-terminal α-helical extensions. Its two subunits associate at the point where the α-helical tails exit from the globular BIR motifs.

Results and Discussion

Structure Determination and Overall Structure

N-terminal GST-tagged human survivin was expressed as recombinant protein in *E. coli*. The protein was purified by affinity chromatography, and the GST was excised by Factor Xa restriction protease cleavage on the column. The purified protein has 151 amino acids and a molecular mass of 17,159 Da. The apparent molecular mass in solution, as determined by ultracentrifugation, is 36 kDa, consistent with the formation of a 2.6 S dimer. The dimer is very stable and does not dissociate upon dilution during size exclusion chromatography.

Survivin crystals grew in space group C2 and formed nonmerohedral twins. They have unit cell parameters a = 113.75 A, b = 71.67 A, c = 81.59 A, β = 128.74°, and contain two monomers in the asymmetric unit. Diffraction can be detected up to 2.6 A using a high-intensity synchrotron beam. The structure was determined by multiple anomalous dispersion (MAD) methods (Hendrickson et al., 1990), using the anomalous signal of the native zinc of the protein. Phases were extended and improved considerably from the first experimental electron density map by density modification (Cowtan and

* To whom correspondence should be addressed (e-mail: margolis@ibs.fr).
‖ These authors contributed equally to this work.

Molecular Cell
184

Table 1. Crystallographic Analysis Statistics

Data Collection	D_{min} (A)	Unique Reflections	Redundancy[a]	Completeness (%)[a]	$\langle I \rangle / \langle \sigma \rangle$[a]	R_{sym} (%)[a,b]
Edge (λ1, 1.28283 A)	3.6	4770	4.09 (2.25)	76.0 (45.3)	21.3 (3.07)	5.9 (13.4)
Peak (λ2, 1.28243 A)	3.6	4661	5.50 (3.68)	78.1 (43.9)	25.5 (3.13)	8.1 (11.2)
Remote (λ3, 1.27557 A)	3.6	4837	3.95 (2.75)	80.2 (45.5)	22.1 (2.10)	7.2 (16.6)
Remote (λ4, 1.60478 A)	3.6	5110	4.14 (3.04)	83.5 (50.7)	19.5 (2.52)	10.9 (21.1)
Native (λ, 0.933 A)	2.7	12978	2.46 (1.77)	92.8 (75.9)	13.9 (2.34)	6.4 (22.9)

Phasing	Edge (λ1)	Peak (λ2)	Remote (λ3)	Remote (λ4)	FOM
Phasing power[c]		0.24	1.01	0.96	0.47[f]
R_{Cullis}[d]		0.97	0.85	0.83	0.71[g]
R_{Cullis} (ano)[e]		0.82	0.84	0.99	

Refinement	
Number of reflections	12968
R_{work}/R_{free}	23.5%/27.0%
Rmsd bonds/Rmsd angles	0.009 A/1.5°
Rmsd NCS Cα atoms, all/BIR motif	0.78 A/0.27 A
Quality of Ramachandran plot	
Percentage of residues in most favored regions	86.4
Percentage of residues in additional favored regions	13.6
No. of protein/water/ion atoms	2333/7/3 (2 zinc, 1 cobalt)

[a] Numbers in parentheses correspond to the last resolution shell.
[b] $R_{sym} = \Sigma\Sigma|I - I_j|/\Sigma I_j$
[c] Phasing power = F_h/A, where F_h is the heavy atom structure factor and A is the residual lack of closure.
[d] R_{Cullis} (dispersive) = $\Sigma|F_{ph} - F_p + F_{hc}|/\Sigma|F_{ph} - F_p|$ for centric reflections.
[e] R_{Cullis} (anomalous) = $\Sigma|D_{ph} - D_{phc}|/\Sigma|D_{ph}|$ for acentric reflections.
[f] Figure of Merit to 3.6 A after MLPHARE.
[g] Figure of Merit after density modification and phase extension to 2.7 A with DM.

Main, 1998). The new map enabled us to trace the chain without ambiguity. The structure was refined at 2.7 A resolution to a R_{work} and R_{free} (Brunger, 1992) of 23.5% and 27.0%, respectively. Crystallographic analysis statistics are reported in Table 1. The current model consists of two molecules of survivin, two zinc ions, one cobalt ion, and seven water molecules. The protein structure includes all but a few disordered amino acid residues: three from the GST fusion linker and the first four N-terminal, the three C-terminal residues of survivin, and two residues in a loop region between β1 and β2 for each monomer.

The survivin dimer shows a unique bow tie shape (Figure 1). The two monomers are related by a noncrystallographic 2-fold axis; they can be superimposed with 0.78 A rmsd for 136 Cα atoms and 0.27 A for Cα atoms from the BIR motif. The Cα-Cα distance between the two C-terminal residues, the height (Figure 1A), and the thickness of the dimer (Figure 1B) are 109.5, 43.6, and 56.3 A, respectively. The long C-terminal helix consists of 42 amino acids.

The surface of survivin displays asymmetric chemical properties. Looking down the 2-fold axis (Figure 2A), the convex face is covered by small patches of basic (blue), acidic (red), hydrophobic (yellow), or polar (white) amino acids. On the contrary, the concave face is on average mainly hydrophobic (Figures 2B and 2C), with in particular two large hydrophobic clusters located at the C terminus of helix α4.

Monomer Structure and Comparison with IAP Domains

The overall shape of a monomer is highly asymmetric and can be described as a pipe (Figure 1). The monomer consists of a globular N-terminal zinc finger domain (M1-S88), a linker segment (V89-T97), and a long C-terminal helix (L98-D142). The zinc finger domain and helix α4 pack tightly together. The monomer contains a total of four helices of more than one turn, three β strands, a few 3_{10} helices, and helical turns. Secondary structures were assigned based on Cα-Cα distances between consecutive amino acids. The overall topology of survivin is unique. A search for a similar fold with DALI (Holm and Sander, 1995) using the entire molecule yielded no results. When the zinc finger domain was submitted to DALI, the structure of the third domain (268 356) of the mammalian IAP homolog B (Hinds et al., 1999) (MIHB, PDB code 1QBH) was selected from the PDB database (Berman et al., 2000) with a Z score of 3.4 and a rmsd of 2.7 A. The amino acid sequence identity between the zinc finger domain of survivin and MIHB is only 31% (Figure 3). The structure of MIHB has been determined by NMR spectroscopy (Hinds et al., 1999). The structural similarity between the two zinc finger domains is evident (Figure 4A). The two helices α2 and α3 are well superimposed. However, the N-terminal regions of the two proteins have a different trajectory in space. The model of the second BIR domain (1242 60) of a human IAP family member also shows structural similarities with the zinc finger domain of survivin (Sun et al., 1999). All three domains bear the BIR motif (Prosite database: PDOC00987) (http://www.expasy.ch/prosite). The BIR motif has four strictly conserved zinc ligands with the CCHC configuration separated by variable amino acid segments (Figure 3). The signature of the zinc finger is $CX_2CX_{15\ 27}HX_{3\ 10}C$ (Mackay and Crossley, 1998). In addition, two amino acids (R18 and G42 of survivin) are highly conserved.

The first observable residue in the electron density is T5. This leads immediately into a short 3_{10} helix, and

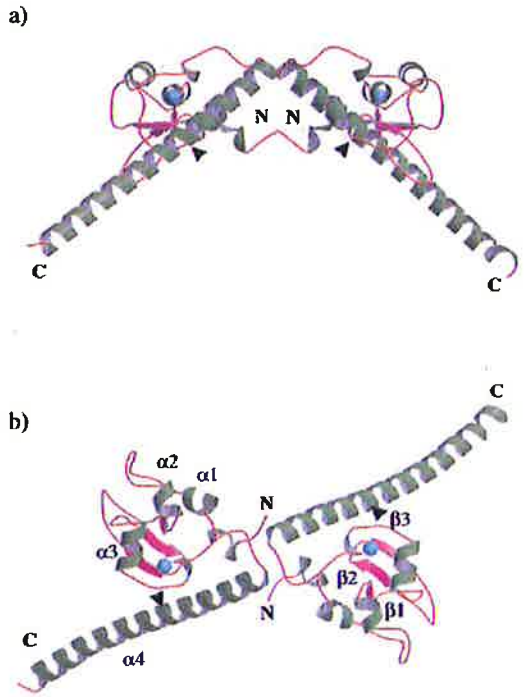

Figure 1. Ribbon Representation of the Survivin Dimer

The β strands, α helices, and loops are represented as violet arrows, green coils, and brown lines, respectively. The zinc atoms are shown as blue spheres, and black arrows indicate the trypsin cleavage sites. Figures were drawn as described in Chantalat et al. (1999).
(A) The dimer 2-fold axis is in the plane.
(B) The view in (A) rotated by 90° around the horizontal axis; the 2-fold axis is perpendicular to the plane.

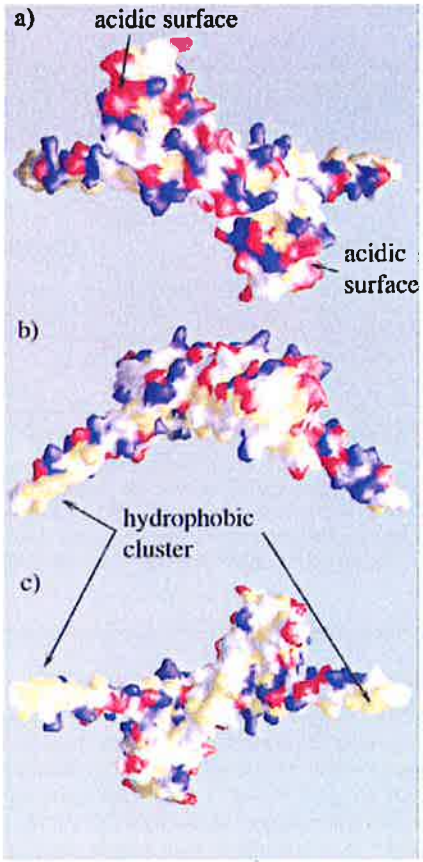

Figure 2. Molecular Surface of the Survivin Dimer

Colored according to the local chemical properties: acidic, basic, polar, and hydrophobic are in red, blue, white, and yellow, respectively.
(A) The view is along the 2-fold axis going into the convex surface of the dimer.
(B) The view in (A) rotated by 90° around the horizontal axis.
(C) The view in (A) rotated by 180° around the horizontal axis. The 2-fold axis now going into the concave surface of the dimer.

then, after a turn, into the BIR motif. In brief, the BIR motif consists of three helices (142 1, 314 1, 68 80) and a three-stranded antiparallel β sheet (434 5, 555 8, 616 4). Amino acids C57, C60, H77, and C84 form the zinc finger stabilizing most of the domain. Another key residue is R18, whose side chain is buried (Figure 4A). R18 makes two hydrogen bonds with main chain oxygens (P12 and A39) and hydrophobic interactions with residues I44 and F58, stabilizing the N-terminal part of the zinc finger domain. Finally, G42 increases the flexibility of the main chain between helix α2 and strand β1 (Figure 4A). The (ϕ, ψ) angles of G42 for each monomer are (83°, 5°) and (95°, -11°), respectively. These angles correspond to conformational angles of a left-handed α helix in the Ramachandran plot.

As in the other two IAP structures, the core of the zinc finger domain is stabilized by hydrophobic interactions involving residues F22, W25, F27, M38, F43, F58, L64, W67, and F86. The domain is followed by a linker of eight residues (899 7) that curves back toward the N terminus. F93 makes hydrophobic interactions with F13 and L14. The linker leads to the C-terminal α4 helix. Here, extensive hydrophobic contacts can be found between the zinc finger domain and helix α4. They include F58, F59, and F61 of the zinc finger domain and F101 and L104 of α4. Interestingly, out of three hydrophobic amino acids of the zinc finger domain, only one is conserved in the two IAP structures (Figure 3), which supports the presence of a unique topology in survivin. In addition, a salt bridge (E63 K115) and three hydrogen bonds are observed: F59O to N111ND2 and F58O to both R108NE and R108NH2.

Dimer Formation

From sequence analysis, the C-terminal region of survivin was predicted to be a coiled-coil (Li et al., 1998). Both solution studies and crystal analysis support the presence of a dimer. However, when the first model emerged from this work, surprisingly the coiled-coil region (end of helix α4) was not involved in the dimer formation but in crystal packing. To confirm this unexpected result, survivin was submitted to limited trypsin proteolysis. A single protein cleavage product was observed on polyacrylamide gels. Mass spectrometry demonstrated it was the N-terminal region of survivin, cleaved at K115 of the native protein. Light scattering and gel filtration of the purified product, lacking part of the C-terminal α helices, both demonstrated it was still dimeric (data not shown). We defined the functional dimer by the presence of an asymmetric unit that contains

Molecular Cell
186

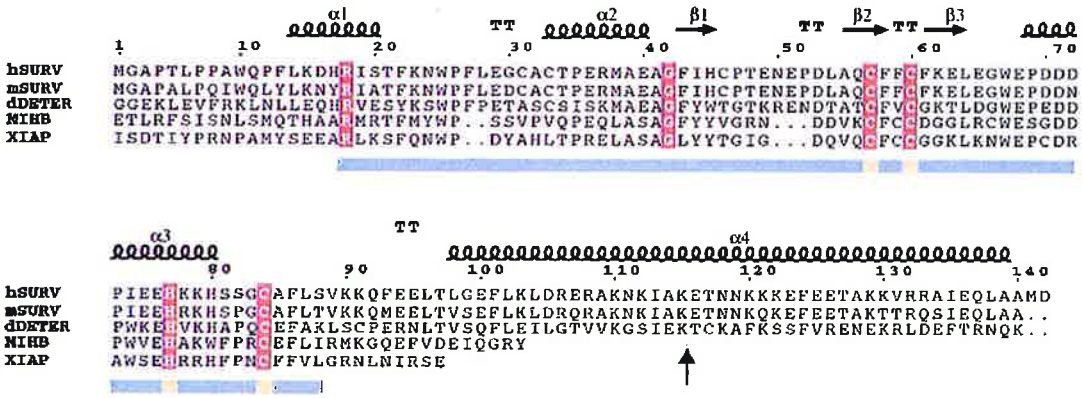

Figure 3. Sequence Alignment of Survivin-Related Proteins

The figure shows alignment between human (hSURV) and mouse (mSURV) survivin, *Drosophila* deterin (dDETER), and two IAP domains of known 3D structure (residues 255 352 of MIHB and residues 149 240 of XIAP; GenBank accession numbers: hSURV, U75285; mSURV, AF115517; dDETER, AI260030; MIHB, U37547; and XIAP, U32974). The secondary structural elements for human survivin are indicated above the alignment. Conserved residues in the zinc finger domain are boxed in red. The BIR domain and zinc ligands are underlined with horizontal stripes in blue and yellow, respectively. The trypsin cleavage site is marked by a black arrow.

two monomers related by a 2-fold noncrystallographic axis.

Figures 4B and 4C illustrate the characteristics of the dimer interface. Three segments are involved in the interaction: the N-terminal region, the linker region, and the N terminus of helix α4. The molecular dimer interface is mostly hydrophobic since 75% of the residues are nonpolar. In the core region of the interface, F93, L98, and F101 make hydrophobic contacts with their counterpart residues on the other monomer. In addition, four hydrogen bonds between main chain atoms are observed (E94O G99N, L96O L98N, and symmetrical interactions).

Only 532 A^2 (5.7% of the overall surface) of a monomer contributes to the dimer interface. A systematic comparison of the structure of oligomeric proteins reported that interface areas in small dimers range from 670 A^2 in superoxide dismutase (Mr 15 710 Da) to 3470 A^2 in phosphorylase a (Mr 95 410 Da) (Janin et al., 1988). This analysis showed no simple correlation between the molecular mass of the monomer and the interface area. Nevertheless, the survivin value compares well with the value of 540 A^2 found recently in the β subunit dimer of human protein kinase CK2 (CK2β) (Chantalat et al., 1999). In the mouse survivin structure, a second zinc ion (Zn2) was observed to mediate dimer formation (Muchmore et al., 2000). In the structure presented here, the Zn2 ligands are conserved (E76 and H80) and exposed to the solvent. For monomer A only, there is a cobalt hexamine binding site nearby. However, the smallest distance between the cobalt and the protein is 3.8 A (D70 OD1), supporting the presence of the Co hexamine complex. The Co is therefore not substituting for a Zn ion.

Survivin and Proteins Involved in Apoptosis

All proteins involved in apoptosis for which the 3D structure is known were compared with the 3D structure of survivin. Special attention was paid to protein complexes. In addition to the two inhibitors of apoptosis discussed above (MIHB and XIAP) bearing a BIR domain, we found only one structure showing a structural similarity with survivin. The crystal structure of the complex of the activating factor Apaf-1 and the caspase-9 prodomain was determined at 2.5 A resolution (Qin et al., 1999) (PDB file code 3YGS). The caspase recruitment domain (CARD) of Apaf-1 binds to caspase-9 to trigger a proteolytic cascade that leads to apoptotic cell death (Vaughn et al., 1999). Most CARD domains adopt a six-helix bundle fold with a Greek Key topology (Vaughn et al., 1999). CARDs are part of a large superfamily of proteins or domains present in apoptotic receptors, adaptor molecules, caspases, and inhibitors of apoptosis, suggesting that the CARD fold is likely to be a general module for proteinpr otein interactions in apoptosis.

Three helices of survivin (α1, α2, and α3) can be superimposed on three helices of Apaf-1 (α5, α2, and α3), respectively, having almost the same length (data not shown). Two pairs, (α1, α5) and (α2, α2), run in opposite directions. However, they both define a negatively charged convex surface. Interestingly, in the Apaf-1 prodomain/caspase-9 prodomain complex (Qin et al., 1999), the convex surface formed by the negatively charged helices α2 and α3 is recognized by the concave surface of the caspase-9 prodomain formed by the positively charged helices α1a /α1b and α4. Since a short form of mouse survivin, called $survivin_{121}$, lacking the end of helix α4 still inhibits caspase-3 activity (Conway et al., 2000), it is tempting to assign a functional role to the negatively charged surface defined by helices α2 and α3 of survivin (referred to as acidic surface in Figure 2A). Many acidic residues are located on the solvent-exposed surface of α2 and α3 or nearby for both structures: D16, E36, E40, D70, D72, and E75 for survivin, and D27, D32, E40, E41, D66, and E78 for Apaf-1 (data not shown). Interestingly, T34, D71, E76, and H80, which are important for survivin function (Muchmore et al., 2000), line the acidic surface.

Finally, one of the most striking features of the survivin

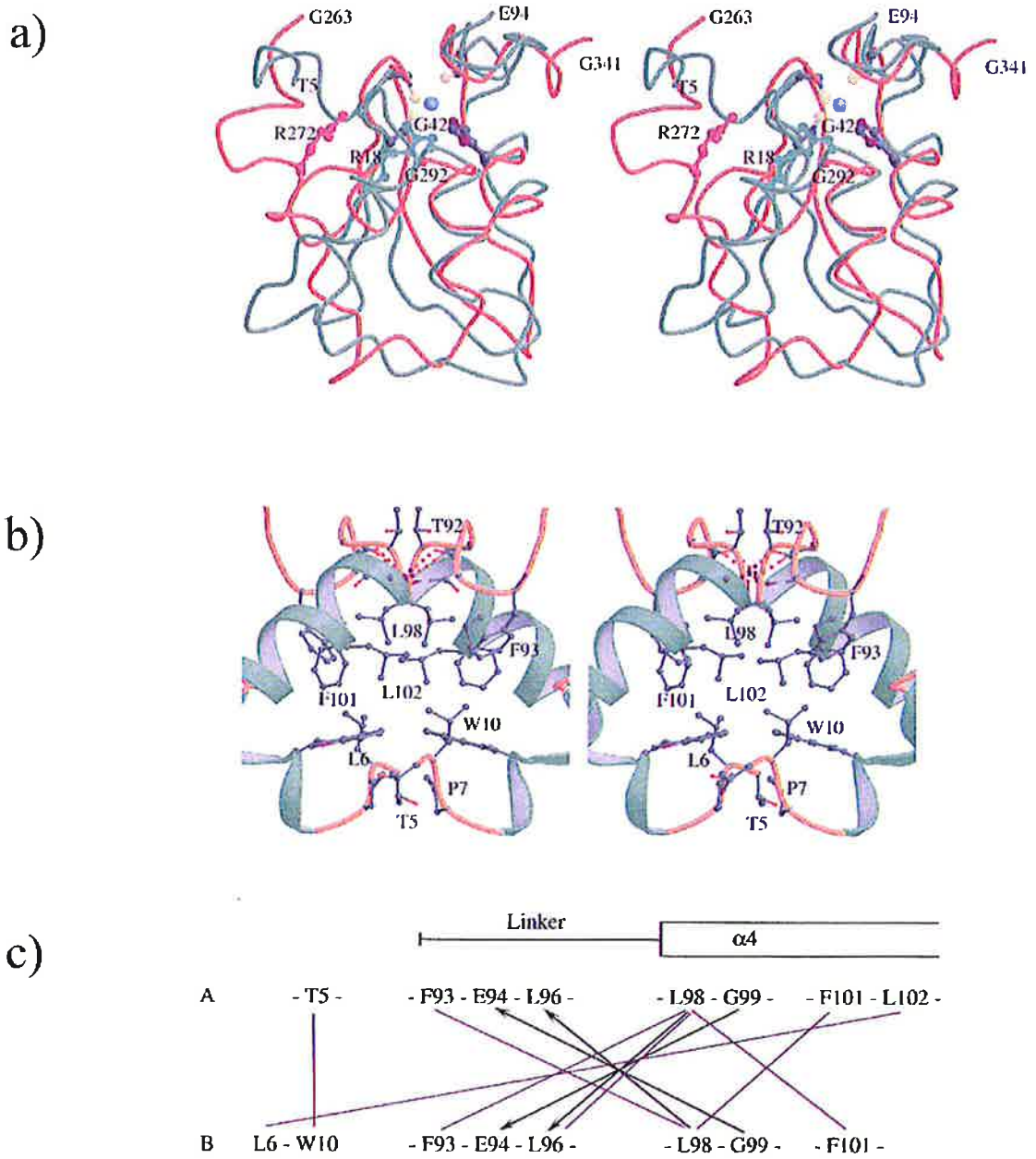

Figure 4. Structure Conservation of the Zinc Finger Domain and Detail of the Dimer Interface

(A) Superimposition of two zinc finger domains, MIHB (G263G 341 in cyan) and survivin (T5-E94 in green), shown in stereo view. For clarity, only the zinc ligands (cysteines in yellow and histidine in deep blue) and the zinc ion (light blue) of survivin are represented. The two conserved arginines (R272 and R18 of MIHB and survivin, respectively) are shown color coded as the main chain. The two conserved glycines (G294 and G42 of MIHB and survivin, respectively) are also marked.

(B) Ribbon stereo view of the dimer interface. The α helices are shown as green coils and loops as brown lines. Amino acid side chains involved in proteinp rotein interactions are represented in ball-and-stick in black. Hydrogen bonds are shown as dotted red lines.

(C) The various contacts at the dimer interface are displayed as a schematic diagram. Hydrogen bonds and van der Waals interactions are indicated by black arrows (donor to acceptor) and blue lines, respectively.

is the hydrophobic cluster located on one face of the C terminus of helix α4 (Figure 2). In the crystal, these hydrophobic clusters are involved in the packing of dimers. In solution they may play a role in protein protein interactions. The unusual angular shape of survivin may give it the potential to fill a unique adaptor role.

Conclusions

Survivin clearly links mitotic spindle function to control of the apoptotic pathway. In keeping with these functions, it contains a BIR motif and is reported to associate with microtubules of the mitotic spindle (Li et al., 1998), as well as with the centrosome (Li et al., 1999). We have

demonstrated that survivin is a dimer linked not through a C-terminal coiled-coil but through interactions located mainly in the linker region and N-terminal region of α4 and that it contains two C-terminal α-helical extensions that give it a singular shape and span. The C termini of survivin are reported to be required for binding to microtubules in vitro. The shape of the survivin dimer permits a unique adaptor or docking function on the microtubule polymer or elsewhere.

Consistent with the absence of a coiled-coil C-terminal motif, trypsin cleavage of survivin at residue 115 demonstrates that the N-terminal region alone is sufficient for dimerization. It is of interest that there is a mouse survivin isoform that terminates at residue 120 and thus lacks a portion of the C-terminal α helix (Conway et al., 2000). This isoform, of unknown function, is most likely also dimeric.

Close homologs of survivin in other species are linked to spindle and cell cleavage function (Fraser et al., 1999; Uren et al., 1999; Yoon and Carbon, 1999; Li et al., 2000). In addition, suppression of survivin is linked to multiple mitotic defects in mammalian cells (Li et al., 1999). The interaction of survivin with the mitotic spindle is therefore of importance for more than control of apoptosis. The survivin structure that we have described here should now open approaches to analyze how it associates with the spindle, linking spindle function and cell survival.

Experimental Procedures

Cloning, Expression, and Purification of Recombinant Human Survivin

The survivin cDNA was amplified by PCR, using IMAGE clone #937208, by standard methods. The insert was cloned into a pGEX expression vector (Pharmacia, Piscataway, NJ), driving expression of the GST-survivin, and was completely sequenced from both ends. Recombinant survivin was expressed in BL21(DE3) *E. coli*. Following culture, cells were frozen and thawed in lysis buffer (20 mM Tris [pH 8] and 0.5 M NaCl) and then lysed in a French Press. GST-survivin was purified from the lysate on glutathione Sepharose 4B beads (Pharmacia) by standard procedures, and then survivin was released with 30 μg of Factor Xa (Boehringer Mannheim), run on a Q HYPERD 10 column (BIOSEPRA) preequilibrated in Buffer A (50 mM Tris [pH 8], 100 mM NaCl, and 1 mM DTT), and eluted with a 100 to 300 mM NaCl gradient in Buffer A at a flow rate of 1 mL/min in a Beckman BioSYS-2000 liquid chromatography system. Purified survivin had the predicted molecular mass and was recognized on Western blots using a C-terminal peptide (amino acids 103 123) human survivin antibody (α Diagnostic International). Mass spectrometry of the pooled peak revealed a single polypeptide with a molecular mass of 17,159 Da, in agreement with the expected mass of full-length survivin, plus an additional nine amino acids (GIP EFGGGG) at the N terminus derived from the cloning procedures. Pooled fractions were dialyzed against 10 mM Tris (pH 8), 100 mM NaCl, and 1 mM DTT (Buffer B), and then concentrated to 10 mg/mL or higher, and small aliquots of protein were stored at 80 °C until use.

Analytical Ultracentrifugation

Survivin at 0.8, 0.5, and 0.25 mg/ mL in Buffer B was centrifuged at 42,000 rpm at 20°C in two channel cells in an Optima XL-A analytical ultracentrifuge (Beckman) equipped with a four-hole An-60 Ti rotor. The observed values were constant in all concentrations, suggesting there is no association-dissociation process and the molar mass values were relevant only in the case of a homogeneous noninteracting system. The results suggested that survivin is a 2.6 S dimer with a molecular mass of 36 kDa.

Limited Proteolysis

Purified recombinant survivin was digested by limited proteolysis with trypsin (Sigma) at 1/2000 weight ratio at 16°C for 30 min. Proteolysis was stopped by the addition of PMSF at 1 mM final concentration. SDS PAGE electrophoresis of the digested protein revealed the presence of a single polypeptide with an apparent molecular mass of 15 kDa. Mass spectrometry data revealed the presence of a single polypeptide with a molecular mass of 14,840 Da. Proteolytic map analysis of the survivin amino acid sequence suggested that the resulting C-terminal amino acid of the digested protein is K115 in native human survivin.

Dynamic Light Scattering

DLS measurements were performed using a DynaPro-801 Molecular sizing Instrument (Protein Solutions, Inc., Charlottesville, VA). The molecular masses found for the full-length and trypsinized survivin proteins were around 51 and 41 kDa, which for both cases correspond to elongated dimers.

Crystallization and Data Collection

Although two crystal forms were obtained by hanging drop vapor diffusion using a sparse matrix screen (Hampton Research), none diffracted better than 7 A. Therefore, additive screens (Hampton Research) were used with the previously found conditions in order to improve these poorly diffracting crystals. In this way, a new crystal form was found that diffracted to at least 3 A. Crystals grew from a HEPES buffer (pH 6.8), 4% polyethylene glycol monomethylether 2000, 5% ethylene glycol, and 1 mM hexamine cobalt chloride. From the first diffraction patterns, it was clear that the crystals showed nonmerohedral twinning, i.e., the reciprocal lattices of the two twin components were perfectly overlapping in some regions of the reciprocal space. In our case, the twin is generated by a 2-fold axis along the c axis. Each image had to be scrutinized until one was found where the two lattices could be distinguished. Both lattices were indexed manually with DENZO (Otwinowski and Minor, 1997), which was further used to integrate the two data sets. Spots closer to each other than five pixels were discarded. Each data set could be scaled and merged with SCALEPACK. The self-rotation function suggested a dimer in the asymmetric unit (a.u.). Assuming a partial specific volume of 0.73 cm^3/g and a dimer in the a.u., the solvent content would be 63%. This value is in the range observed for protein crystals (Matthews, 1968).

MAD Structure Determination and Refinement

The multiwavelength anomalous dispersion (MAD) data were collected from frozen twinned crystals around the K absorption edge of zinc on a MAR CCD at the BM14 beam line, ESRF-Grenoble, France, at four wavelengths (Table 1). The four wavelengths were chosen from a fluorescent scan of the crystal. The rod-like crystals could readily be oriented with the crystallographic 2-fold axis aligned along the spindle. This allowed us to collect Friedel mates very close in time. The data were processed as described above (Table 1). The scaled and reduced intensity data were then converted to amplitudes using TRUNCATE (CCP4, 1994), and cross-wavelength scaling was performed using SCALEIT (CCP4), treating data set λ1 as the native (Table 1). After careful removal of overlapping spots due to twinning and of large anomalous differences, the native Zn structure could be determined from the anomalous Patterson synthesis calculated with data set λ2 (Table 1). Phase calculation and heavy atom refinement with MLPHARE (CCP4) gave a final figure of merit of 0.47 to 3.6 A (Table 1). Then a new native data set was collected to 2.7 A on a single crystal at station ID14-EH2 (ESRF-Grenoble), which was used in a final step of density modification, 2-fold averaging and phase extension with DM (CCP4, 1994). Map interpretation with O (Jones et al., 1991) was initiated from the long C-terminal helix and around the zinc site and facilitated by the descriptions of the solution structures of two other BIR domain containing proteins, XIAP (Sun et al., 1999) and MIHB (Hinds et al., 1999). The refinement was initially done with REFMAC (CCP4) with DM phase restraints using the native data set to 2.7 A, with the maximum likelihood target function. The final stages of refinement were performed with CNS (Brunger et al., 1998).

Acknowledgments

This work was supported by grants from the Association pour la Recherche sur le Cancer and La Ligue (R. L. M.). D. A. S. was supported by an EMBO fellowship. We thank Drs. G. Sainz and E. Mitchell (ESRF-Grenoble) for assistance in data collection and Drs. C. Ebel and E. Forest for help with ultracentrifugation and mass spectrometry, respectively.

Received May 15, 2000; revised June 13, 2000.

References

Ambrosini, G., Adida, C., and Altieri, D.C. (1997). A novel anti-apoptosis gene, survivin, expressed in cancer and lymphoma. Nat. Med. *3*, 9179 21.

Ambrosini, G., Adida, C., Sirugo, G., and Altieri, D.C. (1998). Induction of apoptosis and inhibition of cell proliferation by survivin gene targeting. J. Biol. Chem. *273*, 111771 1182.

Berman, H.M., Westbrook, J., Feng, Z., Gilliland, G., Bhat, T.N., Weissig, H., Shindyalov, I.N., and Bourne, P.E. (2000). The protein data bank. Nucleic Acids Res. *28*, 235 242.

Brunger, A.T. (1992). Free R value: a novel statistical quantity for assessing the accuracy of crystal structures. Nature *355*, 472 475.

Brunger, A.T., Adams, P.D., Clore, G.M., DeLano, W.L., Gros, P., Grosse-Kunstleve, R.W., Jiang, J.S., Kuszewski, J., Nilges, M., Pannu, N.S., et al. (1998). Crystallography & NMR system: a new software suite for macromolecular structure determination. Acta Crystallogr. D *54*, 905 921.

CCP4 (Collaborative Computational Project 4) (1994). The CCP4 suite: programs for protein crystallography. Acta Crystallogr. D *50*, 760 763.

Chantalat, L., Leroy, D., Filhol, O., Nueda, A., Benitez, M.J., Chambaz, E.M., Cochet, C., and Dideberg, O. (1999). Crystal structure of the human protein kinase CK2 regulatory subunit reveals its zinc finger-mediated dimerization. EMBO J. *18*, 2930294 0.

Conway, E.M., Pollefeyt, S., Cornelissen, J., DeBaere, I., Steiner-Mosonyi, M., Ong, K., Baens, M., Collen, D., and Schuh, A.C. (2000). Three differentially expressed survivin cDNA variants encode proteins with distinct antiapoptotic functions. Blood *95*, 1435144 2.

Cowtan, K., and Main, P. (1998). Miscellaneous algorithms for density modification. Acta Crystallogr. D *54*, 487493.

Deveraux, Q.L., and Reed, J.C. (1999). IAP family proteins suppressors of apoptosis. Genes Dev. *13*, 239 252.

Fraser, A.G., James, C., Evan, G.I., and Hengartner, M.O. (1999). Caenorhabditis elegans inhibitor of apoptosis protein (IAP) homologue BIR-1 plays a conserved role in cytokinesis. Curr. Biol. *9*, 292 301.

Hendrickson, W.A., Horton, J.R., and LeMaster, D.M. (1990). Selenomethionyl proteins produced for analysis by multiwavelength anomalous diffraction (MAD): a vehicle for direct determination of three-dimensional structure. EMBO J. *9*, 166516 72.

Hinds, M.G., Norton, R.S., Vaux, D.L., and Day, C.L. (1999). Solution structure of a baculoviral inhibitor of apoptosis (IAP) repeat. Nat. Struct. Biol. *6*, 648651 .

Holm, L., and Sander, C. (1995). Dali: a network tool for protein structure comparison. Trends Biochem. Sci. *20*, 47848 0.

Janin, J., Miller, S., and Chothia, C. (1988). Surface, subunit interfaces and interior of oligomeric proteins. J. Mol. Biol. *204*, 155164.

Jones, T.A., Zou, J.Y., and Cowan, S.W., and Kjeldgaard, M. (1991). Improved methods for binding protein models in electron density maps and the location of errors in these models. Acta Crystallogr. A *47*, 110119.

Jones, G., Jones, D., Zhou, L., Steller, H., and Chu, Y. (2000). Deterin, a new inhibitor of apoptosis from *Drosophila Melanogaster*. J. Biol. Chem., in press.

Kobayashi, K., Hatano, M., Otaki, M., Ogasawara, T., and Tokuhisa, T. (1999). Expression of a murine homologue of the inhibitor of apoptosis protein is related to cell proliferation. Proc. Natl. Acad. Sci. USA *96*, 1457146 2.

Li, F., Ambrosini, G., Chu, E.Y., Plescia, J., Tognin, S., Marchisio, P.C., and Altieri, D.C. (1998). Control of apoptosis and mitotic spindle checkpoint by survivin. Nature *396*, 580584.

Li, F., Ackermann, E.J., Bennett, C.F., Rothermel, A.L., Plescia, J., Tognin, S., Villa, A., Marchisio, P.C., and Altieri, D.C. (1999). Pleiotropic cell-division defects and apoptosis induced by interference with survivin function. Nat. Cell Biol. *1*, 461466.

Li, F., Flanary, P.L., Altieri, D.C., and Dohlman, H.G. (2000). Cell division regulation by BIR1, a member of the inhibitor of apoptosis family in yeast. J. Biol. Chem. *275*, 6707671 1.

Lu, C.D., Altieri, D.C., and Tanigawa, N. (1998). Expression of a novel antiapoptosis gene, survivin, correlated with tumor cell apoptosis and p53 accumulation in gastric carcinomas. Cancer Res. *58*, 1808 1812.

Mackay, J.P., and Crossley, M. (1998). Zinc fingers are sticking together. Trends Biochem. Sci. *23*, 14 .

Matthews, B.W. (1968). Solvent content of protein crystals. J. Mol. Biol. *33*, 491497.

Muchmore, S.W., Chen, J., Jakob, C., Zakula, D., Matayoshi, E.D., Wu, W., Zhang, H., Li, F., Ng, S.-C., and Altieri, D.C. (2000). Crystal structure and mutagenic analysis of the inhibitor-of-apoptosis protein survivin. Mol. Cell *6*, this issue, 1731 82.

Otwinowski, Z., and Minor, W. (1997). Processing of X-ray diffraction data collected in oscillation mode. Methods Enzymol. *276*, 3073 26.

Qin, H., Srinivasula, S.M., Wu, G., Fernandes-Alnemri, T., Alnemri, E.S., and Shi, Y. (1999). Structural basis of procaspase-9 recruitment by the apoptotic protease- activating factor 1. Nature *399*, 5495 57.

Sun, C., Cai, M., Gunasekera, A.H., Meadows, R.P., Wang, H., Chen, J., Zhang, H., Wu, W., Xu, N., Ng, S.C., et al. (1999). NMR structure and mutagenesis of the inhibitor-of-apoptosis protein XIAP. Nature *401*, 818822.

Tamm, I., Wang, Y., Sausville, E., Scudiero, D.A., Vigna, N., Oltersdorf, T., and Reed, J.C. (1998). IAP-family protein survivin inhibits caspase activity and apoptosis induced by Fas (CD95), Bax, caspases, and anticancer drugs. Cancer Res. *58*, 531553 20.

Uren, A.G., Beilharz, T., O Connell, M.J., Bugg, S.J., van Driel, R., Vaux, D.L., and Lithgow, T. (1999). Role for yeast inhibitor of apoptosis (IAP)-like proteins in cell division. Proc. Natl. Acad. Sci. USA *96*, 1017010 175.

Vaughn, D.E., Rodriguez, J., Lazebnik, Y., and Joshua-Tor, L. (1999). Crystal structure of Apaf-1 caspase recruitment domain: an alpha-helical Greek key fold for apoptotic signaling. J. Mol. Biol. *293*, 439447.

Yoon, H.J., and Carbon, J. (1999). Participation of Bir1p, a member of the inhibitor of apoptosis family, in yeast chromosome segregation events. Proc. Natl. Acad. Sci. USA *96*, 1320813 213.

Protein Data Bank ID Code

Atomic coordinates have been deposited with the ID code 1E31.

11484 *Biochemistry* **2003,** *42,* 11484−11493

Unusual Ca^{2+}-Calmodulin Binding Interactions of the Microtubule-Associated Protein F-STOP†,‡

Denis Bouvier,§ Cécile Vanhaverbeke,§ Jean-Pierre Simorre,§ Gérard J. Arlaud,|| Isabelle Bally,|| Vincent Forge,⊥ Robert L. Margolis,# Pierre Gans,*,§ and Jean-Philippe Kleman#

Laboratoire des Protéines du Cytosquelette, Laboratoire de Résonance Magnétique Nucléaire, Laboratoire d'Enzymologie Moléculaire, Institut de Biologie Structurale J-P Ebel (UMR CNRS 5075), 41 rue Jules Horowitz, 38027 Grenoble Cedex 1, France, and Laboratoire de Biophysique Moléculaire et Cellulaire (UMR CNRS 5090), Département Réponse et Dynamique Cellulaire, CEA-Grenoble, 17 rue des Martyrs, 38054 Grenoble Cedex 1, France

Received May 7, 2003; Revised Manuscript Received August 6, 2003

ABSTRACT: F-STOP is a microtubule-associated protein that stabilizes microtubules in a calmodulin (CaM)-dependent manner. All members of the stable tubule only polypeptide (STOP) family have a central domain that contains nearly identical multiple repeats, and a CaM binding motif is present in multiple copies within this domain. We present here an analysis of this CaM binding interaction and find that it is highly unusual in nature. For this work, we synthesized two model peptides of a single STOP central repeat motif and analyzed their binding to CaM by fluorescence, circular dichroism, infrared and NMR spectroscopy. Both peptides bind to CaM with an affinity of 4 μM, similar to that of the native protein. Results indicate that the peptides bind CaM in an atypical manner. Binding is highly dependent on the concentration of cations, indicating that it is to some extent electrostatic. Further, IR and CD analysis shows that, in contrast to typical CaM binding reactions, CaM does not change in helical structure on binding. NMR mapping confirms that CaM remains in extended conformation on binding a single STOP peptide. Binding of a single peptide to CaM occurs principally in the CaM C-terminal region, and the C-terminal domain of CaM effectively competes for STOP binding. Our results establish that CaM binds STOP in an unusual manner, involving mainly the C-terminus of CaM, thus leaving CaM potentially accessible for another binding partner at the N-terminus. This intriguing possibility could be of physiological importance in F-STOP mediated CaM regulation of microtubule dynamics or stability, specifically during mitosis where CaM and STOP colocalize.

Microtubules are ubiquitous components of the cytoskeleton in eucaryotic cells. They are intrinsically labile polymers of tubulin, physiologically stabilized by the association with microtubule-associated proteins (MAPs)[1] (*1*). Among the MAPs, stable tubule only polypeptide (STOP) family members have the unique capacity to prevent in vitro dissociation of microtubules after exposure to cold temperature, dilution, or microtubule depolymerizing drugs (*2*, *3*). STOP protein variants are produced from a single gene by alternate splicing (*4*, *5*). The short F-STOP splice variant is expressed in cycling cells. E- and N-STOP are longer forms, respectively expressed during embryogenesis or in neurons. Physiological roles of STOPs are not at present clearly understood, but STOP inhibition in cultured neuronal cells impairs neuronal differentiation (*6*). Furthermore, knockout mice for STOPs exhibit synaptic defects associated with a severe behavioral phenotype (*7*), suggesting that STOP might be implicated in synaptic functions. F-STOP is physiologically associated with specific microtubules of the mitotic spindle (*5*), and is thus believed to play a role in cell cycle progression during mitosis.

CaM is known to bind STOP and to regulate its microtubule stabilizing capacity in a calcium-dependent manner (*8*, *9*). CaM is a major sensor of cytoplasmic Ca^{2+} concentration, and is implicated in hundreds of cellular processes through calcium specific binding to effectors (*10*). The diverse STOP variants are all implicated or colocalized with CaM, in nerve terminals and in the mitotic spindle (*11*, *12*),

† This work was supported by the Centre National de la Recherche Scientifique, the Commissariat à l'Energie Atomique and the University Joseph Fourier.

‡ Chemical shift assignments of the backbone atoms of VU-1 calmodulin and of calmodulin in the complex VU-1 calmodulin/STP23 have been deposited in the BioMagResBank (accession numbers 5893 and 5896, respectively).

* To whom correspondence should be addressed: E-mail: pierre.gans@ibs.fr. Tel: (33) 4 38 78 57 98. Fax: (33) 4 38 78 54 94.

Laboratoire des Protéines du Cytosquelette, Institut de Biologie Structurale J-P Ebel (UMR CNRS 5075).

§ Laboratoire de Résonance Magnétique Nucléaire, Institut de Biologie Structurale J-P Ebel (UMR CNRS 5075).

|| Laboratoire d'Enzymologie Moléculaire, Institut de Biologie Structurale J-P Ebel (UMR CNRS 5075).

⊥ Laboratoire de Biophysique Moléculaire et Cellulaire (UMR CNRS 5090), Département Réponse et Dynamique Cellulaire, CEA-Grenoble.

[1] Abbreviations: CaM, calmodulin; TR2C, C-terminal domain of calmodulin deletion mutant; STOP, stable tubule only polypeptide; N-STOP, neuronal form of STOP; F-STOP, fibroblastic form of STOP; STP23, STOP 23-mer peptide (Mc motif); STP42, STOP 42-mer peptide (repeat unit); NATA, *N*-acetyl-L-tryptophan amide; SAXS, small-angle X-ray scattering; nOe, nuclear Overhauser effect; bHLH, basic helix−loop−helix; MARCKS, myristoylated alanine-rich C kinase substrate; SEF2-1mp, SL3 enhancer factor 2-1 mimicking factor; M13, CaM-binding domain of myosin-light chain kinase; C20W, N-terminal portion of the CaM-binding domain of the plasma membrane pump; TFP, trifluoroperazine; W-7, *N*-(6-aminohexyl)-5-chloro-1-naphthalenesulfonamide.

where CaM has been implicated in chromosome segregation (*13*). CaM activation is also known to be essential for mitotic progression (*14*, *15*). These observations suggest a physiological role for CaM/STOP binding in various cell processes.

A recent study of STOP sequence properties using immobilized-peptide array revealed that multiple putative CaM binding motifs are present on STOP, and overlap with the microtubule binding sequences (*16*). The short splicing variant, F-STOP, exhibits one CaM/microtubule Mn binding motif and four Mc motifs, occurring once in each of the four conserved repeats in the central region. Bosc et al. (*16*) showed that only F-STOP constructs containing Mc repeats were retained on column-immobilized CaM, signifying that Ca^{2+}-CaM interaction with F-STOP is restricted to the Mc motifs present in its central repeated region. Sequence comparison showed that these motifs are not related to conventional CaM-binding motifs (*17*). Taken together, these observations suggest an unusual binding interaction between CaM and the F-STOP repeated central region.

Several unusual modes of interaction between CaM and its binding partners have been reported (*18*−*25*). However, none of these complexes, as described in Discussion, is representative of the binding mode of STOP. We wanted to understand the unique binding interaction between CaM and F-STOP. To gain structural knowledge on the complex formed between F-STOP and CaM, we decided to study their mode of interaction using a simplified peptide model. We have thus synthesized peptides corresponding either to the element within the repeat that contains the CaM/microtubule Mc binding motif (STP23), as described by Bosc et al. (*16*), or to the full-length repeat (STP42). We show that, in solution, these peptides bind to CaM in a calcium-dependent manner and that binding occurs in the C-terminal domain of CaM. Structural changes that are typical for CaM binding do not occur in the reaction between CaM and STOP. Our results thus demonstrate a unique mode of CaM binding, with potential physiological consequences.

EXPERIMENTAL PROCEDURES

Peptide Synthesis. The 23-mer peptide (STP23, rat sequence from EMBL NM_017204) corresponding to the consensus Mc motif (*16*), QRDTRRKAGPAWMVTRTEGHEEK was obtained commercially (Eurogentec France S. A.). The 42-mer peptide corresponding to a single repeat (STP42, mouse sequence from EMBL NM_010837) AQSQTQEGGPAAGKASGADQRDTRRKAGPAWMVTRSEGHEEK was synthesized chemically (Applied Biosystems 430A automated synthesizer). The *tert*-butyloxycarbonyl group was used for protection of the N-*a*-amino terminus of all amino acids, and synthesis was carried out on a phenylacetamidomethyl resin. Protecting groups for relevant amino acid side chains were as follows: R, mesitylene sulfonyl; D, cyclohexyl; E, benzyl; H, 2,4-dinitrophenyl; K, 2-chlorobenzyl oxycarbonyl; S and T, benzyl; W, formyl. All couplings were performed by the dicyclohexylcarbodiimide/1-hydroxybenzotriazole method, using *N*-methyl pyrrolidone and dimethyl sulfoxide as coupling solvents, according to the protocol recommended by Applied Biosystems. All amino acids except glycine were double-coupled, and amino groups left unreacted at the end of each coupling cycle were capped with acetic anhydride. Deprotection and cleavage of the peptide from the resin were achieved by HF treatment. Deprotection of histidine by thiophenol and deformylation of tryptophan by ethanolamine were achieved as recommended by Applied Biosystems. Purification was achieved by preparative reverse-phase HPLC on a 30-nm Vydac C18 column (2.2 × 25 cm, 10 μm). Fractions of the peptide were first loaded onto the column equilibrated with solvent system 1, consisting of 0.1% trifluoroacetic acid and CH_3CN in the ratio 95:5 (v/v), and elution was carried out with a gradient to give a final ratio of 40:60. Further purification was achieved on the same column using a second solvent system containing 0.07% pentafluorophosphoric acid and CH_3CN, using a 30-min linear gradient from 15 to 55% CH_3CN. Desalting of the peptide was obtained by a final chromatographic step using solvent system 1.

CaM Subcloning, Expression, and Purification. CaM clone containing synthetic calmodulin (AF084412; *26*, *27*) was a kind gift of Dr. D. M. Watterson. The open reading frame was subcloned into $pHAT_2$ (*28*) between EcoRI and BamHI sites. *Escherichia coli* BL21(DE3) strain, transformed by the pHAT-CaM construct, was used to overexpress normal or uniformly $^{15}N/^{13}C$-labeled CaM. For labeled CaM, 10 mL of minimal M9-ampicillin medium containing 2 g/L ^{13}C-glucose and 1 g/L $^{15}NH_4Cl$, was inoculated with 100 μL of a saturated culture grown overnight at 37 °C in LB-Amp from a single colony. The culture was then used to inoculate 990 mL of minimal M9-ampicillin medium at 37 °C which was further induced by 1 mM IPTG for 2.5 h at 37 °C after OD600 had reached 0.5. For normal expression, the induction was achieved under the very same conditions, after growing of 1 L LB−Amp first inoculated with 20 to 50 mL of an overnight culture from a single colony, until the OD600 reaches 0.5. After induction of normal or labeled CaM expression, pelleted cells were resuspended in 15 mL of 50 mM Tris pH 8, 100 mM NaCl, 1 mM EDTA, 1 mM DTT, 0.1 mM PMSF, and lysed using French-press. Following centrifugation (18 000 rpm, 30 min at 4 °C) of the sample, the supernatant was cleared by 0.2 μm filtration before $CaCl_2$ was added to a final concentration of 5 mM. Purification to homogeneity was achieved according to Roberts et al. (*27*), using a 15 mL low-sub Phenyl-Sepharose (AP-Biotech) column on a Beckman Biosys2000 FPLC system. After elution with 50 mM Tris pH 7.5, 1 mM EGTA, Apo-CaM was further concentrated and desalted using 5000 Da cutoff centricon (Amicon) and dialyzed against water before freeze-drying. Purity of the samples was monitored by mass spectrometry. Concentrations were measured using OD at 280 nm with a ϵ value of 1580 cm^{-1} M^{-1}. This molar absorption coefficient was estimated from UV−visible spectra after determination of the protein concentration by total amino acid analysis.

CaM C-Terminal Domain Cloning and Overexpression. CaM C-terminal (TR2C) domain clone was a kind gift of Dr. T. Drakenberg (Biophysical Chemistry Department, Lund University, Sweden). The coding sequence was amplified by PCR using conventional methods, with $^{5'}$CTGATGGGATCCAAGATGAAAGAC-ACTGA$^{3'}$ and $^{5'}$AGGGCCCTCGAGCCTACTTAGCCATCATAA$^{3'}$ (MWG-Biotech AG) as primers. The fragment was then subcloned in BamHI and XhoI sites of pGEX4T-3 (AP-Biotech), as a fusion protein with GST. *E. coli* BL21(DE3) strain, transformed by the

above construct, was used to overexpress the recombinant protein in the conditions described above for CaM. After 3 h induction at 37 °C, cells were harvested by centrifugation, and lysed as described above. Purification of TR2C was achieved after loading of the lysis supernatant on 1.5 mL glutathione-Sepharose according to manufacturer's instructions (AP-Biotech). The fusion protein was further purified after direct cleavage by thrombin on the column (50 U, 4 °C). After overnight incubation, remaining thrombin was captured from the eluate by clearing through a 500 μL *p*-amino benzamidine-Sepharose 6B column (Sigma Aldrich). The final eluate, which contained TR2C, was then dialyzed against water and lyophilized. Integrity and purity of the protein were estimated by mass spectrometry.

Dansyl CaM (DNS−CaM) Synthesis. Apo-CaM (20 mg) was dansylated with dansyl-chloride (Sigma Aldrich) as described by Kincaid et al. (*29*). One or two DNS molecules were incorporated per CaM moiety as determined by mass spectrometry; native: *m/e*: 18 390 100%; *m/e*: 18 622 (+232, 1 dansyl) 83%; *m/e*: 18 854 (+464, 2 dansyl) 59%.

Circular Dichroism. Circular dichroism spectra were recorded at 25 °C between 190 and 250 nm on a Jobin-Yvon CD6 spectro-dichrograph, using a quartz cell of 1-mm path length, with a 2 s integration time for each 0.5-nm step. For each experimental condition, two spectra were averaged and corrected from the baseline for buffer solvents.

Fluorescence Emission Spectroscopy. Intrinsic tryptophan emission fluorescence measurements were performed using eithera Bowman 2 Amincon or a Jobin Yvon Spex Fluoro-Max spectrofluorimeter. Unless otherwise specified in the text, experiments were performed in the following conditions: measurements were recorded at room temperature in a 1 × 1 cm cuvette under continuous stirring. The excitation wavelength was set to 295 nm (4 nm band-pass). Emitted light was detected at 90° between 310 and 380 nm (4 nm band-pass). Assays were performed with peptides in the concentration range of 3−10 μM in 20 mM Tris pH 7.7, 1 mM $CaCl_2$. For CaM binding assays, CaM from 0.5 mM stock solution was added stepwise up to a final concentration of 21 μM. For salt-dependence experiments, salts from 4 M stock solutions were added stepwise to peptide/Ca^{2+}-CaM complexes up to a final concentration of 300 mM for NaCl, $NaNO_3$ and KCl or 100 mM for $CaCl_2$, $Ca(NO_3)_2$, and $MgCl_2$. For the TFP-dependence experiments, TFP from 1 mM stock solution was added stepwise up to 25 μM to peptide/Ca^{2+}-CaM complexes formed in the presence of 0.5 mM $CaCl_2$. For the CaM/TR2C competition experiments, CaM (1.3 mM stock solution) or its C-ter domain (1.5 mM stock solution) were added stepwise up to a final concentration of 21 μM to a 5 μM solution of preformed STP23/DNS-CaM complex. The excitation wavelength was set at the maximal excitation wavelength of the DNS-CaM (335 nm, 4 nm band-pass). Emitted light was detected at 90° between 450 and 550 nm (4 nm band-pass). For each experimental point, the intrinsic fluorescence was determined as the difference between the observed fluorescence (F) and the baseline fluorescence determined with an equivalent concentration of NATA (F_{NATA}) under the same conditions, normalized by corrected initial fluorescence ($F_{max} - F_{NATA}$) using the following expression: $(F - F_{NATA})/(F_{max} - F_{NATA})$.

Infrared Spectroscopy. For Fourier transform infrared spectroscopy (FT-IR) studies, the solutions of STP42 and $^{15}N/^{13}C$-labeled CaM were prepared as 0.85 and 0.9 mM solutions, respectively, in a D_2O buffer (20 mM Tris, 5 mM $CaCl_2$, pH 7.7). The complex was obtained by mixing the two latter solutions in a 1/1 ratio. A total of 60 μL of the solutions were inserted between CaF_2 windows (Spectra tech) using a 100 μm spacer. IR spectra were recorded with a JASCO 610 Fourier transform spectrometer. For each spectrum, 1000 interferograms were recorded at 20 °C with a resolution of 4 cm^{-1}. Then, the water vapor was subtracted and the baseline was corrected using the software provided by JASCO (Japan). The spectrum of the peptide bound to CaM was obtained by subtracting the spectrum of the free $^{15}N/^{13}C$-labeled CaM from the spectrum of the complex (peptide/CaM), as described by Zhang et al. (*30*). The spectra of the peptide were normalized using the band of TFA. Then, the second derivatives of the spectra were calculated with the software provided by JASCO.

Nuclear Magnetic Resonance Spectroscopy. A Ca^{2+}-loaded uniformly $^{15}N/^{13}C$-labeled CaM sample was prepared as a 0.7 mM solution in a Shigemi tube (Shigemi Inc., Allison Park, PA) containing 18 mM Tris-base buffer, pH 7.7, 0.05% NaN_3, anti-proteases (Complete, Boehringer, Mannheim) and 10% D_2O. The sample was degassed under argon. The Ca^{2+}-CaM/peptide complex was prepared by direct addition of a concentrated solution of unlabeled STP42 (typically 6 mM) to the NMR sample of labeled Ca^{2+}-CaM to reach a 1:1 stoichiometry. NMR spectra were recorded at 27 °C on Varian Inova 600 and 800 MHz spectrometers equipped with a triple-resonance (^1H, ^{13}C, ^{15}N) probe including shielded z-gradients. To be able to compare the backbone chemical shifts of free and peptide-bound CaM, the backbone chemical shifts of the CaM/peptide complex were assigned under the same conditions as the free CaM. This was done with the following experiments: 2D ^1H-^{15}N HSQC, 3D HNCA, 3D HNCO (*31*−*34*), 3D HN(CO)CA (*35*), and 3D (H)CC(CO)-NH (*36*) spectra. For the HNCA, HN(CO)CA, HNCO, and (H)CC(CO)NH experiments, 1228 × 120 × 58, 1024 × 100 × 55, 1024 × 128 × 52, and 1024 × 70 × 50 (^1H, ^{13}C, ^{15}N) complex points were acquired, respectively. All triple resonance experiments used the pulse sequences provided by the Varian protein pack (available at ftp site: ftp.nmr.varianinc.com). All data were processed using FELIX 2000 (Accelrys). Proton chemical shifts were reported with respect to the H_2O signal relative to DSS at 27 °C. The ^{15}N and ^{13}C chemical shifts were referenced indirectly using the $X/^1H$ frequency ratios of the zero-point: 0.101329118 (^{15}N) and 0.251449530 (^{13}C) (*37*).

RESULTS

Fluorescence Measurements. Initially, we verified whether F-STOP peptide models were able to bind CaM in solution. As illustrated in Figure 1, addition of increasing concentrations of CaM to the STOP peptide STP23 in the presence of 1 mM calcium, induced an increase of the fluorescence intensity and a blue shift of the maximum of reemission of 19 nm. This indicates a more hydrophobic environment in the tryptophan vicinity and demonstrates formation of a complex between Ca^{2+}-CaM and the peptide. Addition of 10 mM EGTA totally reversed the observed changes, indicating that the binding was calcium dependent. The calculated dissociation constant yielded a value of 3.9 ± 1.4 μM, which lies in the range of the published values for CaM/

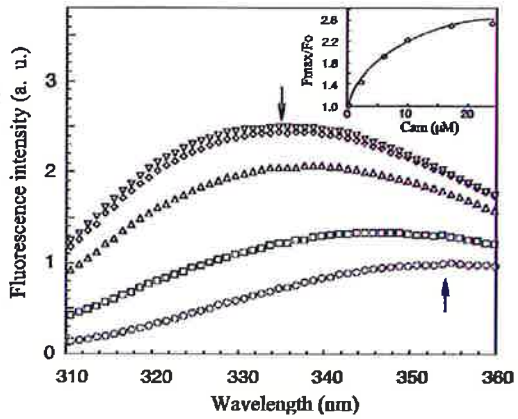

FIGURE 1: Steady-state intrinsic tryptophan fluorescence spectra of STP23 peptide as a function of CaM concentration. 3 μM peptide (open circles); in the presence of 2 μM (open squares), 8 μM (open triangles), 17 μM (open diamonds), and 24 μM CaM (open inverted triangles). Spectra were recorded at 25 °C in the presence of 0.5 mM $CaCl_2$. Excitation was set at 300 nm. The inset shows the evolution of the fluorescence intensity at the maximum emission wavelength as a function of CaM concentration.

F-STOP binding affinities (*16*). Similar results were obtained for the longer peptide corresponding to a single repeat motif (STP42) with a calculated K_d of 5.6 ± 1.2 μM (Supporting Information, Figure S1).

Our result clearly indicates that a single peptide motif binds Ca^{2+}-CaM. We next tested the influence of ionic strength on the binding of CaM to STP23 (Figure 2). Starting from the complex in solution, our data show that an increase in ionic strength leads to a decrease of the fluorescence maximum (Figure 2). The dissociation of the peptide from CaM under increased ionic strength environment is confirmed by a red shift of the λ_{max} toward the value of the unbound form (data not shown), with an almost complete dissociation above 200 mOsm sodium chloride. This is not due to the increase of the chloride concentration, as half-dissociation is obtained only at about 100 mM Cl^- with NaCl, whereas it is quasi-complete at 50 mM Cl^- with $CaCl_2$ (Figure 2A,B). Moreover, we also observed dissociation at similar cation concentrations using nitrate salts instead of chloride salts (Supporting Information, Figure S2). Using STP42 (Supporting Information, Figure S3), we further tested a series of monovalent or divalent ions. Since no specific difference was observed in the dissociation efficiency using sodium or potassium (Figure S3A,C) and calcium or magnesium (Figure S3B,D), we conclude that the nature of the salt used is not responsible for the dissociation observed. We also tested the effect of acidic pH, and observed an increase in dissociation efficiency using divalent ions (data not shown). Taken together our data suggest that CaM interaction with STOP peptides is at least partly electrostatic.

Peptide α-Helical Content. Generally, an increase of the α-helical content in the secondary structure of a CaM-binding peptide is induced by the formation of the complex (*38*). This can be observed by CD spectroscopy as an increase of the ellipticity at 208 and 222 nm. Surprisingly, no significant increase of the negative ellipticity took place at 208 and 222 nm when STOP peptides were added, even in the presence of peptide excess (Figure 3A). The only variations we observed in the range of 200−210 nm were due to the intrinsic

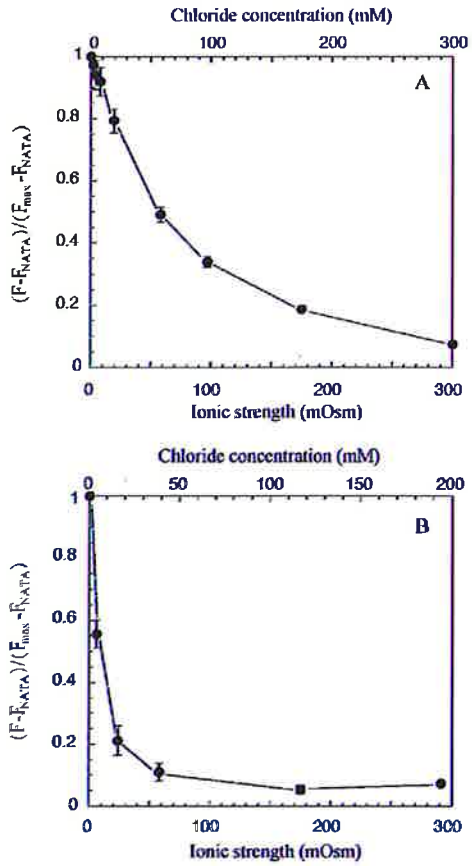

FIGURE 2: Effect of the ionic strength on the STP23/CaM binding. Plotted here is the emitted W-fluorescence, corrected from the NATA-fluorescence recorded in the same conditions and normalized by the complex fluorescence before addition of salts, as a function of the osmolarity: $I = 1/2\ \Sigma(C_i z_i^2)$ where C_i and z_i are the concentration and charge of the i species (lower abscissa) or as a function of the chloride concentration (upper abscissa). Fluorescence was measured for increasing concentrations of NaCl (A) or $CaCl_2$ (B). Spectra were recorded in the presence of 5 μM peptide complexed with 10 μM CaM.

absorption of the peptides (data not shown). We verified by intrinsic W fluorescence using the same samples that, under the conditions used for the CD experiments, binding occurred. The peptides do not adopt a helical conformation by themselves in solution as indicated by a negative ellipticity minimum at 200 nm, nor exhibit a propensity to adopt this conformation, as no significant increase of the helicity was induced by TFE below 15% (data not shown). No spectral variations were observed when 100 mM $CaCl_2$ was added to the peptides, indicating that no structural change takes place in the peptide under these conditions (data not shown). Thus, the ion-dependent inhibition of the binding is not due to a specific folding of the peptides.

To confirm the unusual lack of peptide α-helicity upon binding, we used FTIR spectroscopy to investigate the structure changes induced within STP23 in the presence of CaM. The amide I band, which is due to carbonyl stretching, is particularly valuable for study of the secondary structure of polypeptides. Moreover, by using $^{15}N/^{13}C$-labeled protein it is possible to distinguish the contributions to the FTIR spectrum of the two partners of the complex (*30*, *39*). When

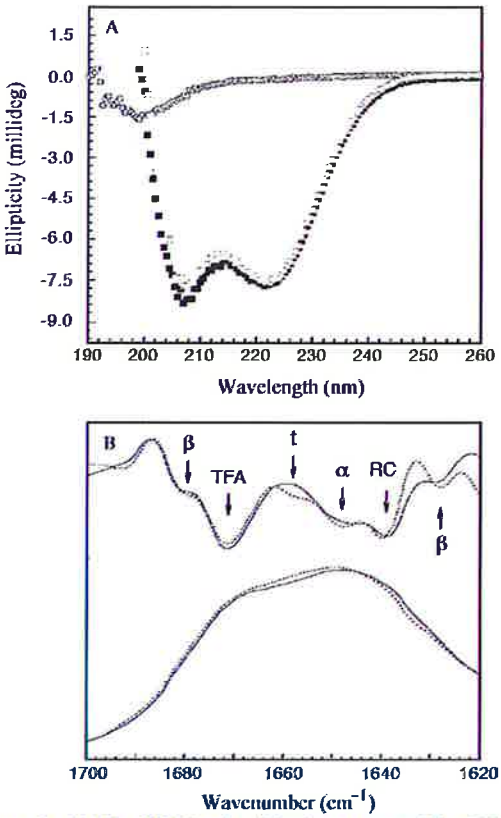

FIGURE 3: (A) Far UV circular dichroism spectra of the STP23/CaM. STP23 alone (open circles); CaM alone (filled squares); STP23/CaM (open squares). Spectra were recorded with 40 μM CaM complexed with a final concentration 40 μM STP23. (B) FTIR spectra of the peptide: effect of the binding to CaM. (Lower panel) Raw spectra of the free peptide (plain line) and the CaM-complexed peptide (dashed line). The spectrum of the peptide bound to CaM was obtained by subtracting the amide I band of the $^{15}N/^{13}C$-labeled CaM (see Experimental Procedures). (Top panel) Second derivatives of the raw spectra: free peptide (plain line), CaM-complexed peptide (dashed line). The band assignment is shown on the figure: (β) extended structures; (TFA) TFA; (t) turns; (α) α-helices; (RC) random coil.

$^{15}N/^{13}C$-labeled CaM is used, its amide I band is shifted (*30*). It is then possible to distinguish the contribution of the bound peptide from that of CaM. In agreement with previous studies (*30*, *40*), the maximum of the amide I band of the unlabeled CaM is at 1644 cm^{-1} (data not shown). The maximum is shifted at 1598 cm^{-1} in the case of the $^{15}N/^{13}C$-labeled protein (data not shown). This maximum is not changed when CaM forms a complex with the peptide. Therefore, the spectrum of the peptide bound to CaM can be extracted from the spectrum of the complex by subtracting the spectrum of the free $^{15}N/^{13}C$-TR2C, as described by Yuan et al. (*39*).

The maximum of the amide I band in the spectrum of the peptide in solution is at 1646 cm^{-1} (Figure 3B). This maximum is shifted to 1648 cm^{-1} when the protein is bound to CaM. This indicates that the secondary structure of the peptide is modified upon binding to CaM. The second derivative of the spectrum is calculated to distinguish the various components of the amide I band. Aside from a band at 1671 cm^{-1} that is due to residual TFA (used for the peptide synthesis), bands that can be assigned to random coil (1640 cm^{-1}), α-helices (1648 cm^{-1}), and extended structures (1629 and 1680 cm^{-1}) were detected. These extended structures are probably due to a small amount of the peptide, which is aggregated and does not interfere in the binding to CaM. In agreement with the CD spectra, the preponderant band was that of random coil. The band of α-helices was broad as a result of highly fluctuating structures. The main changes detected in the spectrum of the peptide bound to CaM were the narrowing of the bands (except those assigned to extended structures), particularly those of α-helices, and the appearance of a small band at 1658 cm^{-1} that can be assigned to turns (Figure 3B). The sharpening of the band of α-helices suggests that the highly fluctuating α-helical structure in solution is more constrained upon binding to CaM.

NMR Spectroscopy. Despite previous reports of CaM assignments (*31*), complete ab initio reassignment of our CaM sample appeared to be necessary. Slight experimental variations, in particular, the salt concentrations between our conditions and the published ones combined with the primary sequence difference led to chemical shift variations which did not allow unambiguous assignment of the peaks from the published results, in particular, in the central part of the HSQC spectra. Consequently, we performed four 3D experiments (HNCA, HN(CO)CA, HNCO, and (H)C(CCO)NH) which allowed us to assign all the atoms of the backbone protein except the N-terminal His-tag $_1$MSHHHHHHS$_9$. We also obtained 80% of the ^1H and ^{13}C chemical shifts of the side chains of the nonaromatic residues. The proton, nitrogen, and carbon chemical shifts of the backbone are reported in Supporting Information (Table S1).

An interaction between proteins is expected to induce structural and dynamic changes, giving raise to chemical shift and line width variations of the signals. The residues of CaM affected by the interaction with the peptide have thus been identified from 2D HSQC spectra. We observed only one CAM species upon addition of aliquots of peptide, indicating that the complex is in a fast exchange regime. Residues were considered to be affected when $[(\Delta^{15}N_{Hz})^2 + (\Delta^1H_{Hz})^2]^{1/2} \geq$ **30 Hz. This value corresponds to twice the experimental** resolution at 800 MHz either for the proton ($|\Delta H^N| \geq 0.04$ ppm) or the nitrogen ($|\Delta N| \geq 0.4$ ppm). About two-thirds of the $^{15}N/^1H$ backbone amide chemical shifts remained unaffected by complex formation indicating that the global structure of the domains of CaM was not strongly modified upon complex formation. The assignment was confirmed via a 3D HNCA experiment. The ^1H, ^{15}N, and $^{13}C\alpha$ chemical shifts of the backbone are reported in Supporting Information (Table S2). Figure 4 shows the major variations induced on the H^N and amide ^{15}N chemical shifts by the addition of STP42 to a Ca^{2+}-CaM solution. Surprisingly, the major changes are located in the C-terminal domain. The affected residues in the C-terminal domain are about twice as many as those in the N-terminal domain (see legend to Figure 4), and the main chemical shift changes are principally located in the C-terminal domain of CaM. Interestingly, among residues exhibiting large variations are hydrophobic residues that show nOe contacts with the peptide in the CaM/M13 (*41*) or CaM/CaMKK (*42*) complexes. This suggests that hydrophobic interactions may play an important role in the CaM/STP42 binding. The secondary structure of the complex was estimated from the differences between the experimental and the random coil Cα chemical shifts ($\Delta C\alpha$). These $\Delta C\alpha$

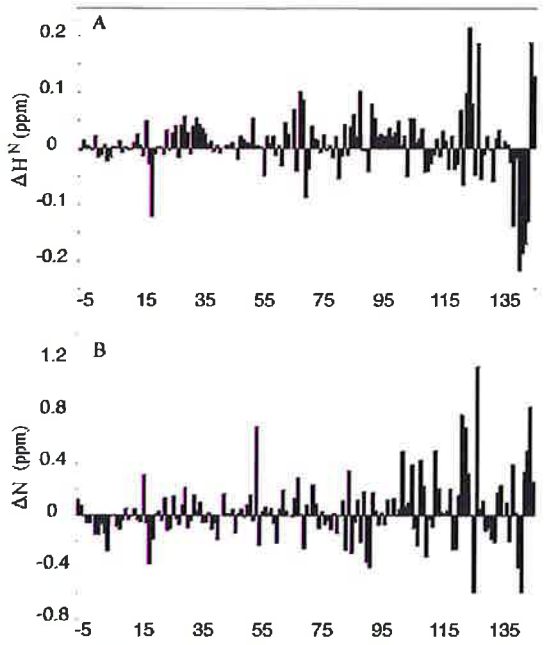

FIGURE 4: Variations of the ^1H and ^{15}N chemical shifts of CaM on complex formation. The STP42 peptide was at a final molar ratio of 1/1 Ca^{2+}-CaM/peptide. The difference of the chemical shifts observed in the ^{15}N-HSQC spectra is displayed as a function of the sequence number. Residues were considered to be affected when $[(\Delta^{15}N_{Hz})^2 + (\Delta^1H_{Hz})^2]^{1/2} \geq 30$ Hz. This value corresponds to twice the experimental resolution at 800 MHz either for the proton ($|\Delta H^N| \geq 0.04$ ppm) or the nitrogen ($|\geq N| \geq 0.4$ ppm). The 18 residues affected in the N-terminal domain are S17, F19, I27, T29, K30, GTV33−35, N53, V55, A57, D64, EFLNL67−71, A73. The 32 residues affected in the C-terminal domain are E82, E84, E87, F89, FDK92−94, A102, ELRH104−107, TNL110−112, K115, EMIREADV123−130, G134, F141, QVMMAK143−148.

shifts indicate that the secondary structures of the N- and C-terminal domains are basically the same as for free CaM and the CaM/M13 complex (data not shown). This result strongly suggests, as for the other peptide complexes, that the two domains do not change their tertiary backbone structure upon binding to the peptide. ΔCα values for the central region of the protein are presented on Figure 5. Surprisingly, we did not observe any significant change in the central region of CaM corresponding to the α-helix connecting the N-terminal and C-terminal domains. This strongly suggests that the central helix is not disrupted in the binding in contrast to classical CaM/peptide complexes (*43*) and that CaM retains an open conformation in our case. This observation could be related to our finding that most residues affected upon binding are located in the C-terminal region of the protein, indicating that the peptide binds mainly to this domain in a manner which may not require central helix disruption (as illustrated in Figure 6).

The Peptide Binds to CaM C-Terminal Domain. To further analyze the nature of the CaM/STOP interaction, and to confirm the implication of the CaM C-terminal domain in STOP peptide binding, we tested the effect of trifluoroperazine (TFP) on binding characteristics. TFP is a classical inhibitor of CaM-dependent activation of its effectors through direct interaction with CaM. TFP binding is complex, but involves mostly the C-terminal CaM subdomain (*44*). Using

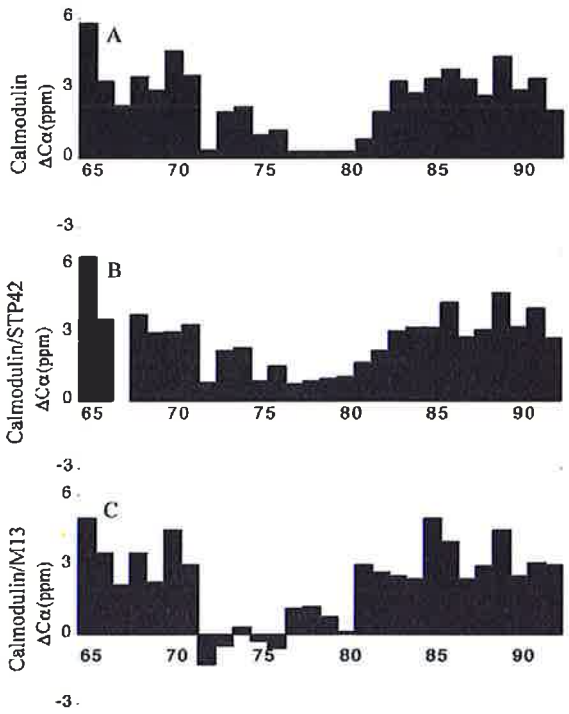

FIGURE 5: The differences between the experimental and the random coil Cα chemical shifts (ΔCα) of free CaM (A), the CaM/STP42 complex (B), and the CaM/M13 complex (C) for the central helix. Here the ΔCα shifts of the free CaM (A) and the CaM/STP42 complex (B) closely follow each other while those of the CaM/M13 complex (C) are significantly different.

CD spectroscopy as described by Vertessy et al. (*45*), we first measured TFP affinity for our CaM sequence (data not shown), and obtained a constant in the range of 1−2 μM, as expected from published data (*45*, *46*). As shown in Figure 7A, the addition of TFP led to a large decrease of the maximal fluorescence associated with a red shift of the maximum toward the λ_{max} value of the free peptide. This indicates that TFP inhibits peptide binding and suggests that the Mc motif competes with TFP for the same binding site, which comprises the hydrophobic pocket in the C-terminal domain.

To further investigate the mode of interaction of CaM with the peptide, we then performed competition experiments between CaM and its C-terminal domain (TR2C). As illustrated in Figure 7B, TR2C displaced dansylated-CaM (DNS-CaM) from STOP peptide with an efficiency similar to that of wild-type CaM. These convergent data strongly suggest that CaM-binding modules of F-STOP interact predominantly with CaM C-terminal domain, whereas the N-terminal domain has only an accessory role in STOP binding.

DISCUSSION

In this work, we have characterized the interaction between Ca^{2+}-CaM and peptide models corresponding to the Mc motif of the repeated microtubule-binding domain of F-STOP protein. We demonstrate that peptide binding to Ca^{2+}-CaM is unusual, mostly involving its C-terminal domain, and implicating to some extent electrostatic interactions. Moreover, NMR spectra analyses strongly suggest that CaM remains in an extended conformation.

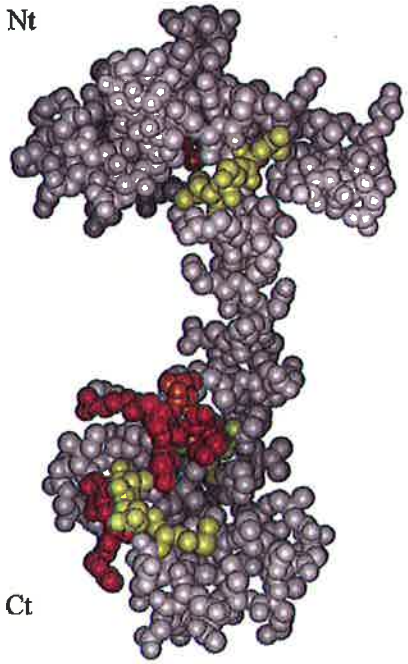

FIGURE 6: Spatial distribution of the chemical shift variations observed between CaM and the CaM complexed with STP42 at a molar ratio of 1/1 Ca^{2+}-CaM/peptide. The variations are mapped onto the crystallographic structure of free *P. tetraurelia* Ca^{2+}-CaM (*59*). Major variations are observed in the C-terminal domain. Yellow, orange, and red indicate the locations of amino acids whose $[(\Delta^{15}N_{Hz})^2 + (\Delta^{1}H_{Hz})^2]^{1/2}$ were between 60 and 90 Hz (L69, N70, L71, F89, D93, M124, E127, A128), between 90 and 120 Hz (F19, I125, F141, M146, K148), and over 120 Hz (R126, D129, Q143, V144, M145, A147), respectively.

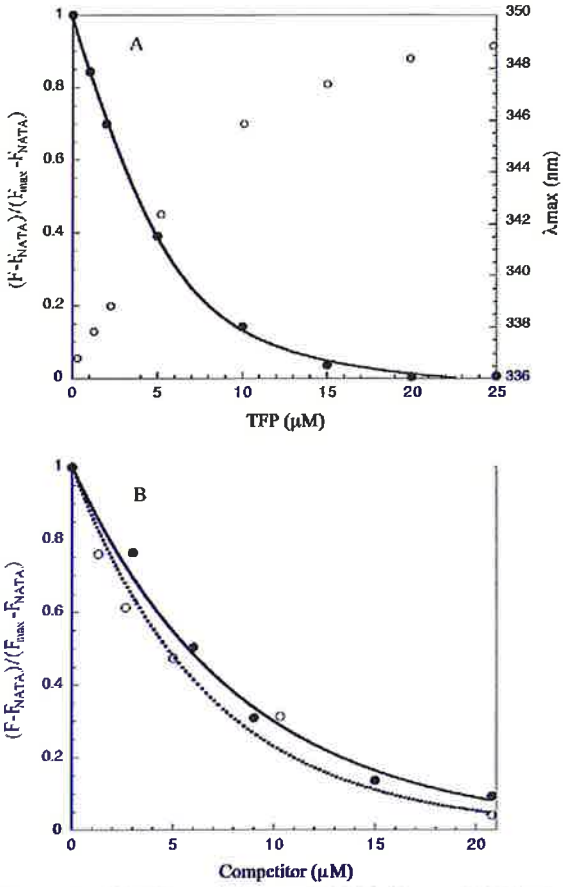

FIGURE 7: (A) Effect of TFP on CaM binding to STP23. The W-fluorescence corrected from the NATA fluorescence, recorded in the same conditions and normalized by the initial steady-state complex fluorescence (filled circles), and the emission wavelength at the maximum of each fluorescence spectrum (open circles) were expressed as a function of the TFP concentration. Spectra were recorded in the presence of 10 μM peptide complexed with 10 μM CaM. Excitation was set at 290 nm to avoid interference with TFP fluorescence. Reemitted fluorescence signals were integrated 20 nm around the maximum of each individual emission spectrum. (B) Competition between integral CaM and its C-terminal domain for STP23 binding. The DNS fluorescence corrected from the NATA fluorescence, recorded in the same conditions and normalized by the initial steady-state complex fluorescence, was expressed as a function of the competitor concentration: CaM (open circles) and TR2C (filled circles). Spectra were recorded in the presence of 0.5 mM $CaCl_2$ for a concentration of 6 μM peptide complexed with 5 μM DNS-CaM. Output signals were integrated between 450 and 550 nm.

Previously reported data showed that at least a tandem repeat of the Mc motif was required for proper CaM-Agarose binding (*16*), suggesting that two Mc motifs might bind a single CaM molecule. To our knowledge, a 2:1 peptide to CaM binding stoichiometry has been only reported for the complex formed between CaM and the carboxy-terminal domain of the Petunia glutamate decarboxylase (*18*). An even more complex situation has been described for the phosphorylase kinase, where one CaM interacts with two distinct peptides of its gamma subunit (*19*). Structures of two complexes where CaM binds to more than a single peptide have been determined, in complex with the edema factor of *Bacillus anthraxis* (*20*), or with the gating-domain of a Ca^{2+}-activated K^+ channel (*21*). In our hands, however, 2D ^{15}N-HSQC spectra in the presence of 1:1 and 2:1 peptide versus CaM ratios show equivalent variations of the ^1H and ^{15}N chemical shifts when compared to Ca^{2+}-CaM alone (data not shown). It is thus highly probable that the weak binding of a single Mc motif to immobilized CaM described in published work (*16*) is related to the experimental conditions used, i.e., 100 mM NaCl. We indeed clearly demonstrate here that Mc binding is very sensitive to ionic strength, as is native F-STOP binding (unpublished results), decreasing association efficiency by 70% in the presence of 100 mOsm NaCl (Figures 2A and S3A). In their published study (*16*), Bosc et al. suggest, from Scatchard plots, that F-STOP bears two types of CaM-binding sites: low affinity and high affinity. However, this hypothesis does not correlate with the presence of both Mc and Mn CaM binding motifs, since only Mc repeats in F-STOP bind immobilized Ca^{2+}-CaM (*16*). Thus, we cannot exclude the possibility that STOP binding to CaM through repeated Mc motifs is cooperative, suggesting that F-STOP might undergo a global structural rearrangement upon CaM binding.

Generally, complexes formed between specific peptides and Ca^{2+}-CaM share typical features: (i) high affinity binding in the 10−100 nM range; (ii) sensitivity to hydrophobic inhibitors such as TFP or W-7; (iii) essentially hydrophobic interaction due to contacts between methionines of CaM and aromatic or bulky hydrophobic residues of the peptide which is thus insensitive to high ionic strength; and

(iv) from the structural point of view, wrapping of the two CaM subdomains around the peptide which in turn adopts an α-helical conformation (*10*, *47*, *48*). The complex we have characterized between CaM and a single Mc motif of F-STOP repeated region exhibits very unusual features, which contrast with the classical model. Although the binding is calcium dependent, the affinity is low, in the micromolar range, more similar to that observed for calcium-independent binding domains (*10*, *47*, *48*). Second, the binding is very sensitive to ionic strength, which also contrasts with most of the other peptide binding motifs. Such a property suggests a mainly ionic interaction between the negatively charged amino acids of CaM and the basic residues of the peptide. In our case, although the exact location of the binding zone in the peptide cannot be precisely determined as yet, the sequence corresponding to the Mc motif exhibits a high proportion, about 60%, of basic and polar residues. Moreover, CD spectra (Figure 3A) indicate that the binding of the peptide to CaM has no effect on the overall α-helical structure in the complex. The possibility of a loss of CaM structure, compensated by gain of peptide structure induced by binding can be ruled out by our NMR results which show only slight variations of the CaM chemical shifts, in particular, the $^{13}C\alpha$ chemical shifts which are highly dependent on the structure. This analysis is corroborated by infrared spectroscopy, which does not indicate any significant structural change in CaM, while the signals associated with the peptide are clearly perturbed. These convergent results indicate that Mc peptide motif binds CaM without adopting the canonical α-helical conformation, in contrast to typical hydrophobic CaM-binding peptides. To date, in three-dimensional structures of peptides in complex with Ca^{2+}-CaM, the interacting peptide is found to adopt an α-helical conformation upon binding (*21*, *41*, *42*, *49*−*53*).

In complex with the Mc motif peptide, Ca^{2+}-CaM appears to retain a conformation similar to that of free Ca^{2+}-CaM (Figure 5). In the usual cases described to date, the wrapping of Ca^{2+}-CaM around the bound peptide is indeed accompanied by a disruption of the central α-helix connecting the two subdomains (*43*). This conformational transition induces very typical changes of the Cα chemical shifts in the interdomain α-helix of Ca^{2+}-CaM (*43*). Moreover, we clearly demonstrate both by NMR and direct competition assays that the Mc motif peptide of STOP interacts mainly with the C-terminal part of CaM (Figures 6 and 7). Indeed, chemical mapping indicates that the most affected region upon peptide binding is the C-terminal half of CaM (cf. Figure 4), suggesting the N-terminal half of CaM has only an accessory role (if any) in the binding. Interestingly, we demonstrate that the binding of the STP23 Mc motif peptide to Ca^{2+}-CaM is inhibited by TFP with an IC_{50} of about 4 μM (Figure 7A), which suggests a competition for the same site between the two species. This is further supported by the published mapping of the C-terminal binding site of TFP on Ca^{2+}-CaM, where 9 residues out of 13 having contacts with TFP in CaM/TFP complex (*44*) are also involved in Mc peptide binding (F92, L105, E123, M124, I125, E127, A128, F141, V144). Our data suggest that competition with TFP could be at least partly the result of steric hindrance.

These very atypical features for Ca^{2+}-CaM/peptide complexes have been observed in two other cases: CaM-binding domains of the SEF2-1/E12 protein and the MARCKS and MARCKS-related proteins. Binding inhibition has been reported in both cases for model-peptide binding to Ca^{2+}-CaM above 25 mM $CaCl_2$ for MARCKS, and 200 mM NaCl for SEF2-1/E12 (*22*, *54*), i.e., comparable to what we observe for the Mc motif studied here. In both cases, the peptides bear very high content in basic amino acids (50%) and low content in hydrophobic amino acids when compared to typical CaM-binding domains, a property which has been related to the observed salt sensitivity (*22*, *54*). In the formed complexes, the peptides have been also reported to bind to Ca^{2+}-CaM without acquiring any α-helical conformation as determined by CD spectroscopy for the MARCKS CaM-binding domain (*24*, *54*), the F52/MARCKS-related CaM-binding domain (*25*, *54*), the Ral-A protein (*55*) and by NMR for the SEF2-1mp domain (*23*). In the latter case, absence of chemical shift variations between free Ca^{2+}-CaM and Ca^{2+}-CaM/peptide complexes has been observed, suggesting an extended conformation of Ca^{2+}-CaM in solution (*23*). Such an extended conformation for complexed Ca^{2+}-CaM has been also proposed for the basic CAP-23/NAP22 CaM-binding domain using SAXS spectroscopy (*23*, *56*). Functionally, a preferential interaction with the C-terminal domain of CaM has been reported for the bHLH protein E12, which exhibits a basic domain analogous to SEF2-1mp (*22*). Thus, the recently reported structure of the CaM/MARCKS peptide complex could give interesting insights into the interaction mode of Ca^{2+}-CaM/Mc motif binding. Indeed, the MARCKS peptide is found to take an elongated structure, with only a short one-turn α-helix surrounded by two loops (*57*). Such a conformation would be, for our peptide, in agreement with the CD and IR results, which indicate only the stabilization upon CaM binding of a preexisting fluctuating α-helical structure in solution. MARCKS peptide also binds to Ca^{2+}-CaM through interaction of a single hydrophobic residue with the hydrophobic pocket of the C-terminal lobe of CaM. This role could be mimicked in the Mc module by the tryptophan. Unfortunately, we have not been able yet to assign the peptides within the complex and consequently to determine either the CaM-binding region or the Mc motif conformation in the bound state. These points are under investigation using a labeled-peptide sample.

MARCKS peptide interacts with the N-terminal lobe of CaM in crystals, leading it to wrap around the peptide, with a disruption of CaM central α-helix (*57*). This is a major difference with the conformation of CaM in complex with the F-STOP Mc motif. First, major contacts between N-terminal domain and the MARCKS peptide are observed for CaM residues 10−15, a zone that is unaffected in our complex. Second, we do not observe any significant change for the central helix, suggesting an open conformation of CaM similar to that observed in free Ca^{2+}-CaM. In this species, the tumbling of the two domains remains independent, as described in the "flexible tether" model (*58*). Thus, we suggest that in the CaM/STP-peptide complex, the chemical shift variations we observed in the N-terminal lobe of CaM are related to its temporary interaction with the C-terminal lobe of the complex. In the MARCKS complex, wrapping of CaM might still be the consequence of the steric constraint imposed by crystal stacking. Even though previous NMR results have been interpreted as due to the disruption of the central helix and a closed CaM conformation (*25*), it is notable that data are missing for residues in the CaM

central α-helix, leaving open the possibility of a restrained flexibility rather than true wrapping around the peptide.

Our results reinforce the recent views on CaM binding modes, pointing out that Ca^{2+}-CaM interacts with its targets with more variety than previously imagined (*59*). Nonglobular wrapping of bound CaM has been described in complexes formed with Ca^{2+}-activated K^+ channel and Anthrax edema factor (*20*, *21*). This is also illustrated in the complex formed between the C20W peptide of the plasma membrane calcium pump and the C-terminal lobe of Ca^{2+}-CaM (*60*). Ca^{2+}-CaM interaction with STOP-Mc motif involves mainly its C-terminal lobe, leaves CaM in an extended conformation, and potentially permits interaction of its N-terminal domain with another partner. This intriguing possibility remains to be investigated.

Physiological CaM-binding to F-STOP may represent an even more unusual complex formation. Mc motifs are repeated in the central domain of cloned STOP proteins, raising the possibility that several Ca^{2+}-CaM interact with a single STOP under physiological conditions. Interestingly, homology searches in EST databases for STOP-related proteins in different organisms have shown that Mc motif is not always repeated, and may even be absent (*16*). As mentioned above, F-STOP colocalizes with CaM at the microtubule spindle during mitosis (*11*). The measured K_d of Ca^{2+}-CaM for Mc motif is in the micromolar range. Such an affinity rules out the possibility that microtubule associated F-STOP is responsible for the specific relocalization of CaM during mitosis. On the other hand, their colocalization may lead to specific interaction of F-STOP and CaM in the close vicinity of the spindle. In fact, microtubule dynamics are a key to mitotic progression (*61*). CaM is also known to be required for proper progression through mitosis (*14*, *15*). The fact that CaM is the only known regulator of microtubule stabilization by STOP suggests that their interaction may have a physiological function during mitosis. It will be of interest to know how the unusual CaM binding to STOP may be implicated in this process.

ACKNOWLEDGMENT

We thank J. P. Andrieu (LEM-IBS) for amino acid analyses, LSMP-IBS for mass spectrometry analyses, L. Blanchoin for technical assistance, and E. Denarier and C. Bosc for helpful reagents. D.B. and C.V. were recipients of a CEA fellowship.

SUPPORTING INFORMATION AVAILABLE

Steady-state intrinsic tryptophan fluorescence spectra of STP42 peptide as a function of CaM concentration (Figure S1), effect of nitrate salts on STP23/CaM binding (Figure S2), and effect of the ionic strength on the STP42/CaM binding (Figure S3). Proton, nitrogen-15, and carbon-13 chemical shift assignment of Ca^{2+}-calmodulin backbone atoms (Table S1) and STP42-complexed Ca^{2+}-calmodulin backbone atoms (Table S2). This material is available free of charge via the Internet at http://pubs.acs.org.

REFERENCES

1. Chapin, S., and Bulinski, J. (1992) Microtubule stabilization by assembly promoting microtubule-associated proteins: a repeat performance. *Cell Motil. Cytoskeleton 23*, 236−243.
2. Margolis, R. L., Rauch, C. T., and Job, D. (1986) Purification and assay of a 145-kDa protein (STOP145) with microtubule-stabilizing and motility behavior. *Proc. Natl. Acad. Sci. U.S.A. 83*, 639−643.
3. Pabion, M., Job, D., and Margolis, R. L. (1984) Sliding of STOP proteins on microtubules. *Biochemistry 23*, 6642−6648.
4. Bosc, C., Cronk, J. D., Pirollet, F., Watterson, M. D., Haiech, J., Job, D., and Margolis, R. L. (1996) Cloning, expression, and properties of the microtubule-stabilizing protein STOP. *Proc. Natl. Acad. Sci. U.S.A. 93*, 2125−2130.
5. Denarier, E., Fourest-Lieuvin, A., Bosc, C., Pirollet, F., Chapel, A., Margolis, R. L., and Job, D. (1998) Nonneuronal isoforms of STOP protein are responsible for microtubule cold stability in mammalian fibroblasts. *Proc. Natl. Acad. Sci. U.S.A. 95*, 6055−6060.
6. Guillaud, L., Bosc, C., Fourest-Lieuvin, A., Denarier, E., Pirollet, F., Lafanechere, L., and Job, D. (1998) STOP proteins are responsible for the high degree of microtubule stabilization observed in neuronal cells. *J. Cell Biol. 142*, 167−179.
7. Andrieux, A., Salin, P. A., Vernet, M., Kujala, P., Baratier, J., Gory-Faure, S., Bosc, C., Pointu, H., Proietto, D., Schweitzer, A., Denarier, E., Klumperman, J., and Job, D. (2002) The suppression of brain cold-stable microtubules in mice induces synaptic defects associated with neuroleptic-sensitive behavioral disorders. *Genes Dev. 16*, 2350−2364.
8. Pirollet, F., Derancourt, J., Haiech, J., Job, D., and Margolis, R. L. (1992) Ca(2+)-calmodulin regulated effectors of microtubule stability in bovine brain. *Biochemistry 31*, 8849−8855.
9. Pirollet, F., Margolis, R., and Job, D. (1992) Ca(2+)-calmodulin regulated effectors of microtubule stability in neuronal tissues. *Biochim. Biophys. Acta 1160*, 113−119.
10. Chin, D., and Means, A. R. (2000) Calmodulin: a prototypical calcium sensor. *Trends Cell Biol. 10*, 322−328.
11. Li, C. J., Heim, R., Lu, P., Pu, Y., Tsien, R. Y., and Chang, D. C. (1999) Dynamic redistribution of calmodulin in HeLa cells during cell division as revealed by a GFP-calmodulin fusion protein technique. *J. Cell Sci. 112 (Pt 10)*, 1567−1577.
12. Erent, M., Pagakis, S., Browne, J. P., and Bayley, P. (1999) Association of calmodulin with cytoskeletal structures at different stages of HeLa cell division, visualized by a calmodulin-EGFP fusion protein. *Mol. Cell Biol. Res. Commun. 1*, 209−215.
13. Moser, M. J., Flory, M. R., and Davis, T. N. (1997) Calmodulin localizes to the spindle pole body of *Schizosaccharomyces pombe* and performs an essential function in chromosome segregation. *J. Cell Sci. 110 (Pt 15)*, 1805−1812.
14. Rasmussen, C. D., and Means, A. R. (1989) Calmodulin is required for cell-cycle progression during G1 and mitosis. *EMBO J. 8*, 73−82.
15. Torok, K., Wilding, M., Groigno, L., Patel, R., and Whitaker, M. (1998) Imaging the spatial dynamics of calmodulin activation during mitosis, *Curr. Biol. 8*, 692−699.
16. Bosc, C., Frank, R., Denarier, E., Ronjat, M., Schweitzer, A., Wehland, J., and Job, D. (2001) Identification of novel bifunctional calmodulin-binding and microtubule- stabilizing motifs in STOP proteins. *J. Biol. Chem. 276*, 30904−30913.
17. Choi, J. Y., Lee, S. H., Park, C. Y., Heo, W. D., Kim, J. C., Kim, M. C., Chung, W. S., Moon, B. C., Cheong, Y. H., Kim, C. Y., Yoo, J. H., Koo, J. C., Ok, H. M., Chi, S. W., Ryu, S. E., Lee, S. Y., Lim, C. O., and Cho, M. J. (2002) Identification of calmodulin isoform-specific binding peptides from a phage-displayed random 22-mer peptide library. *J. Biol. Chem. 277*, 21630−21638.
18. Yuan, T., and Vogel, H. J. (1998) Calcium-calmodulin-induced dimerization of the carboxyl-terminal domain from petunia glutamate decarboxylase. A novel calmodulin-peptide interaction motif. *J. Biol. Chem. 273*, 30328−30335.
19. Dasgupta, M., Honeycutt, T., and Blumenthal, D. K. (1989) The gamma-subunit of skeletal muscle phosphorylase kinase contains two noncontiguous domains that act in concert to bind calmodulin. *J. Biol. Chem. 264*, 17156−17163.
20. Drum, C. L., Yan, S. Z., Bard, J., Shen, Y. Q., Lu, D., Soelaiman, S., Grabarek, Z., Bohm, A., and Tang, W. J. (2002) Structural basis for the activation of anthrax adenylyl cyclase exotoxin by calmodulin. *Nature 415*, 396−402.
21. Schumacher, M. A., Rivard, A. F., Bachinger, H. P., and Adelman, J. P. (2001) Structure of the gating domain of a Ca2+-activated K+ channel complexed with Ca2+/calmodulin. *Nature 410*, 1120−1124.

22. Onions, J., Hermann, S., and Grundstrom, T. (2000) A novel type of calmodulin interaction in the inhibition of basic helix-loop-helix transcription factors. *Biochemistry 39*, 4366−4374.
23. Larsson, G., Schleucher, J., Onions, J., Hermann, S., Grundstrom, T., and Wijmenga, S. S. (2001) A novel target recognition revealed by calmodulin in complex with the basic helix−loop−helix transcription factor SEF2−1/E2−2. *Protein Sci. 10*, 169−186.
24. Matsubara, M., Yamauchi, E., Hayashi, N., and Taniguchi, H. (1998) MARCKS, a major protein kinase C substrate, assumes nonhelical conformations both in solution and in complex with Ca2+-calmodulin. *FEBS Lett. 421*, 203−207.
25. Porumb, T., Crivici, A., Blackshear, P. J., and Ikura, M. (1997) Calcium binding and conformational properties of calmodulin complexed with peptides derived from myristoylated alanine-rich C kinase substrate (MARCKS) and MARCKS-related protein (MRP). *Eur. Biophys. J. 25*, 239−247.
26. Haiech, J., Kilhoffer, M. C., Craig, T. A., Lukas, T. J., Wilson, E., Guerra-Santos, L., and Watterson, D. M. (1990) Mutant analysis approaches to understanding calcium signal transduction through calmodulin and calmodulin regulated enzymes. *Adv. Exp. Med. Biol. 269*, 43−56.
27. Roberts, D. M., Crea, R., Malecha, M., Alvarado-Urbina, G., Chiarello, R. H., and Watterson, D. M. (1985) Chemical synthesis and expression of a calmodulin gene designed for site-specific mutagenesis. *Biochemistry 24*, 5090−5098.
28. Peranen, J., Rikkonen, M., Hyvonen, M., and Kaariainen, L. (1996) T7 vectors with modified T7lac promoter for expression of proteins in *Escherichia coli*. *Anal. Biochem. 236*, 371−373.
29. Kincaid, R. L., Billingsley, M. L., and Vaughan, M. (1988) Preparation of fluorescent, cross-linking, and biotinylated calmodulin derivatives and their use in studies of calmodulin-activated phosphodiesterase and protein phosphatase. *Methods Enzymol. 159*, 605−626.
30. Zhang, M., Fabian, H., Mantsch, H. H., and Vogel, H. J. (1994) Isotope-edited Fourier transform infrared spectroscopy studies of calmodulin's interaction with its target peptides. *Biochemistry 33*, 10883−10888.
31. Ikura, M., Kay, L. E., and Bax, A. (1990) A novel approach for sequential assignment of 1H, 13C, and 15N spectra of proteins: heteronuclear triple-resonance three-dimensional NMR spectroscopy. Application to calmodulin. *Biochemistry 29*, 4659−4667.
32. Grzesiek, S., and Bax, A. (1992) Improved 3D triple-resonance NMR techniques applied to a 31 kDa protein. *J. Magn. Reson. 96*, 432−440.
33. Muhandiram, D. R., and Kay, L. E. (1994) Gradient-enhanced triple-resonance three-dimensional NMR experiments with improved sensitivity. *J. Magn. Reson. B103*, 203-216.
34. Kay, L. E., Xu, G. Y., and Yamazaki, T. (1994) Enhanced-sensitivity triple-resonance spectroscopy with minimal H_2O saturation. *J. Magn. Reson. A109*, 129−133.
35. Yamazaki, T., Lee, W., Arrowsmith, C. H., Muhandiram, D. R., and Kay, L. E. (1994) A suite of triple resonance NMR experiments for the backbone assignment of ^{15}N, ^{13}C, ^{2}H labeled proteins with high sensitivity, *J. Am. Chem. Soc. 116*, 11655−11666.
36. Grzesiek, S., Anglister, J., and Bax, A. (1993) Correlation of backbone amide and aliphatic side-chain resonances in $^{13}C/^{15}N$-enriched proteins by isotropic mixing of ^{13}C magnetization. *J. Magn. Reson. B101*, 114−119.
37. Wishart, D. S., Bigam, C. G., Yao, J., Abildgaard, F., Dyson, H. J., Oldfield, E., Markley, J. L., and Sykes, B. D. (1995) 1H, 13C and 15N chemical shift referencing in biomolecular NMR. *J. Biomol. NMR 6*, 135−140.
38. Fasman, G. D. (1996) *Circular Dichroism and the Conformational Analysis of Biomolecules*, Plenum Press, New York.
39. Yuan, T., Walsh, M. P., Sutherland, C., Fabian, H., and Vogel, H. J. (1999) Calcium-dependent and -independent interactions of the calmodulin-binding domain of cyclic nucleotide phosphodiesterase with calmodulin. *Biochemistry 38*, 1446−1455.
40. Krueger, J. K., Gallagher, S. C., Wang, C. A., and Trewhella, J. (2000) Calmodulin remains extended upon binding to smooth muscle caldesmon: a combined small-angle scattering and Fourier transform infrared spectroscopy study. *Biochemistry 39*, 3979−3987.
41. Ikura, M., Clore, G. M., Gronenborn, A. M., Zhu, G., Klee, C. B., and Bax, A. (1992) Solution structure of a calmodulin-target peptide complex by multidimensional NMR. *Science 256*, 632−638.
42. Osawa, M., Tokumitsu, H., Swindells, M. B., Kurihara, H., Orita, M., Shibanuma, T., Furuya, T., and Ikura, M. (1999) A novel target recognition revealed by calmodulin in complex with Ca^{2+}-calmodulin-dependent kinase kinase. *Nat. Struct. Biol. 6*, 819−824.
43. Ikura, M., Kay, L. E., Krinks, M., and Bax, A. (1991) Triple-resonance multidimensional NMR study of calmodulin complexed with the binding domain of skeletal muscle myosin light-chain kinase: indication of a conformational change in the central helix. *Biochemistry 30*, 5498−5504.
44. Cook, W. J., Walter, L. J., and Walter, M. R. (1994) Drug binding by calmodulin: crystal structure of a calmodulin-trifluoperazine complex. *Biochemistry 33*, 15259−15265.
45. Vertessy, B. G., Harmat, V., Bocskei, Z., Naray-Szabo, G., Orosz, F., and Ovadi, J. (1998) Simultaneous binding of drugs with different chemical structures to Ca2+-calmodulin: crystallographic and spectroscopic studies. *Biochemistry 37*, 15300−15310.
46. Levin, R. M., and Weiss, B. (1977) Binding of trifluoperazine to the calcium-dependent activator of cyclic nucleotide phosphodiesterase. *Mol. Pharmacol. 13*, 690−697.
47. Crivici, A., and Ikura, M. (1995) Molecular and structural basis of target recognition by calmodulin. *Annu. Rev. Biophys. Biomol. Struct. 24*, 85−116.
48. Rhoads, A. R., and Friedberg, F. (1997) Sequence motifs for calmodulin recognition. *FASEB J. 11*, 331−340.
49. Meador, W. E., Means, A. R., and Quiocho, F. A. (1992) Target enzyme recognition by calmodulin: 2.4 A structure of a calmodulin-peptide complex. *Science 257*, 1251−1255.
50. Meador, W. E., Means, A. R., and Quiocho, F. A. (1993) Modulation of calmodulin plasticity in molecular recognition on the basis of X-ray structures. *Science 262*, 1718−1721.
51. Mirzoeva, S., Weigand, S., Lukas, T. J., Shuvalova, L., Anderson, W. F., and Watterson, D. M. (1999) Analysis of the functional coupling between Calmodulin's calcium binding and peptide recognition properties. *Biochemistry 38*, 14117−14118.
52. Wall, M. E., Clarage, J. B., and Phillips, G. N. (1997) Motions of calmodulin characterized using both Bragg and diffuse X-ray scattering. *Structure 5*, 1599−1612.
53. Kurokawa, H., Osawa, M., Kurihara, H., Katayama, N., Tokumitsu, H., Swindells, M. B., Kainosho, M., and Ikura, M. (2001) Target-induced conformational adaptation of calmodulin revealed by the crystal structure of a complex with nematode Ca(2+)/calmodulin-dependent kinase kinase peptide. *J. Mol. Biol. 312*, 59−68.
54. Schleiff, E., Schmitz, A., McIlhinney, R. A., Manenti, S., and Vergeres, G. (1996) Myristoylation does not modulate the properties of MARCKS-related protein (MRP) in solution. *J. Biol. Chem. 271*, 26794−26802.
55. Wang, K. L., Khan, M. T., and Roufogalis, B. D. (1997) Identification and characterization of a calmodulin-binding domain in Ral-A, a Ras-related GTP-binding protein purified from human erythrocyte membrane. *J. Biol. Chem. 272*, 16002−16009.
56. Hayashi, N., Izumi, Y., Titani, K., and Matsushima, N. (2000) The binding of myristoylated N-terminal nonapeptide from neuro-specific protein CAP-23/NAP-22 to calmodulin does not induce the globular structure observed for the calmodulin-nonmyristylated peptide complex. *Protein Sci. 9*, 1905−1913.
57. Yamauchi, E., Nakatsu, T., Matsubara, M., Kato, H., and Taniguchi, H. (2003) Crystal structure of a MARCKS peptide containing the calmodulin-binding domain in complex with Ca-(2+)-calmodulin. *Nat. Struct. Biol. 10*, 226−231.
58. Barbato, G., Ikura, M., Kay, L. E., Pastor, R. W., and Bax, A. (1992) Backbone dynamics of calmodulin studied by 15N relaxation using inverse detected two-dimensional NMR spectroscopy: the central helix is flexible. *Biochemistry 31*, 5269−5278.
59. Vetter, S. W., and Leclerc, E. (2003) Novel aspects of calmodulin target recognition and activation. *Eur. J. Biochem. 270*, 404−414.
60. Elshorst, B., Hennig, M., Forsterling, H., Diener, A., Maurer, M., Schulte, P., Schwalbe, H., Griesinger, C., Krebs, J., Schmid, H., Vorherr, T., and Carafoli, E. (1999) NMR solution structure of a complex of calmodulin with a binding peptide of the Ca2+ pump. *Biochemistry 38*, 12320−12332.
61. Andersen, S. S. (2000) Spindle assembly and the art of regulating microtubule dynamics by MAPs and Stathmin/Op18. *Trends Cell Biol. 10*, 261−267.

BI034746W

Références

1. Earnshaw, W. C., et Cooke, C. A. **1991** Analysis of the distribution of the INCENPs throughout mitosis reveals the existence of a pathway of structural changes in the chromosomes during metaphase and early events in cleavage furrow formation, *J Cell Sci 98 (Pt 4)*, 443-461.
2. Cooke, C. A., Heck, M. M., et Earnshaw, W. C. **1987** The inner centromere protein (INCENP) antigens: movement from inner centromere to midbody during mitosis, *J Cell Biol 105*, 2053-2067.
3. Terada, Y., Tatsuka, M., Suzuki, F., Yasuda, Y., Fujita, S., et Otsu, M. **1998** AIM-1: a mammalian midbody-associated protein required for cytokinesis, *Embo J 17*, 667-676.
4. Adams, R. R., Wheatley, S. P., Gouldsworthy, A. M., Kandels-Lewis, S. E., Carmena, M., Smythe, C., Gerloff, D. L., et Earnshaw, W. C. **2000** INCENP binds the Aurora-related kinase AIRK2 and is required to target it to chromosomes, the central spindle and cleavage furrow, *Curr Biol 10*, 1075-1078.
5. Martineau-Thuillier, S., Andreassen, P. R., et Margolis, R. L. **1998** Colocalization of TD-60 and INCENP throughout G2 and mitosis: evidence for their possible interaction in signalling cytokinesis, *Chromosoma 107*, 461-470.
6. Skoufias, D. A., Mollinari, C., Lacroix, F. B., et Margolis, R. L. **2000** Human Survivin Is a Kinetochore-associated Passenger Protein, *J Cell Biol 151*, 1575-1582.
7. Andreassen, P. R., Palmer, D. K., Wener, M. H., et Margolis, R. L. **1991** Telophase disc: a new mammalian mitotic organelle that bisects telophase cells with a possible function in cytokinesis, *J Cell Sci 99*, 523-534.
8. Mollinari, C., Reynaud, C., Martineau-Thuillier, S., Monier, S., Kieffer, S., Garin, J., Andreassen, P. R., Boulet, A., Goud, B., Kleman, J. P., et Margolis, R. L. **2003** The Mammalian Passenger Protein TD-60 Is an RCC1 Family Member with an Essential Role in Prometaphase to Metaphase Progression, *Dev Cell 5*, 295-307.
9. Ambrosini, G., Adida, C., et Altieri, D. C. **1997** A novel anti-apoptosis gene, survivin, expressed in cancer and lymphoma, *Nat Med 3*, 917-921.
10. Li, F., Ambrosini, G., Chu, E. Y., Plescia, J., Tognin, S., Marchisio, P. C., et Altieri, D. C. **1998** Control of apoptosis and mitotic spindle checkpoint by survivin, *Nature 396*, 580-584.
11. Chantalat, L., Skoufias, D. A., Kleman, J. P., Jung, B., Dideberg, O., et Margolis, R. L. **2000** Crystal structure of human survivin reveals a bow tie-shaped dimer with two unusual alpha-helical extensions, *Mol Cell 6*, 183-189.
12. Wheatley, S. P., Carvalho, A., Vagnarelli, P., et Earnshaw, W. C. **2001** INCENP is required for proper targeting of Survivin to the centromeres and the anaphase spindle during mitosis, *Curr Biol 11*, 886-890.
13. Jiang, W., Jimenez, G., Wells, N. J., Hope, T. J., Wahl, G. M., Hunter, T., et Fukunaga, R. **1998** PRC1: a human mitotic spindle-associated CDK substrate protein required for cytokinesis, *Mol Cell 2*, 877-885.
14. Mollinari, C., Kleman, J. P., Jiang, W., Schoehn, G., Hunter, T., et Margolis, R. L. **2002** PRC1 is a microtubule binding and bundling protein essential to maintain the mitotic spindle midzone, *J Cell Biol 157*, 1175-1186.
15. Denarier, E., Fourest-Lieuvin, A., Bosc, C., Pirollet, F., Chapel, A., Margolis, R. L., et Job, D. **1998** Nonneuronal isoforms of STOP protein are responsible for microtubule cold stability

in mammalian fibroblasts, *Proc Natl Acad Sci U S A 95*, 6055-6060.
16. Margolis, R. L., Rauch, C. T., Pirollet, F., et Job, D. **1990** Specific association of STOP protein with microtubules in vitro and with stable microtubules in mitotic spindles of cultured cells, *Embo J 9*, 4095-4102.
17. Job, D., Rauch, C., Fischer, E., et Margolis, R. **1982** Recycling of cold-stable microtubules: evidence that cold stability is due to substoichiometric polymer blocks., *Biochemistry 21*, 509-515.
18. Margolis, R. L., Rauch, C. T., et Job, D. **1986** Purification and assay of a 145-kDa protein (STOP145) with microtubule- stabilizing and motility behavior, *Proc Natl Acad Sci U S A 83*, 639-643.
19. Bosc, C., Andrieux, A., et Job, D. **2003** STOP Proteins, *Biochemistry 42*, 12125-12132.
20. Li, C. J., Heim, R., Lu, P., Pu, Y., Tsien, R. Y., et Chang, D. C. **1999** Dynamic redistribution of calmodulin in HeLa cells during cell division as revealed by a GFP-calmodulin fusion protein technique, *J Cell Sci 112 (Pt 10)*, 1567-1577.
21. Bouvier, D., Vanhaverbeke, C., Simorre, J. P., Arlaud, G. J., Bally, I., Forge, V., Margolis, R. L., Gans, P., et Kleman, J. P. **2003** Unusual Ca(2+)-Calmodulin Binding Interactions of the Microtubule-Associated Protein F-STOP, *Biochemistry 42*, 11484-11493.
22. Rieder, C. L., et Salmon, E. D. **1998** The vertebrate cell kinetochore and its roles during mitosis, *Trends Cell Biol 8*, 310-318.
23. Adams, R. R., Carmena, M., et Earnshaw, W. C. **2001** Chromosomal passengers and the (aurora) ABCs of mitosis, *Trends Cell Biol 11*, 49-54.
24. Mishima, M., Kaitna, S., et Glotzer, M. **2002** Central spindle assembly and cytokinesis require a kinesin-like protein/RhoGAP complex with microtubule bundling activity, *Dev Cell 2*, 41-54.
25. Toure, A., Dorseuil, O., Morin, L., Timmons, P., Jegou, B., Reibel, L., et Gacon, G. **1998** MgcRacGAP, a new human GTPase-activating protein for Rac and Cdc42 similar to Drosophila rotundRacGAP gene product, is expressed in male germ cells, *J Biol Chem 273*, 6019-6023.
26. Saint, R., et Somers, W. G. **2003** Animal cell division: a fellowship of the double ring?, *J Cell Sci 116*, 4277-4281.
27. Minoshima, Y., Kawashima, T., Hirose, K., Tonozuka, Y., Kawajiri, A., Bao, Y. C., Deng, X., Tatsuka, M., Narumiya, S., May, W. S., Jr., Nosaka, T., Semba, K., Inoue, T., Satoh, T., Inagaki, M., et Kitamura, T. **2003** Phosphorylation by aurora B converts MgcRacGAP to a RhoGAP during cytokinesis, *Dev Cell 4*, 549-560.
28. Oegema, K., Savoian, M. S., Mitchison, T. J., et Field, C. M. **2000** Functional analysis of a human homologue of the Drosophila actin binding protein anillin suggests a role in cytokinesis, *J Cell Biol 150*, 539-552.
29. Martineau, S. N., Andreassen, P. R., et Margolis, R. L. **1995** Delay of HeLa cell cleavage into interphase using dihydrocytochalasin B: retention of a postmitotic spindle and telophase disc correlates with synchronous cleavage recovery, *J Cell Biol 131*, 191-205.
30. Margolis, R. L., et Andreassen, P. R. **1993** The telophase disc: its possible role in mammalian cell cleavage, *Bioessays 15*, 201-207.
31. Honda, R., Korner, R., et Nigg, E. A. **2003** Exploring the functional interactions between Aurora B, INCENP, and survivin in mitosis, *Mol Biol Cell 14*, 3325-3341.
32. Chook, Y. M., Cingolani, G., Conti, E., Stewart, M., Vetter, I., et Wittinghofer, A. **1999** Pictures in cell biology. Structures of nuclear-transport components, *Trends Cell Biol 9*, 310-311.

33. Nishimoto, T. **1999** A new role of ran GTPase, *Biochem Biophys Res Commun 262*, 571-574.
34. Renault, L., Kuhlmann, J., Henkel, A., et Wittinghofer, A. **2001** Structural basis for guanine nucleotide exchange on Ran by the regulator of chromosome condensation (RCC1), *Cell 105*, 245-255.
35. Skoufias, D. A., Andreassen, P. R., Lacroix, F. B., Wilson, L., et Margolis, R. L. **2001** Mammalian mad2 and bub1/bubR1 recognize distinct spindle-attachment and kinetochore-tension checkpoints, *Proc Natl Acad Sci U S A 98*, 4492-4497.
36. Biggins, S., et Walczak, C. E. **2003** Captivating capture: how microtubules attach to kinetochores, *Curr Biol 13*, R449-460.
37. Bosc, C., Cronk, J. D., Pirollet, F., Watterson, M. D., Haiech, J., Job, D., et Margolis, R. L. **1996** Cloning, expression, and properties of the microtubule-stabilizing protein STOP, *Proc Natl Acad Sci USA 93*, 2125-2130.
38. Guillaud, L., Bosc, C., Fourest-Lieuvin, A., Denarier, E., Pirollet, F., Lafanechere, L., et Job, D. **1998** STOP proteins are responsible for the high degree of microtubule stabilization observed in neuronal cells, *J Cell Biol 142*, 167-179.
39. Aguezzoul, M., Andrieux, A., et Denarier, E. **2003** Overlap of promoter and coding sequences in the mouse STOP gene (Mtap6), *Genomics 81*, 623-627.
40. Pirollet, F., Derancourt, J., Haiech, J., Job, D., et Margolis, R. L. **1992** Ca(2+)-calmodulin regulated effectors of microtubule stability in bovine brain, *Biochemistry 31*, 8849-8855.
41. Pirollet, F., Margolis, R., et Job, D. **1992** Ca(2+)-calmodulin regulated effectors of microtubule stability in neuronal tissues., *Biochim Biophys Acta 1160*, 113-119.
42. Roberts, D. M., Crea, R., Malecha, M., Alvarado-Urbina, G., Chiarello, R. H., et Watterson, D. M. **1985** Chemical synthesis and expression of a calmodulin gene designed for site-specific mutagenesis, *Biochemistry 24*, 5090-5098.
43. Bosc, C., Frank, R., Denarier, E., Ronjat, M., Schweitzer, A., Wehland, J., et Job, D. **2001** Identification of novel bifunctional calmodulin-binding and microtubule- stabilizing motifs in STOP proteins, *J Biol Chem 276*, 30904-30913.
44. Yamauchi, E., Nakatsu, T., Matsubara, M., Kato, H., et Taniguchi, H. **2003** Crystal structure of a MARCKS peptide containing the calmodulin-binding domain in complex with Ca(2+)-calmodulin, *Nature structural Biology 10*, 226-231.
45. Matsubara, M., Yamauchi, E., Hayashi, N., et Taniguchi, H. **1998** MARCKS, a major protein kinase C substrate, assumes non-helical conformations both in solution and in complex with Ca2+-calmodulin, *FEBS Lett 421*, 203-207.
46. Vetter, S. W., et Leclerc, E. **2003** Novel aspects of calmodulin target recognition and activation, *Eur J Biochem 270*, 404-414.
47. Calabresi, P., Centonze, D., Gubellini, P., Marfia, G. A., Pisani, A., Sancesario, G., et Bernardi, G. **2000** Synaptic transmission in the striatum: from plasticity to neurodegeneration, *Prog Neurobiol 61*, 231-265.
48. Andrieux, A., Salin, P. A., Vernet, M., Kujala, P., Baratier, J., Gory-Faure, S., Bosc, C., Pointu, H., Proietto, D., Schweitzer, A., Denarier, E., Klumperman, J., et Job, D. **2002** The suppression of brain cold-stable microtubules in mice induces synaptic defects associated with neuroleptic-sensitive behavioral disorders, *Genes Dev 16*, 2350-2364.
49. Robinson, P. J., Wang, X., Xue, J., Assaf, B. T., Kemp, B. E., Larsen, M. R., Milburn, P. J., Kleman, J. P., et Margolis, R. L. **2003** Phosphorylation of N-STOP on Ser-537 by cGMP-dependent protein kinase in nerve terminals is regulated by Ca^{2+}-calmodulin, *J Neuroscience manuscrit en préparation.*

Annexes

Résumé du travail de Thèse de Doctorat

Les collagènes V et XI sont des composants quantitativement minoritaires des fibres de collagène. Dans les tissus, les fibres sont des assemblages formés principalement par les collagènes majoritaires de types I et II. La classification des collagènes fibrillaires est basée sur la séparation des collagènes selon leurs localisations tissulaires. Cependant, de nombreuses études ont montré que la chaîne α1 du collagène de type XI n'est pas uniquement exprimée dans les tissus cartilagineux, comme le postule la classification. J'ai démontré la présence de cette chaîne dans les extraits de placenta humain, et dans les produits de synthèse des cellules A204 en culture, deux sources issues de tissus non cartilagineux. Dans cette lignée tout au moins, une forme hétérotypique inconnue jusqu'alors, [α1(XI)]2 α2(V), est synthétisée (1). Nous avons alors suggéré que les collagènes V et XI sont des isoformes d'un type collagènique unique et de distribution complexe V/XI (2). L'étude de la maturation du collagène V/XI des cellules A204 a montré, contrairement aux données publiées jusqu'alors, que la molécule hétérotypique subissait une maturation complète (3). Nos données suggéraient qu'il existe plusieurs formes moléculaires dans les tissus. Il est maintenant admis que ces différentes formes d'assemblage et de maturation sont directement impliquées dans la régulation de la fibrillogenèse (4).

La suite de notre étude a porté sur la stabilisation par couplage covalent de l'hétérotrimère [α1(XI)]2 α2(V). La matrice des cultures des cellules A204 n'est en effet solubilisée qu'après action de la pepsine, suggérant l'existence de liens covalents inconnus dans les parties "non en triple-hélice". Nous avons démontré que ces liens étaient formés par l'action d'une transglutaminase ubiquitaire. Nos résultats démontrent d'une part que les fibrilles de collagènes sont beaucoup plus complexes qu'on ne l'avait cru, et d'autre part que la transglutamination est la voie de pontage du collagène V/XI en culture, ce qui suggère que cette voie peut être utilisée de façon plus générale dans les processus physiologiques conduisant à l'insolubilisation des matrices extracellulaires (5).

Abréviations

BIR
Baculovirus Inhibitor of Apoptosis Repeat

CAM
Calmoduline

CENP-A
CENtromeric Protein -A

EST
Enhanced Sequence Tag; base de données nucléotidique

GAP
GTPase Activating Protein

GEF
Guanine Exchange Factor; facteur d'échange du GDP en GTP pour les petites GTPases

GFP
Green Fluorescent Protéin

GST
Glutathion S-Transferase

HTGs
Human high-Throughput Genomic Sequence; base de données génomique humaine

INCENP
INner CENtromeric Protein

LTD
Long Term Depotentiation

LTP
Long Term Potentiation

MALDI-TOF
Matrix-Assisted Laser Desorption/Ionization mass spectroscopy – Time Of Flight

MARCKS
Myristoylated, Alanine-Rich protein kinase C Substrate

MgcRacGAP
Male germ cells Rac GTPase Activator Protein; homologue humain de RotundRacGAP (Drosophile)

MKLP1
Mitotic Kinesin-Like Protein-1

PKG
Protein Kinase dépendante du cGMP

PRC1
Protein Required for Cytokinesis 1

Ran
Ras-like nuclear GTPase

RCC1
Regulator of Chromosome Condensation factor 1; GEF de Ran

RNAi
Interférence à l'ARN

SAXS
Small Angle X-ray Scattering

STOP
Stable Tubule Only Polypeptide

TD-60
Telophase disk 60 kDa antigen